

28580117

C.1

MICHIGAN STATE UNIVERSITY LIBRARIES



3 1293 00788 5928



This is to certify that the

dissertation entitled

A Kinetic and XPS Study of the Importance
of Oxygen in Catalyzed and Uncatalyzed
Hydrogen Gasification of Carbon

presented by

Michael Henry Treptau

has been accepted towards fulfillment
of the requirements for

Ph.D. degree in Chem. Engr.

Dennis J. Miller
Major professor

Date 7-28-89

**PLACE IN RETURN BOX to remove this checkout from your record.
TO AVOID FINES return on or before date due.**

DATE DUE	DATE DUE	DATE DUE
_____	_____	_____
_____	_____	_____
_____	_____	_____
_____	_____	_____
_____	_____	_____
_____	_____	_____
_____	_____	_____

1

**A KINETIC AND XPS STUDY OF THE IMPORTANCE
OF OXYGEN IN CATALYZED AND UNCATALYZED
HYDROGEN GASIFICATION OF CARBON**

By

Michael Henry Treptau

A DISSERTATION

Submitted to
Michigan State University
in partial fulfillment of the requirements
for the degree of

DOCTOR OF PHILOSOPHY

Department of Chemical Engineering

1989

ABSTRACT

A KINETIC AND XPS STUDY OF THE IMPORTANCE OF OXYGEN IN CATALYZED AND UNCATALYZED HYDROGEN GASIFICATION OF CARBON

By

Michael Henry Treptau

Gasification of coal to form synthetic natural gas is a potentially attractive method of supplying future energy needs of the U.S. Hydrogen gasification is an important topic of study because it is a direct, exothermic route to methane formation, and the presence of hydrogen also strongly inhibits gasification. Alkali salts are the catalysts of choice because of their low cost and resistance to poisoning. A suggested pathway for gasification is via an oxygen transfer mechanism, in which reactant gas adsorbs on the carbon surface, generating oxygen surface complexes. These complexes desorb to form active sites for gasification. Alkali catalysts enhance gasification by interacting with the carbon to form additional surface complexes postulated to be M-O-C groups.

The objectives of the present work are to clarify the role of oxygen in hydrogen gasification by determining if oxygen surface complexes form active sites in hydrogen, and to determine whether oxidation with HNO_3 enhances the reaction rate. Uncatalyzed and catalyzed gasification experiments are performed in a high pressure differential reactor, and x-ray photoelectron spectroscopy (XPS) is used to measure surface oxygen content and determine the nature of active species formed following oxidation, high temperature degassing, and reaction. A study of various alkali salt catalysts is also undertaken to determine the effects of cation, anion, catalyst loss, and dispersion on the reaction rate. Two different carbons are used to determine the role of carbon structure and composition.

Results show that the uncatalyzed gasification rate depends on the initial surface oxygen content. Oxidation with HNO_3 approximately doubles the reaction rate, while degassing reduces the rate by about the same amount. Under reaction conditions, however, XPS shows that no oxygen is present on the carbon surface. A mechanism is thus postulated whereby oxygen groups on the carbon surface desorb to form nascent active sites. Oxidation enhances gasification by increasing the amount of surface oxygen available to produce active sites, while high temperature degassing both removes surface oxygen and anneals the active sites. The effect of oxidation and degassing also depends to some extent on carbon structure and bulk oxygen content.

Catalyzed gasification results indicate that the same active species present in oxidizing environments also catalyze the hydrogen gasification reaction. Catalysts strongly enhance the reactivity of both fresh and degassed carbons by up to a factor of 200 at high loadings. Oxidation with HNO_3 approximately doubles the catalyzed rate via interaction of the catalyst with basic oxygen groups. XPS results on K_2CO_3 -impregnated carbon indicate the presence of large amounts of oxygen on the surface under reaction conditions, some of which is singly bonded to the carbon and assigned to active K-O-C groups. Catalyst loss is higher than in oxidizing environments due to reduction of active species and subsequent vaporization of free metal.

Dedicated to my wife, Sherri, and both sets of parents, whose faithful support, encouragement, and love have helped immeasurably to make the completion of this work possible, and to Christopher, whose presence during the last three months has been a new source of encouragement and motivation.

ACKNOWLEDGEMENTS

I would like to thank Dr. Dennis J. Miller, the chairman of my doctoral committee, for his guidance and encouragement throughout the course of my graduate studies. I would also like to thank Dr. Martin C. Hawley, Dr. Lawrence T. Drzal, Dr. Klaus Otto, and Dr. Thomas J. Pinnavaia for serving on my doctoral committee and providing constructive suggestions during the preparation of this work.

The financial support of the Department of Chemical Engineering at Michigan State University throughout most of this work is greatly appreciated, as is the funding for the XPS work by the Composite Materials and Structures Center at Michigan State University. I would also like to thank Dr. John T. Wilband of the Department of Geological Science at Michigan State University for the use of the Neutron Activation Analysis facilities.

Finally, I would like to express my gratitude to Dr. Kevin J. Hook of the Composite Materials and Structures Center at Michigan State University for his invaluable assistance in running the XPS experiments, and especially for his help with the interpretation of the results.

TABLE OF CONTENTS

List of Tables	viii
List of Figures	ix
Chapter 1: Introduction and Background	1
1.1 Introduction	1
1.2 Background	3
1.2.1 Steam and Carbon Dioxide Gasification	3
1.2.1.1 Uncatalyzed Gasification	3
1.2.1.2 Catalyzed Gasification	6
1.2.2 Hydrogen Gasification	10
1.2.2.1 Uncatalyzed Hydrogen Gasification	10
1.2.2.2 Catalyzed Hydrogen Gasification	12
1.3 Objectives and Rationale	13
1.3.1 Uncatalyzed Hydrogen Gasification	14
1.3.2 Catalyzed Hydrogen Gasification	15
Chapter 2: Experimental Procedures	17
2.1 Gasification Experiments	17
2.1.1 Carbon Characterization	17
2.1.2 Sample Preparation	18
2.1.3 Reactor System	20
2.1.4 Data Analysis	22
2.1.5 Catalyst Loss Measurements	22
2.2 Surface Analysis of Carbons	23
2.2.1 Background	23
2.2.2 Spectrometer Description	24
2.2.3 Data Analysis	25
2.2.4 Vacuum Pretreatment Reactor	26
2.2.5 Sample Preparation	33
Chapter 3: Comparative Study of Alkali Catalysts	35
3.1 Catalyst Activity	36

3.2 Anion Effects	41
3.3 Catalyst Dispersion	44
3.4 Catalyst Loss	47
3.5 Evolution of CO and CO ₂	53
3.6 Discussion	55
Chapter 4: Effect of Pretreatment on Uncatalyzed Gasification	57
4.1 Carbon Black	58
4.1.1 Pretreatment and Gasification	58
4.1.2 Surface Analysis	58
4.2 Coconut Charcoal	71
4.2.1 Pretreatment and Gasification	71
4.2.2 Surface Analysis	73
4.3 Discussion	76
4.3.1 Carbon Black	76
4.3.2 Coconut Charcoal	78
Chapter 5: Effect of Pretreatment on Catalyzed Gasification	80
5.1 Carbon Black	80
5.2 Coconut Charcoal	83
5.3 Surface Analysis	86
5.3.1 K ₂ CO ₃ Standard	86
5.3.2 K ₂ CO ₃ -Impregnated Carbon Black	90
5.4 Discussion	96
5.4.1 Gasification Results	96
5.4.2 XPS Results	97
Chapter 6: Conclusions and Recommendations	100
6.1 Uncatalyzed Gasification	100
6.2 Catalyzed Gasification	104
List of References	106
Appendix A: Data for Figures 3.1 and 3.2	111
Appendix B: O(1s) Peaks	123

LIST OF TABLES

2.1	Ultimate Analysis of Carbons.	18
2.2	Physical Parameters for Neutron Activation Analysis.	23
2.3	Atomic Sensitivity Factors for XPS.	26
3.1	Catalyst Loss at 725° C on Carbon Black.	51
3.2	Catalyst Loss at 865° C on Carbon Black.	52
3.3	Catalyst Loss at 775° C on Coconut Charcoal (M/C= 0.02).	52
3.4	Effect of Pretreatment on Catalyst Loss at 865° C on Carbon Black (M/C= 0.02).	53
3.5	Gas Evolution During Sample Heatup (M/C= 0.02).	54
4.1	Surface Oxygen Content of Carbon Black.	62
4.2	Summary of curve fits for the C(1s) peak of carbon black.	68
4.3	Surface Oxygen Content of Coconut Charcoal.	74
4.4	Curve fit results for the C(1s) peak of coconut charcoal.	76
5.1	XPS Results for K ₂ CO ₃ -impregnated Carbon Black.	93
A.1	Extrapolations made to obtain rates at 30% conversion.	111

LIST OF FIGURES

2.1	BET surface area of coconut charcoal versus conversion.	19
2.2	Schematic of high pressure gasification system.	21
2.3	Schematic of vacuum pretreatment reactor - top view.	28
2.4	Schematic of vacuum pretreatment reactor - side view.	30
3.1	Specific rate versus catalyst loading for carbon black at 865° C, 500 psig H ₂	37
3.2	Specific rate versus catalyst loading for carbon black at 725° C, 500 psig H ₂	38
3.3	Comparison of K ₂ CO ₃ and Na ₂ CO ₃ -catalyzed carbon black at 865° C, 500 psig H ₂	39
3.4	Comparison of K ₂ CO ₃ and Na ₂ CO ₃ -catalyzed coconut charcoal at 775° C, 500 psig H ₂	40
3.5	Comparison of K ₂ CO ₃ and KOH-catalyzed carbon black at 865° C, 500 psig H ₂	42
3.6	Comparison of Na ₂ CO ₃ and NaOH-catalyzed carbon black at 865° C, 500 psig H ₂	43
3.7	Comparison of impregnated and physically mixed K ₂ CO ₃ on carbon black at 865° C, 500 psig H ₂ , K/ C= 0.019.	45
3.8	Comparison of impregnated and physically mixed Na ₂ CO ₃ on carbon black at 865° C, 500 psig H ₂ , Na/ C= 0.024.	46
3.9	Catalyst loss from carbon black at 725° C, 500 psig H ₂	48
3.10	Catalyst loss from carbon black at 865° C, 500 psig H ₂	49

3.11	Catalyst loss from coconut charcoal at 775° C, 500 psig H ₂	50
4.1	Effect of HNO ₃ oxidation on reactivity of fresh carbon black at 865° C, 500 psig H ₂	59
4.2	Effect of HNO ₃ oxidation on reactivity of degassed carbon black at 865° C, 500 psig H ₂	60
4.3	Effect of partial combustion at 400° C on reactivity of carbon black at 865° C, 500 psig H ₂ (from Zoheidi [16]).	61
4.4	Change in the O(1s) peak of carbon black with temperature.	65
4.5	C(1s) peak and curve fit components of untreated carbon black.	67
4.6	Initial rate versus initial surface oxygen content for carbon black.	70
4.7	Effect of HNO ₃ oxidation on reactivity of uncatalyzed coconut charcoal at 865° C, 500 psig H ₂	72
4.8	Initial rate versus initial surface oxygen for coconut charcoal.	75
5.1	Effect of HNO ₃ oxidation on reactivity of K ₂ CO ₃ -catalyzed carbon black at 865° C, 500 psig H ₂ , K/C= 0.02.	81
5.2	Effect of HNO ₃ oxidation on reactivity of Na ₂ CO ₃ -catalyzed carbon black at 865° C, 500 psig H ₂ , Na/C= 0.02.	82
5.3	Effect of HNO ₃ oxidation on reactivity of K ₂ CO ₃ -catalyzed coconut charcoal at 775° C, 500 psig H ₂ , K/C= 0.02.	84
5.4	Effect of HNO ₃ oxidation on reactivity of Na ₂ CO ₃ -catalyzed coconut charcoal at 775° C, 500 psig H ₂ , Na/C= 0.02.	85
5.5	C(1s) peak of K ₂ CO ₃ standard heated to 200° C.	87
5.6	O(1s) peak of K ₂ CO ₃ standard heated to 200° C.	88
5.7	K(2p) peak of K ₂ CO ₃ standard heated to 200° C.	89
5.8	S(2p) peak of untreated K ₂ CO ₃ -impregnated carbon black.	91

5.9	S(2p) peak of K_2CO_3 -impregnated carbon black after exposure to H_2 at $800^\circ C$, 1 atm.	92
5.10	C(1s) peak of K_2CO_3 -impregnated carbon black exposed to H_2 at $800^\circ C$, 1 atm.	95
A.1	Specific rate versus conversion for Li_2CO_3 -catalyzed carbon black at $725^\circ C$, 500 psig H_2	112
A.2	Specific rate versus conversion for low Li_2CO_3 loadings on carbon black at $865^\circ C$, 500 psig H_2	113
A.3	Specific rate versus conversion for high Li_2CO_3 loadings on carbon black at $865^\circ C$, 500 psig H_2	114
A.4	Specific rate versus conversion for low Na_2CO_3 loadings on carbon black at $725^\circ C$, 500 psig H_2	115
A.5	Specific rate versus conversion for high Na_2CO_3 loadings on carbon black at $725^\circ C$, 500 psig H_2	116
A.6	Specific rate versus conversion for Na_2CO_3 -catalyzed carbon black at $865^\circ C$, 500 psig H_2	117
A.7	Specific rate versus conversion for low K_2CO_3 loadings on carbon black at $725^\circ C$, 500 psig H_2	118
A.8	Specific rate versus conversion for high K_2CO_3 loadings on carbon black at $725^\circ C$, 500 psig H_2	119
A.9	Specific rate versus conversion for low Cs_2CO_3 loadings on carbon black at $725^\circ C$, 500 psig H_2	120
A.10	Specific rate versus conversion for high Cs_2CO_3 loadings on carbon black at $725^\circ C$, 500 psig H_2	121
A.11	Specific rate versus conversion for Cs_2CO_3 -catalyzed carbon black at $865^\circ C$, 500 psig H_2	122
B.1	O(1s) peak of untreated carbon black.	124
B.2	O(1s) peak of carbon black heated to $200^\circ C$	125

B.3	O(1s) peak of carbon black heated to 400° C.	126
B.4	O(1s) peak of carbon black heated to 600° C.	127
B.5	O(1s) peak of carbon black heated to 1000° C.	128
B.6	O(1s) peak of HNO ₃ oxidized carbon black.	129
B.7	O(1s) peak of carbon black; HNO ₃ oxidized, heated to 200° C.	130
B.8	O(1s) peak of carbon black; HNO ₃ oxidized, heated to 400° C.	131
B.9	O(1s) peak of carbon black; HNO ₃ oxidized, heated to 600° C.	132
B.10	O(1s) peak of carbon black; HNO ₃ oxidized, exposed to H ₂ at 750° C, 1 atm.	133
B.11	O(1s) peak of carbon black; degassed, HNO ₃ oxidized, heated to 200° C.	134
B.12	O(1s) peak of carbon black; degassed, HNO ₃ oxidized, heated to 400° C.	135
B.13	O(1s) peak of carbon black O ₂ oxidized at 400° C.	136
B.14	O(1s) peak of carbon black; O ₂ oxidized at 400° C, heated to 600° C.	137
B.15	O(1s) peak of untreated K ₂ CO ₃ -impregnated carbon black.	138
B.16	O(1s) peak of K ₂ CO ₃ -impregnated carbon black heated to 200° C.	139
B.17	O(1s) peak of K ₂ CO ₃ -impregnated carbon black heated to 500° C.	140
B.18	O(1s) peak of K ₂ CO ₃ -impregnated carbon black heated to 750° C.	141
B.19	O(1s) peak of K ₂ CO ₃ -impregnated carbon black exposed to H ₂ at 750° C, 1 atm.	142

B.20	O(1s) peak of K_2CO_3 -impregnated carbon black exposed to H_2 at 800° C, 1 atm.	143
B.21	O(1s) peak of K_2CO_3 -impregnated carbon black 10% gasified, reheated to 200° C.	144

Chapter 1

Introduction and Background

1.1 Introduction

The eventual depletion of domestic natural gas reserves necessitates the development of alternative sources to replace this inexpensive and clean fuel. In the U.S., one logical and potentially plentiful alternative fuel source is substitute natural gas (SNG) produced by gasification of coal, of which the U.S. has abundant reserves. It has long been known that various materials catalyze gasification reactions, including transition metals [1] and alkali salts of weak acids [2]. Transition metal catalysts are the most effective, but are expensive and easily poisoned by sulfur, leading to the choice of alkali salts as the preferred catalysts. In terms of balancing cost with catalytic activity, potassium salts provide the best compromise.

An example of a typical process utilizing alkali catalysts for coal gasification is the Exxon process [3]. Steam is used to gasify the coal and produce synthesis gas via the reaction



In addition, Exxon found that the catalyst enabled the gasifier to be operated at low enough temperatures such that methane formation was also favored and catalyzed via the subsequent reaction



Alternatively, hydrogen can react directly with carbon to form methane



Reaction 1-1 is endothermic, while Reactions 1-2 and 1-3 are exothermic. Overall, conditions in the gasifier are essentially thermoneutral. In the Exxon process, methane is the desired product, and the unreacted synthesis gas is separated and recycled back to the gasifier.

Optimization of the gasification reactor involves finding conditions which maximize methane production, and hydrogen plays a role in several ways. First, hydrogen strongly inhibits the steam gasification reaction, and knowledge of the mechanism of inhibition is necessary in order to minimize its effect. Secondly, enhancing the rate of hydrogen gasification (Reaction 1-3) directly increases methane production in the gasifier and provides a source of heat for the strongly endothermic steam gasification reaction.

In addition to its role in the steam gasification process, hydrogen gasification is a direct, exothermic route to the production of SNG in one step with very few byproducts. This potential route to SNG, in addition to the role

Reaction 1-3 plays in other gasification processes, provides the motivation for specifically studying the hydrogen gasification reaction.

Finally, studying the hydrogen gasification reaction will aid in understanding the processes occurring in other reactant gases. Oxygen appears to play an important role in both catalyzed and uncatalyzed gasification, and the use of pure hydrogen as a reactant gas provides a unique environment for studying the role of oxygen initially present in or added to the carbon, and for studying the interaction of the catalyst with the carbon and/or oxygen groups on the surface of the carbon.

1.2 Background

1.2.1 Steam and Carbon Dioxide Gasification

The majority of gasification research has traditionally focused on the use of steam or carbon dioxide as reactant gases, and much progress has been made over the last 15 years in clarifying the mechanisms of both the catalyzed and uncatalyzed reactions. The most recent review of the various proposed catalytic mechanisms is by Moulijn and Kapteijn [4]. Many of these results are worth discussing in some detail, since they may have important implications for the hydrogen gasification reaction as well.

1.2.1.1 Uncatalyzed Gasification

For uncatalyzed gasification, the major results from steam and carbon dioxide gasification which may also be relevant to hydrogen gasification involve the presence of oxygen groups on the surface of carbon and their involvement in the reaction mechanism. It has long been known that the presence of oxygen

species on the surface of carbon black [5] and carbon fibers [6] greatly enhances the surface properties of these materials for many applications, and that various treatment procedures are able to increase the concentration of these oxygen species [7-10]. Much work has also been done to identify the chemical forms of these groups [8-15], which can generally be categorized as acidic, basic, neutral, or inert [11]. Carboxyl, phenol, and lactone groups have been proposed [12] as acidic complexes. They are formed by oxidation at temperatures around 400° C and decompose to give CO₂ above 500° C. Carbonyl and quinone groups are neutral or weakly acidic and decompose to CO around 750° C [15]. Basic surface groups include chromene or pyrone complexes and can persist on the surface at temperatures above 1000° C [13]. Aromatic ethers are generally inert and are postulated to make up the majority of surface oxygen [5]. An in-depth review of the characterization of oxygen groups on carbon is given by Zoheidi [16] and will not be duplicated here. Only recently have oxygen groups been recognized for their important role in the gasification mechanism itself.

In oxidizing environments such as steam or carbon dioxide, the reactant gas is thought to dissociatively adsorb at an active site, forming the surface oxygen species which then desorb to produce carbon monoxide and nascent active sites [17]. For steam gasification, a plausible mechanism can be written as

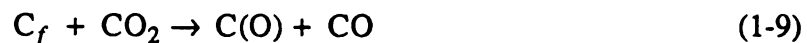


Reaction 1-7 describes inhibition by dissociative hydrogen adsorption at active sites. At high pressures, non-dissociative hydrogen adsorption would be expected to dominate.



This reaction describes the likely first step in the hydrogen gasification process. From a thermodynamic viewpoint, dissociative adsorption would be expected to be more significant at lower hydrogen pressures such as are found in steam gasification. Giberson and Walker [18] concluded from kinetic measurements that dissociative hydrogen adsorption is the primary mode of inhibition of the steam gasification reaction.

For carbon dioxide gasification, a similar oxygen transfer mechanism can be written:



In both steam and carbon dioxide gasification, desorption of the C(O) complexes is thought to be the rate-limiting step.

This leads to the question of whether increasing the concentration of surface oxygen complexes by pretreatment of the carbon can enhance the gasification rate. Keleman and Freund [19] found that the ability of CO₂ and O₂ to undergo dissociative chemisorption depended on the extent of prior oxidation of a glassy carbon by HNO₃. In other words, HNO₃ oxidation increased the active surface area (ASA) of the carbon.

Since desorption of oxygen complexes from the surface of the carbon appears to control the kinetics of steam and carbon dioxide gasification, efforts have also been underway to identify the chemical form of these active species. Keleman and Freund [20] used Auger electron spectroscopy (AES) to study the adsorption step of reactant gases on a glassy carbon. They concluded that carbonyl groups are the primary intermediates on the surface of the carbon. Marchon, *et. al.* [15] used x-ray photoelectron spectroscopy (XPS) and temperature-programmed desorption (TPD) to conclude that on graphite, lactone and semi-quinone groups are the primary participants in the uncatalyzed reaction with any oxygen-containing molecule.

1.2.1.2 Catalyzed Gasification

Recent studies of alkali-catalyzed steam and carbon dioxide gasification have attempted to provide a better understanding of how the catalyst interacts with the carbon and the reactant gas, and to determine the chemical form of the catalyst in its active state. Early postulated mechanisms of catalytic activity include electron transfer [21] and oxidation-reduction [22] cycles of the catalyst, as well as the possibility of intercalation of free metal into the carbon matrix [23]. Intercalation compounds have since been shown to be unstable under reaction conditions [24,25]. It has been shown many times that the active form of the catalyst is not bulk carbonate, and that the catalyst interacts strongly with the carbon before it becomes active. The primary evidence for this interaction is the release of large quantities of CO and CO₂, and the disappearance of the carbonate peak in the x-ray diffraction pattern under reaction conditions.

Identification of the active form of the catalyst took a large step forward when Mims and Pabst [26] used surface methylation of catalytically gasified carbon to show that the catalyst is present in the form of C-O-K groups under

reaction conditions. Since then, most results have supported the presence of these groups, or the results have at least been interpreted with the assumption that these groups exist.

One of the most effective methods in determining the reactions occurring in the presence of alkali catalysts has been the use of temperature-programmed reaction (TPR) of isotopically labelled catalysts and/or reactant gases. Saber, *et al.* [27-29] showed that K_2CO_3 interacts strongly with the carbon and/or surface oxygen groups on the carbon and decomposes between 500 and 1000 K to form surface complexes. Once formed, these surface complexes participate in carbon and oxygen exchange with the gas phase, and oxygen in these complexes also exchanges with oxygen initially on the carbon surface. Catalytic gasification does not occur until a significant number of these surface groups decompose further at higher temperatures, releasing CO_2 . It was proposed [27] that once decomposed to its active form, the catalyst undergoes a redox cycle between elemental potassium bound to the carbon and the C-O-K groups proposed by Mims and Pabst.



The free potassium can also be vaporized, accounting for the catalyst loss observed by most investigators.



The rate of catalyst loss was found to depend on the initial surface oxygen

content of the carbon, suggesting that oxygen stabilizes the catalyst. Differences in activity between K_2CO_3 and Na_2CO_3 were explained by a much weaker interaction between Na_2CO_3 and the carbon, as evidenced by lower exchange rates and higher temperatures required for complete decomposition of the carbonate.

Cerfontain, *et al.* [30] concluded that the catalyst is present in three forms: the alkali phenolates proposed by Mims and Pabst, alkali oxide clusters containing chemisorbed CO_2 which are anchored by the phenolates, and bulk carbonate which is inactive. At low catalyst loadings, the majority of the catalyst would tend to be in the phenolate form. Low temperature exchange reactions were also seen [30,31]. The actual gasification intermediate was proposed to be a C-O group on the surface of the carbon. The catalyst can thus be viewed as increasing the number of gasification sites rather than altering the mechanism or reducing the activation energy. Differences between Na_2CO_3 and the higher molecular weight alkali metal carbonates were explained by the tendency for Na_2CO_3 to either remain in or return to the carbonate form and agglomerate, as opposed to remaining highly dispersed.

Mims and Pabst [32] postulated that the surface phenoxides associated with the catalyst are the gasification intermediates. The surface phenoxides are reversibly oxidized to phenoxy radicals, which decompose to give CO. The remainder of the catalyst is in a basic salt phase viewed as an electrolyte acting to stabilize the surface phenoxide groups. Again, differences in dispersion were seen as the main difference between Na_2CO_3 and the other alkali carbonates.

Other analytical tools which have provided insight into catalyzed gasification are surface sensitive techniques such as AES, XPS, and ultraviolet photoemission spectroscopy (UPS) in conjunction with TPR. Keleman, *et al.* [33] used XPS and UPS to show that KOH forms stable potassium-oxygen

species on preoxidized glassy carbon and graphite edge surfaces. They report O(1s) peaks at 531 and 535 eV. The 531 eV peak disappears upon heating from 500 to 950° C and is thus assigned to a K-O-C structure. The peak at 533 eV remains at 950° C and is assigned to strongly bound oxygen. Potassium hydroxide also interacts with clean graphite edge surfaces, but the groups are much less stable. The UPS results of the valence band spectrum confirm that the active species do not involve bulk KOH, K₂O, or K₂CO₃.

Keleman and Freund [34] also showed that catalyzed carbon surfaces are much more active for CO₂ adsorption and dissociation, thus increasing the active site density and gasification rate. The uncatalyzed surface, on the other hand, contained strongly bound oxygen after exposure to CO₂. They postulated that the surface C-O-K groups modify the surface electronic properties of the carbon, as seen by a decrease in the work function measured by UPS. They attributed this effect to partial charge donation to the carbon surface.

While the details may vary somewhat, the results presented in this section provide a much clearer picture of the steps involved in catalyzed gasification. The major points of agreement which may have direct implications for hydrogen gasification are: 1) The catalyst interacts strongly with the carbon surface, forming stable groups distinct from bulk alkali carbonate or oxide species. 2) These groups are apparently stabilized to a greater extent by oxygen groups already present on the surface of the carbon. 3) The function of the catalyst is most likely to increase the number of active sites on the carbon, rather than to alter the mechanism or reduce the activation energy. 4) Sodium carbonate has a much weaker interaction with the carbon surface, and tends to agglomerate and remain in the inactive carbonate form.

1.2.2 Hydrogen Gasification

Much less work has been focused on the hydrogen gasification reaction, especially for the catalyzed reaction. The reaction is both thermodynamically and kinetically much less favorable than the reactions with either steam or carbon dioxide. Recently, however, the reaction has received renewed attention because of the important role hydrogen plays in the inhibition of the steam gasification reaction.

1.2.2.1 Uncatalyzed Hydrogen Gasification

The uncatalyzed hydrogen gasification reaction has been studied in significant detail. Both the reaction equilibrium [35] and hydrogen chemisorption characteristics on carbon [36,37] have been investigated; hydrogen strongly bonds to carbon and is removed completely only at temperatures above 1400° C. As mentioned earlier, adsorption can occur dissociatively or non-dissociatively, depending on conditions. Kinetics of the reaction have been studied by Blackwood [38-40], Cao and Back [41], and Zielke and Gorin [42] for several carbons and chars. They report a Langmuir-Hinshelwood expression at high pressure which reduces to first order in hydrogen at lower pressures far from equilibrium. Other hydrogen gasification studies have been reported for coal-based carbons [43-46] and graphite [47-49]. A mechanism involving stepwise formation of CH, CH₂, CH₃, and CH₄ on the carbon surface has been postulated [41,42] and is consistent with kinetic results. The possibility of some reactions occurring in the gas phase has also not been ruled out. Another possibility consistent with kinetic results is two-step hydrogenation to form CH₂ and then CH₄ [40]. This mechanism is also more consistent with the postulate that non-dissociative hydrogen adsorption leads to gasification, while dissociative adsorption leads to inhibition.

Some of the differences between gasification in hydrogen compared to steam or CO_2 may be due to differences in the preferred orientation of edge sites formed as gasification proceeds. Yang and Duan [50] analyzed etch pits formed in hydrogen and oxygen and found that hydrogen produces hexagonal basal plane edges, while oxygen produces arm-chair edges. In addition, hydrogen gasification of graphite is extremely slow and is not catalyzed by alkali carbonates [16,51].

Of particular interest to this work are the relationships observed between the presence of oxygen and the rate of methane formation. Cao and Back [52] showed that the addition of 0.1% oxygen to the hydrogen reactant gas increases the rate of methane evolution by an order of magnitude over that of pure hydrogen. Blackwood [38] found that the rate of hydrogen gasification is strongly dependent on the oxygen content of the reacting wood char. He postulated that some of the oxygen-containing groups such as pyrone/chromene groups are lost upon heating and cannot be regenerated upon exposure to molecular oxygen. Mühlen, *et al.* [46] found that the hydrogen gasification rate of a coal char was strongly dependent on the temperature and pressure of the initial coal pyrolysis, suggesting that removal of oxygen and annealing of active sites results in reduced hydrogen gasification rates. Otake and Jenkins [14] showed that methane evolution could be directly correlated to the desorption of oxygen complexes evolved as CO.

Finally, Zoheidi [16] showed that heat treatment at 1000°C reduces the reactivity of carbon black significantly, and that partial combustion at 400°C enhances the reactivity of both fresh and degassed carbon black by fixing acidic oxygen groups on the surface. He postulated that oxygen groups on the surface of the carbon desorb and form nascent active sites similar to those believed to be involved in steam and CO_2 gasification. Treatment at 1000°C removes the

oxygen groups and then thermally anneals the active sites, greatly reducing the reactivity of the carbon. Gasified and degassed samples were found to contain a predominance of basic groups. These groups were postulated to be responsible for the low residual activity of degassed and gasified carbons.

1.2.2.2 Catalyzed Hydrogen Gasification

Relatively little work has been done regarding alkali-catalyzed hydrogen gasification compared to steam or CO₂ gasification. Gardner, *et al.* [53] showed that K₂CO₃ effectively catalyzes hydrogen gasification of coal char, and Walker, *et al.* [54] report enhanced methane formation in the presence of the carbonate. Kokorotsikos, *et al.* [55] report lignite gasification rates as a function of K₂CO₃ impregnation conditions, and Cypres, *et al.* [56] studied the effect of loading for several alkali salts in hydrogen gasification of coal.

As in the case of uncatalyzed hydrogen gasification, studies demonstrating the importance of surface oxygen on catalyst effectiveness are of primary interest in relation to this work. Mims and Krajewski [57] showed using TPD of isotopically labelled species that for a mixture of H₂O, CO₂, CO, and H₂ over K₂CO₃-catalyzed carbon, the dominant mode of methane formation is by direct hydrogenation of the carbon substrate. Gas phase methanation reactions are only favored under conditions where carbon deposition from CO and CO₂ is expected. They also found that the reactivity in pure hydrogen decreased rapidly, but was recovered upon exposure to an H₂/H₂O mixture, wherein C(O) groups are reestablished on the surface. They postulated that catalyzed hydrogen gasification activity is associated in some way with surface oxygen, possibly the same carbanionic sites induced by the surface salt groups of the catalyst postulated to be the active sites in steam and CO₂ gasification. These sites could

either activate hydrogen for further reaction with other surface groups, or be the carbon atoms which are hydrogenated.

Zoheidi [16] showed that catalyst loss and catalytic activity depend to some extent on the pretreatment of the carbon, although catalyst loss is always significant. He postulated that the catalyst interacts with the carbon and oxygen groups on the surface of the carbon to form species with varying degrees of activity and stability. Partial combustion at 400° C, which fixes acidic groups on the surface, was found to reduce catalyst loss but not enhance the reaction rate. Partial combustion at 800° C fixes basic groups on the surface and was found to enhance the catalyzed reaction rate.

Significant differences between catalyzed and uncatalyzed hydrogen gasification were also noted by Zoheidi. While the specific rate decreases rapidly with conversion for uncatalyzed carbon black, the rate with ten weight percent K_2CO_3 ($K/C = 0.02$) remains approximately constant. The effect can be seen by comparison of Figures 4.1 and 5.1, for example. This difference suggests that active sites are irreversibly lost in the uncatalyzed case, whereas the presence of a catalyst provides a stabilized source of active sites.

1.3 Objectives and Rationale

The findings of many of the investigators summarized in this chapter have helped to clarify the role oxygen plays in catalyzed and uncatalyzed steam and carbon dioxide gasification. Understanding of the role oxygen plays in hydrogen gasification, however, is much less complete, although it certainly appears to have a significant effect on the reaction. Since enhancement of the hydrogen gasification rate is important for the variety of reasons set forth in the

Introduction, the objectives of this work are aimed at achieving a better understanding of the hydrogen gasification reaction in general, and the effect of oxygen in catalyzed and uncatalyzed hydrogen gasification in particular. The global objective of this work is to enhance the formation of methane from coal, thus making hydrogen gasification a more attractive process for satisfying world energy needs.

1.3.1 Uncatalyzed Hydrogen Gasification

The role of oxygen in uncatalyzed hydrogen gasification will be investigated by determining the relationship between the surface oxygen content of a carbon and its reactivity in hydrogen. The surface oxygen content of carbon following reaction and various treatments will be measured by XPS, and the results will be correlated to the kinetic results obtained from gasification experiments. X-ray photoelectron spectroscopy has been chosen for surface analysis because it provides elemental surface compositions as well as information regarding the binding energy of core electrons. Measurement of core electron binding energies enables XPS to provide information on the nature of the species present in addition to surface compositions. The fact that XPS is performed in a vacuum permits the analysis of potentially air-sensitive samples which have been prepared in a pretreatment reactor designed for the transfer of such samples to the XPS system without exposure to air.

Nitric acid, which has been shown to be a simple and effective oxidizing agent for carbon, will be used to fix oxygen groups on the surface of untreated carbons and carbons which have been degassed at 1000° C in a vacuum. The ability of HNO₃ oxidation (which fixes both acidic and basic groups on carbon) to enhance the uncatalyzed hydrogen gasification rate will be compared to the

results obtained by Zoheidi for partial combustion in O_2 . Partial combustion can fix acidic or basic groups on the surface depending on the reaction temperature.

To determine the effect of carbon structure and composition on oxidation and gasification, two different carbons of considerably different structure and impurity content will be studied. One is a graphitic, petroleum-based carbon black with low oxygen content. The other is an amorphous, biomass-based coconut charcoal with high oxygen content.

1.3.2 Catalyzed Hydrogen Gasification

Because alkali carbonate catalysts have been shown to strongly enhance hydrogen gasification rates, the effect of catalysts on fresh, degassed, and oxidized carbons will be investigated. The first part of the study of catalyzed hydrogen gasification is aimed at achieving a better understanding of the characteristics of the alkali-catalyzed reaction in general. This will be accomplished by performing a comparative study of several alkali salts to better understand the effect of the cation, anion, catalyst loading, and catalyst dispersion on the reaction rate.

The second part of the catalyzed gasification study will focus on assessing the effectiveness of HNO_3 oxidation in enhancing the catalyzed reaction rate. Again, the results will be compared to the results of Zoheidi for partial combustion in order to better understand which oxygen groups (*i.e.* acidic or basic) are effective in enhancing the catalyzed reaction rate. The stoichiometry and nature of the active catalyst species will be studied by using XPS as a probe of the partially gasified carbon surface, as XPS can identify potassium as well as oxygen and carbon on the surface. As in the case of uncatalyzed gasification,

two different carbons will be studied to determine the role of carbon structure and composition on the effectiveness of pretreatment procedures in catalyzed hydrogen gasification.

Chapter 2

Experimental Procedures

2.1 Gasification Experiments

2.1.1 Carbon Characterization

Gasification experiments were performed with both carbon black and coconut charcoal in an attempt to distinguish effects related to carbon structure and composition. The carbon black used is Raven 16 furnace black (Cities Service Co., Columbian Chemicals). It is a graphitic carbon black with a particle size of about 65 nm. The initial surface area as measured by the nitrogen BET method is 13-20 m²/g. The surface area increases linearly with conversion to a value of 400 m²/g at 60% conversion [16]. Ultimate analysis results are given in Table 2.1. The most significant impurity in the carbon black is sulfur, at 1.5 weight percent.

The coconut charcoal is a 50-200 mesh activated coconut charcoal from Fisher Scientific. The ash content of this char is 3.7%. The ash content was reduced to 1.5% by washing in concentrated HCl at room temperature prior to use. The char has an amorphous structure and an initial BET surface area of

about 610 m²/g, which increases to about 790 m²/g at 20% conversion and then remains approximately constant, as shown in Figure 2.1. Ultimate analysis results for the acid-washed char are given in Table 2.1. The most notable differences in impurity content between the carbon black and the coconut charcoal are the negligible amount of sulfur and the much higher oxygen and ash content of the coconut charcoal.

Table 2.1. Ultimate Analysis of Carbons

Ultimate Analysis, wt. %	Carbon Black	Coconut Charcoal
Moisture	0.46	1.02
Carbon	96.92	91.82
Hydrogen	0.27	0.43
Nitrogen	0.29	1.81
Sulfur	1.54	0.06
Ash	0.31	1.48
Oxygen (diff)	0.21	3.38

2.1.2 Sample Preparation

Alkali carbonate and hydroxide catalysts were deposited on the carbons by wet impregnation unless otherwise noted. For low catalyst loadings, the concentration of catalyst in solution was such that about 2 ml of solution per gram of carbon was required. When necessary, about 1 ml of acetone per gram of carbon was also added to aid in wetting the carbon. The resulting slurry was then dried at room temperature with frequent stirring until no free moisture was visible. The sample was then dried for at least 24 hours in an oven at 120° C. After drying, the sample was ground with a mortar and pestle when necessary.

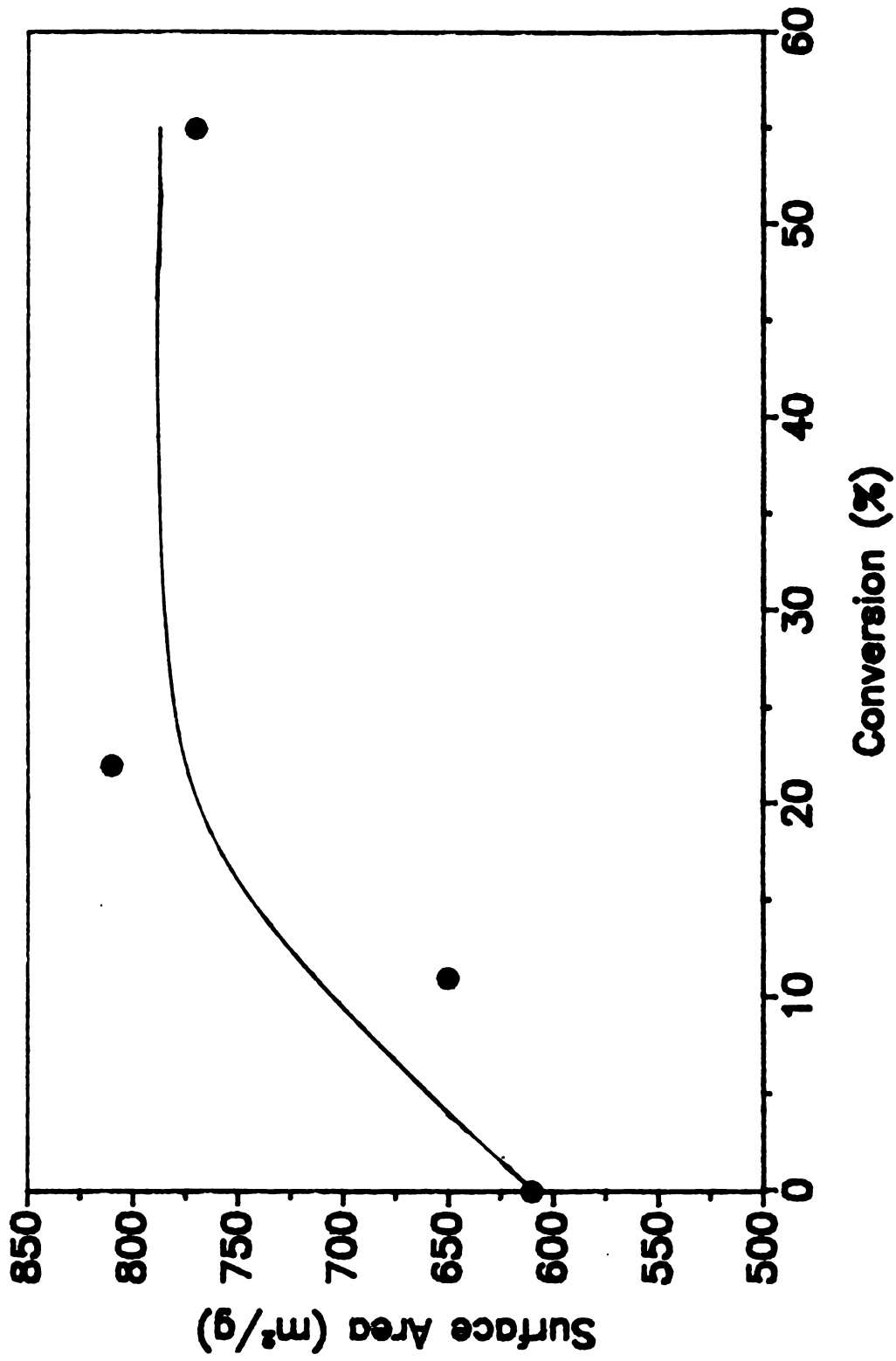


Figure 2.1. BET surface area of coconut charcoal versus conversion.

For high catalyst loadings or cases where the solubility of the catalyst was extremely low, the solution to carbon ratio was adjusted as high as necessary to dissolve the catalyst. High loadings of Li_2CO_3 were not prepared by wet impregnation because of the extremely low solubility of Li_2CO_3 in water. Even at the relatively low loading of $M/C = 0.025$, a large excess of water was required to dissolve the catalyst and impregnate it into the carbon. With such a large excess of water, it is difficult to prevent the catalyst from precipitating onto the walls of the beaker as the water evaporates. Instead of wet impregnation, the catalyst was added by thoroughly mixing the appropriate weight of Li_2CO_3 with the carbon. The validity of using this procedure instead of wet impregnation will be discussed in Chapter 3.

Oxidation with nitric acid was performed at room temperature overnight in a concentrated (70%) HNO_3 solution. The mixture was then filtered, washed thoroughly with water, and oven dried at 120°C . Degassing of carbons was accomplished by heating to 1000°C in a vacuum of approximately 0.01 torr for 15 hours.

2.1.3 Reactor System

Gasification experiments were performed in the same reactor that was designed and used by Zoheidi [16]. A schematic of the reactor system is shown in Figure 2.2. It is a fixed bed differential reactor designed for operation up to 1000°C and 1000 psi simultaneously. Reaction rates were determined by measuring the methane evolution rate by timed collection of the product gas. The amount of methane collected was then measured by gas chromatography. Products other than methane were not detected in any gasification experiments. All gasification experiments were performed in pure hydrogen (99.999%) at 500 psig and a flow rate of approximately 300 ml/min (STP). Under these

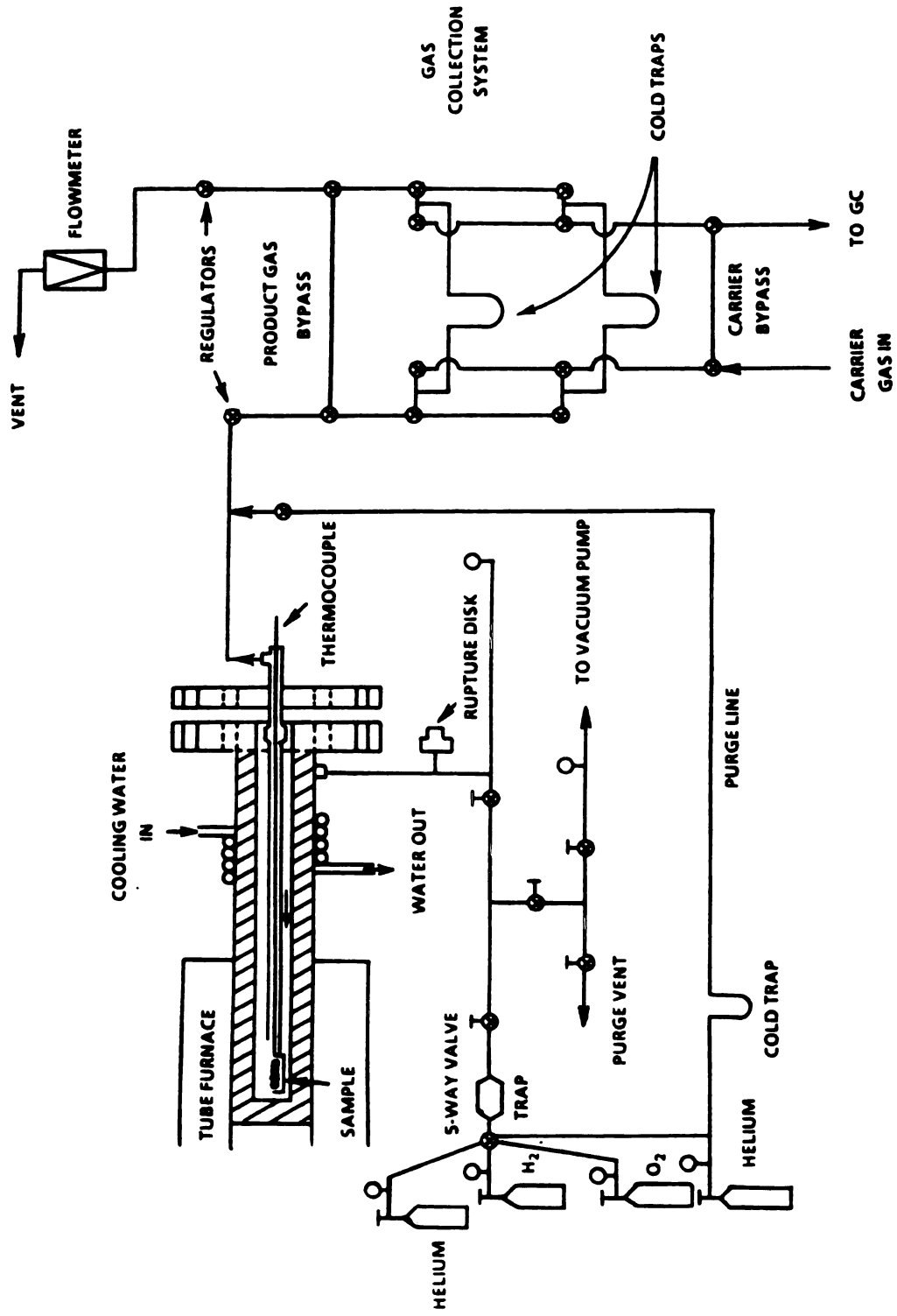


Figure 2.2. Schematic of high pressure gasification system.

conditions, Zoheidi [16] showed that for the observed carbon black reaction rates, heat and mass transfer effects are negligible in this reactor. For all experiments, the reactor was evacuated to approximately 0.01 torr during initial heatup, and the hydrogen gas flow was started as the temperature reached 500° C. Typical sample size was 40-70 mg for carbon black and 90-110 mg for coconut charcoal, due to differences in bulk density. A detailed description of the design and operation of the reactor is given by Zoheidi [16].

2.1.4 Data Analysis

The raw data from the gasification experiments were obtained in the form of reaction rate (ml CH₄/min-g) versus time. For consistency, the reaction rates were normalized so that the conversion obtained by integration of the raw data matched the conversion measured by weighing the residual sample after reaction. After normalizing, the data were transformed to reaction rate per unit total surface area (TSA) versus conversion. Ideally, the rates should be expressed per unit active surface area (ASA), but measurements of ASA have not been made for these carbons or for hydrogen gasification in general. Since the TSA of both carbon black and coconut charcoal is well characterized and depends only on conversion, the use of TSA eliminates consideration of the effects of surface area on the gasification rate.

2.1.5 Catalyst Loss Measurements

Catalyst loss measurements were performed by neutron activation analysis (NAA) on the residual samples after gasification. Following gasification, a sample containing potassium, sodium, or cesium was bombarded with a high flux of neutrons (10^{12} – 10^{13} neutrons/cm²-s) inside the TRIGA nuclear reactor located in the College of Engineering at Michigan State University. The

intensity of γ -radiation emitted by the unstable isotopes which are formed can then be compared to a set of standards that were activated at the same time. The area under the Gaussian curve of counts versus energy is assumed to be proportional to the quantity of the unstable isotope. The quantity of alkali metal remaining on the sample can thus be calculated after correcting for the loss of intensity due to the half-life of the isotope. A list of the physical parameters necessary for performing NAA is given in Table 2.2. The detection equipment is located in the Geology Department of Michigan State University, and included a GeLi detector with associated signal shaping and amplification electronics, and a Canberra multi-channel analyzer. The typical counting time necessary to obtain an adequate signal-to-noise ratio was five minutes per sample.

Table 2.2. Physical Parameters for Neutron Activation Analysis

	Sodium	Potassium	Cesium
half-life (hr)	15.0	12.4	8760
cross section (barns)	0.4	1.3	27.4
relative abundance (%)	100	1.2	100
activation time (min)	30	45	120
γ energy (MeV)	1.37	1.52	0.605

2.2 Surface Analysis of Carbons

2.2.1 Background

In order to better understand the effects of oxidation and catalysts on the reactivity of carbons, XPS was used as a probe of the carbon surface composition following various pretreatment procedures. The primary reason for

choosing XPS over other techniques is the fact that XPS provides elemental surface compositions and is performed in a vacuum. Thus, a sample can be treated in an appropriate reactor system and then be transferred to the XPS system and analyzed without exposure to air. This is especially important when studying hydrogen gasification, since the catalyst is thought to be in a highly reduced state under reaction conditions. The reason for choosing XPS over other vacuum techniques is that XPS affords the possibility of providing information not only about what elements are on the surface of the carbon, but also the chemical environment in which they exist.

The procedure for XPS involves irradiating a sample with x-rays of sufficient energy to remove core electrons from the atoms in the sample. The kinetic energy of an ejected photoelectron depends on its binding energy to the nucleus from which it was ejected. The binding energy depends on the specific element and to a lesser extent on the chemical environment of the atom. Since the escape depth of an electron is only approximately 50 Å, depending on its kinetic energy, the technique is highly surface sensitive.

2.2.2 Spectrometer Description

The XPS system used in these experiments is the Perkin-Elmer PHI 5400 ESCA system located in the Composite Materials and Structures Center at Michigan State University. The x-ray beam is a non-monochromated $Mg_{K\alpha}$ source operated at 15 kV, 300 W, and 20 mA. The detector consists of a hemispherical energy analyzer with a position sensitive detector. The electron takeoff angle was 45°, and the analyzer was operated at a pass energy of 35.75 eV, step size of 0.1 eV/step, and a sampling time of 50 ms/step. The sampling area was approximately a 1 mm circle, and typical counting times to obtain adequate

signal were 8 minutes for oxygen, potassium, and other trace elements, and 3 minutes for carbon. The system pressure during analysis was typically less than 10^{-8} torr.

2.2.3 Data Analysis

Data reduction and analysis were performed with software associated with the Perkin-Elmer system. All binding energies were referenced to a bulk C(1s) binding energy of 285 eV. Smoothing prior to curve fitting was accomplished with a 25-point smooth. Atomic concentration calculations were performed on the raw, unsmoothed data, using atomic sensitivity factors provided by Perkin-Elmer. These sensitivity factors are shown in Table 2.3, and depend on both the element and the analyzer type and configuration. Using the appropriate sensitivity factors, atomic concentrations were then calculated using the following equation:

$$C_x = \frac{I_x / S_x}{\sum (I_n / S_n)} \quad (2-1)$$

where I_x and S_x are the peak area and sensitivity factor of the element in question, and I_n and S_n are the peak areas and sensitivity factors of all elements present. Atomic concentration calculations were performed by the software except when potassium was present. In this case, a potassium x-ray satellite is located in the same position as the C(1s) peak. A satellite subtraction was therefore performed by the software before applying Equation 2-1 to the resulting peak areas.

Table 2.3. Atomic Sensitivity Factors for XPS

Element	Sensitivity Factor
C (1s)	0.296
O (1s)	0.711
K (2p)	1.466
S (2p)	0.666
Mo (3d)	3.321
Cr (2p)	2.427
W (4f)	3.523

2.2.4 Vacuum Pretreatment Reactor

As mentioned earlier, the success of performing XPS experiments on treated carbons depends on the ability to treat the sample under various environments and then transfer it to the XPS system without exposure to air. A pretreatment reactor was built with these objectives in mind, since the original gasification reactor was not capable of meeting these criteria. The new reactor has a base pressure of less than 10^{-8} torr, and is capable of reaching 1000° C at 10^{-4} torr. The reactor can also be operated at elevated temperatures in a variety of gases at pressures up to one atmosphere.

A schematic of the reactor system is shown in Figures 2.3 and 2.4. The system is pumped by a 50 l/min Balzers TPU 050 turbomolecular pump. Since the same pump is used to pump both the main chamber and the introduction chamber, two butterfly valves and a gate valve are used to isolate the two chambers. The introduction chamber can thus be brought up to atmospheric pressure and pumped back down without disturbing the main chamber. A butterfly valve and bellows valve are also used to isolate the gas introduction section from the high vacuum system.

Figure 2.3. Schematic of Vacuum Pretreatment Reactor - Top View

- a. Mechanical Pressure Gauge
- b. Bellows Valve
- c. Thermocouple Gauge
- d. Butterfly Valve
- e. Viewport
- f. Ionization Gauge
- g. Power and Thermocouple Feedthroughs (out of page)
- h. Linear Transport Arm
- i. Viewport (out of page); Turbomolecular Pump (into page)
- j. Reactor Vessel
- k. Gate Valve
- l. Bellows Valve
- m. Sample Loading Hatch
- n. Sample Introduction Attachment

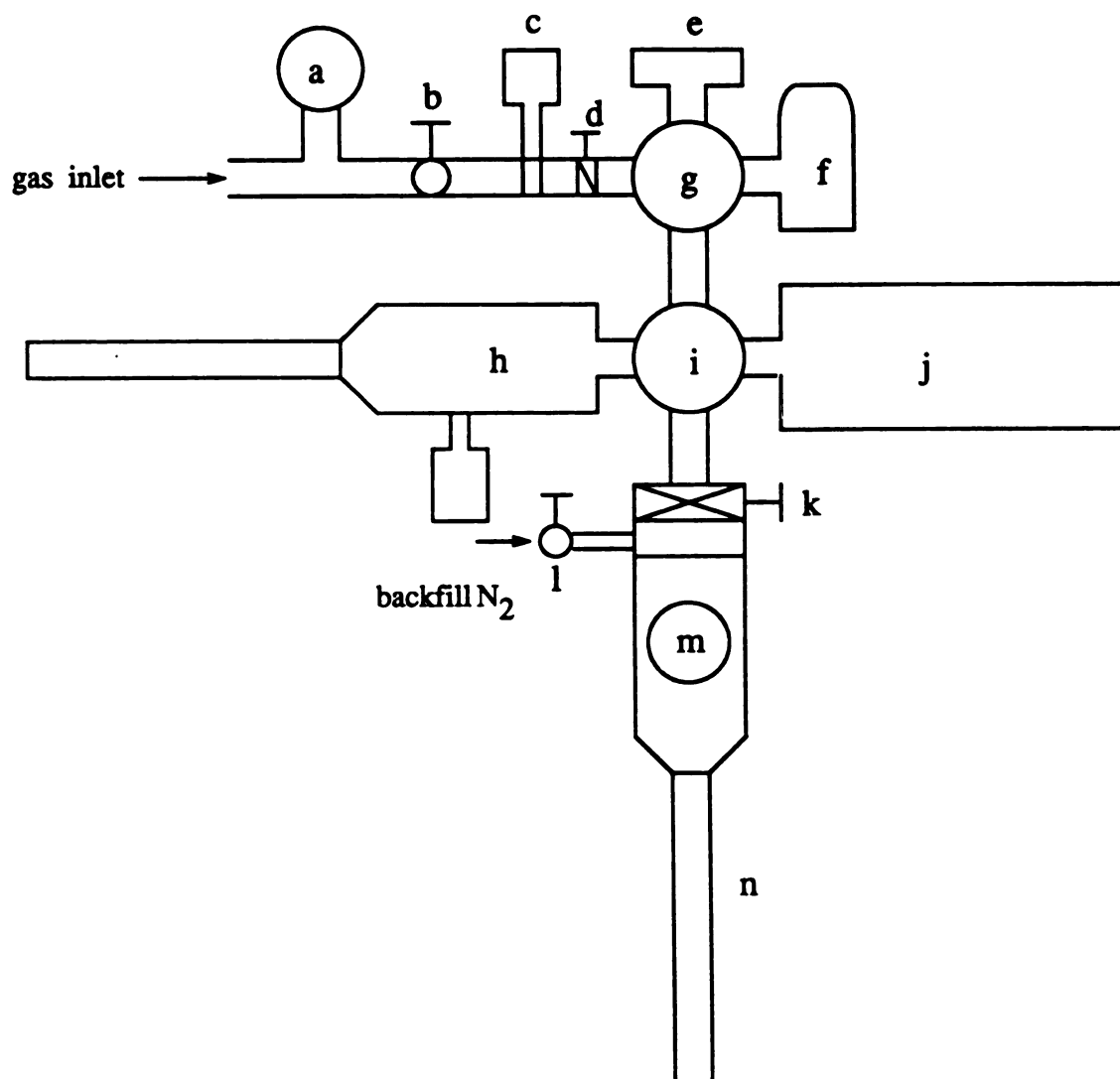


Figure 2.3. Schematic of Vacuum Pretreatment Reactor - Top View

Figure 2.4. Schematic of Vacuum Pretreatment Reactor - Side View

- a. Sample Introduction Attachment
- b. Sample Loading Hatch
- c. Gate Valve
- d. Butterfly Valve
- e. Reactor Vessel (out of page); Linear Transport Arm (into page)
- f. Viewport
- g. Butterfly Valve
- h. Ionization Gauge (out of page); Gas Inlet (into page)
- i. Viewport
- j. Power and Thermocouple Feedthroughs
- k. Turbomolecular Pump

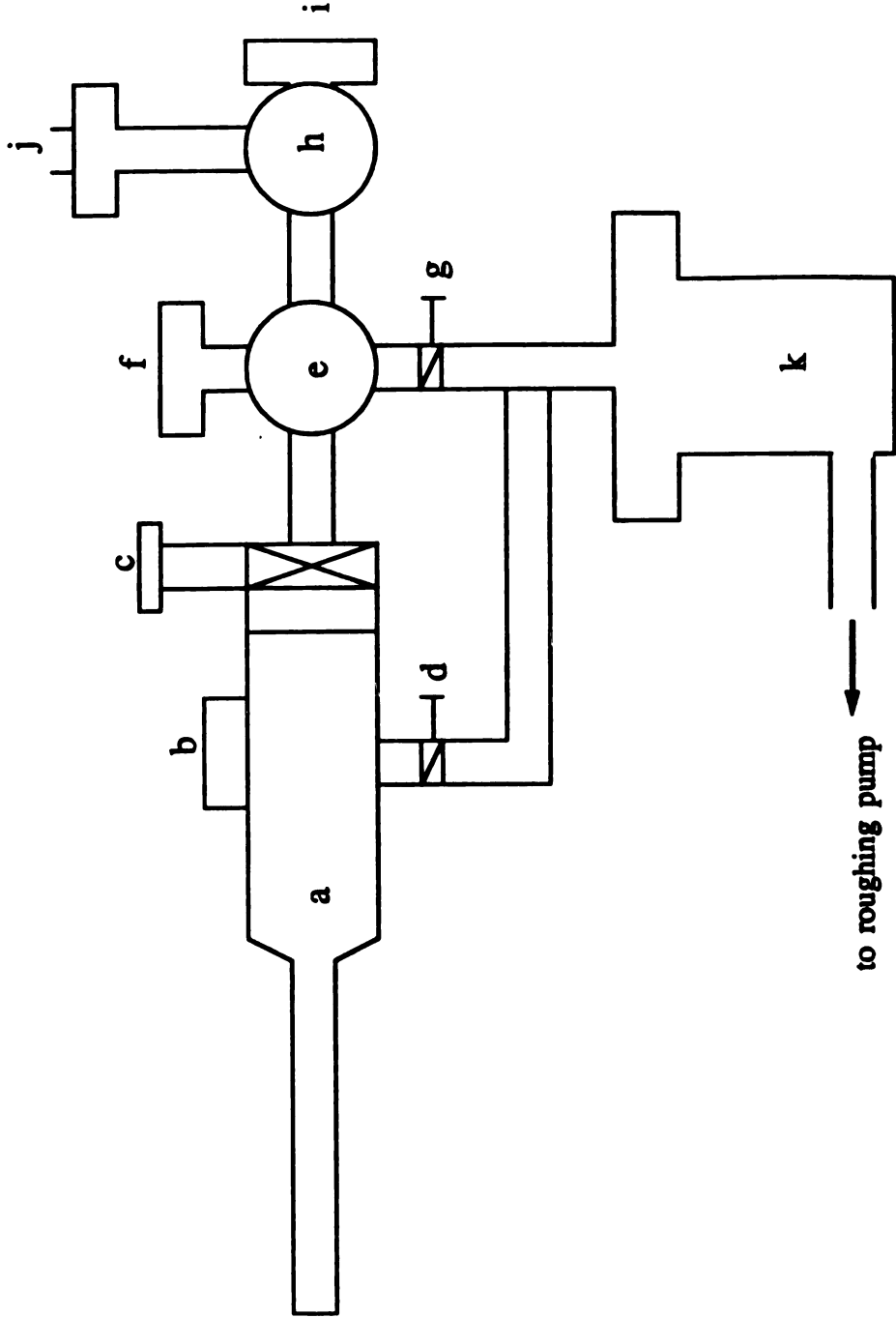


Figure 2.4. Schematic of vacuum pretreatment reactor - side view.

Three different means of pressure measurement are available, depending on the range of operating pressure desired. For high vacuum, an ionization gauge with an operating range of 10^{-8} – 10^{-3} torr is used. For low vacuum, a thermocouple gauge with a range of $\sim .01$ – 1 torr, and a mechanical gauge with a range of 0–30 inches Hg are used.

The Perkin-Elmer PHI Model 04-725 specimen introduction attachment allows for the use of a Vacuum Transfer Vessel (VTV) for transferring the sample to the XPS system without exposure to air. After being placed in the introduction attachment, the sample is carried to the intersection, where it is picked up by the Perkin-Elmer PHI Model 04-745 linear transport attachment mounted a right angles to the introduction attachment. The linear transport arm then carries the sample into the reactor vessel for treatment. Since the arm remains in the hot zone of the reactor along with the sample holder, the standard aluminum-bronze fork was replaced with a stainless steel fork that could withstand temperatures to 1000° C. After treatment, the reverse procedure is followed to bring the sample back into the introduction attachment, and finally into the VTV. The transfer procedure into the VTV and to the XPS unit can be accomplished at pressures less than 10^{-5} torr.

The reactor vessel itself is cylindrical, and consists of a 1.5 inch diameter quartz liner surrounded by two half-cylinder, 350 watt, 240 VAC, ceramic resistance heaters. The quartz liner protects the sample from direct contamination from the heaters as they outgas at high temperatures. The outer shell of the reactor, a 12 inch long, 4 inch diameter stainless steel tube, is insulated by three concentric stainless steel radiation shields, as well as axial radiation shields at each end. The radiation shields are very effective; at 1000° C and high vacuum, the outside shell remains below 200° C even after six hours.

Insulation to prevent conductive heat losses is not used, since outgassing would be difficult to eliminate in a highly porous, low thermal conductivity ceramic insulation. The maximum operating temperature of the reactor at atmospheric pressure thus depends on the maximum allowable temperature of the outer shell. In hydrogen at 750° C, the outer shell reaches a temperature of about 260° C within one hour.

Temperature is measured with a chromel-alumel thermocouple situated as close to the sample holder as practical without touching it. The thermocouple and power wires are insulated with ceramic fish-spline insulation.

Degassing was accomplished by heating the sample at a rate of approximately 4° C/min to the degassing temperature of 1000° C. The sample was held at 1000° C and 10^{-4} torr for seven hours. Degassing was originally performed for 15 hours as in the gasification reactor, but the XPS results show that little or no additional reduction in the oxygen content of carbon black was achieved. In addition, sample contamination from migration or vaporization of metals became significant at long degassing times.

The procedure for experiments where a reactant gas was used involved pumping the reactor at approximately 0.05 torr while the sample temperature was ramped at a rate of about 4° C/min until the desired temperature was reached. At that point, the reactor was isolated from the pump, and the reactant gas was let in until the desired pressure was reached. The reactant gases used in these experiments were air and hydrogen. To remove impurities, the hydrogen was passed through a silica gel cold trap immersed in liquid nitrogen prior to entering the reactor, and air was passed through a cold trap immersed in a dry ice/acetone mixture. After treatment, samples treated in air were cooled approximately 20° C, and samples treated in hydrogen were cooled approximately 250° C before evacuating the reactor. After evacuating, the

sample was partially withdrawn from the hot zone of the reactor. The sample and reactor were then allowed to cool overnight prior to transfer to the XPS system.

2.2.5 Sample Preparation

Carbon black samples were pressed into thin pellets with a hydraulic press at 20 tons in a one inch die. A pellet was then cut into smaller pieces, and one piece was placed on a flat, stainless steel sample mount. A typical sample weighed about 6 mg and was about 0.5 mm in thickness. The sample was held in place by covering it with a tungsten mask with a 3/8 inch hole in the center. The mask was held in place by two stainless steel screws. With this arrangement, the sample could be treated and analyzed by XPS without being disturbed.

A different procedure was used for coconut charcoal, since it was found that the char would not form pellets. For treatment in the reactor, the powder was placed in a recessed sample holder and covered with a 325 mesh stainless steel screen held in place by two stainless steel screws. After treatment, the sample holder was placed in the VTV and transferred to a flexible glove cabinet. The glove cabinet was then pumped down and purged with nitrogen. The sample holder was then removed from the VTV, and some of the coconut charcoal was mounted on a flat sample holder using double-sided tape. This sample holder was then placed in the VTV and was transferred to the XPS system under nitrogen.

To avoid introducing changes in the properties of the carbons due to x-ray beam damage, a new sample was prepared for each step in a treatment sequence. Kelemen and Freund [58] found that long-term exposure to the x-ray

beam reduced the amount of carboxyl groups on coal and increased the reactivity of the sample to subsequent oxidation.

Chapter 3

Comparative Study of Alkali Catalysts

The effects of the alkali metal cation, the anion, and catalyst loading on gasification activity have been studied extensively for steam and carbon dioxide gasification [24,59-61], but this topic has been relatively unexplored in the case of hydrogen gasification. Cypres, *et al.* [56] found that the effectiveness of catalysts in hydrogen gasification of coal followed the order $K_2CO_3 > Na_2CO_3 > K_2SO_4 > KCl$. They also found that KOH did not have any catalytic activity, concluding that it vaporizes at reaction temperatures. Gardner, *et al.* [53] found that $KHCO_3$ and K_2CO_3 had approximately the same activity for hydrogen gasification of coal char. Zoheidi [16] showed that for hydrogen gasification of carbon black, K_2CO_3 has significant catalytic activity, while KCl has little or no activity. To provide a more thorough understanding of the effects of the cation, anion, and catalyst loading on hydrogen gasification activity, the results of experiments with Cs_2CO_3 , K_2CO_3 , Na_2CO_3 , Li_2CO_3 , KOH, and NaOH are presented in this chapter. Rubidium carbonate was not investigated.

3.1 Catalyst Activity

The effect of initial catalyst loading on the reactivity of carbon black at 865° C and 30% conversion for the various carbonates is shown in Figure 3.1. For high loadings, the reaction rate became too high to be measured accurately at 865° C. Thus Figure 3.2 shows curves of rate at 30% conversion and 725° C versus initial loading. Because the reaction rates are extremely low at 725° C and low catalyst loadings, 30% conversion was not attained in some cases. In these cases, rate data were extrapolated from data at lower conversions. The assumption used for these extrapolations is that at low loadings, the absolute reaction rate is approximately constant with conversion. The curves of rate versus conversion from which this figure was constructed are presented in Appendix A, as is a table listing the points where an extrapolation was used. Figure 3.1 and 3.2 show clearly that catalytic activity increases gradually with the molecular weight of the cation and increases significantly with initial loading up to a saturation loading of $M/C = 0.1$. Both of these results closely match the findings for steam and carbon dioxide gasification [59,62], although there have been some discrepancies as to the effectiveness of Li_2CO_3 as a catalyst.

The specific rate versus conversion curves in Figures 3.3 and 3.4 for carbon black and coconut charcoal samples catalyzed by K_2CO_3 and Na_2CO_3 demonstrate more clearly the distinct difference in activity between the two catalysts. It also shows that the differences in activity depicted in Figures 3.1 and 3.2 depend strongly on conversion. While both catalysts initially exhibit approximately the same activity, the catalyzed reaction rate decreases with conversion in the presence of Na_2CO_3 for both carbons, while the K_2CO_3 -catalyzed rate increases or remains constant with conversion.

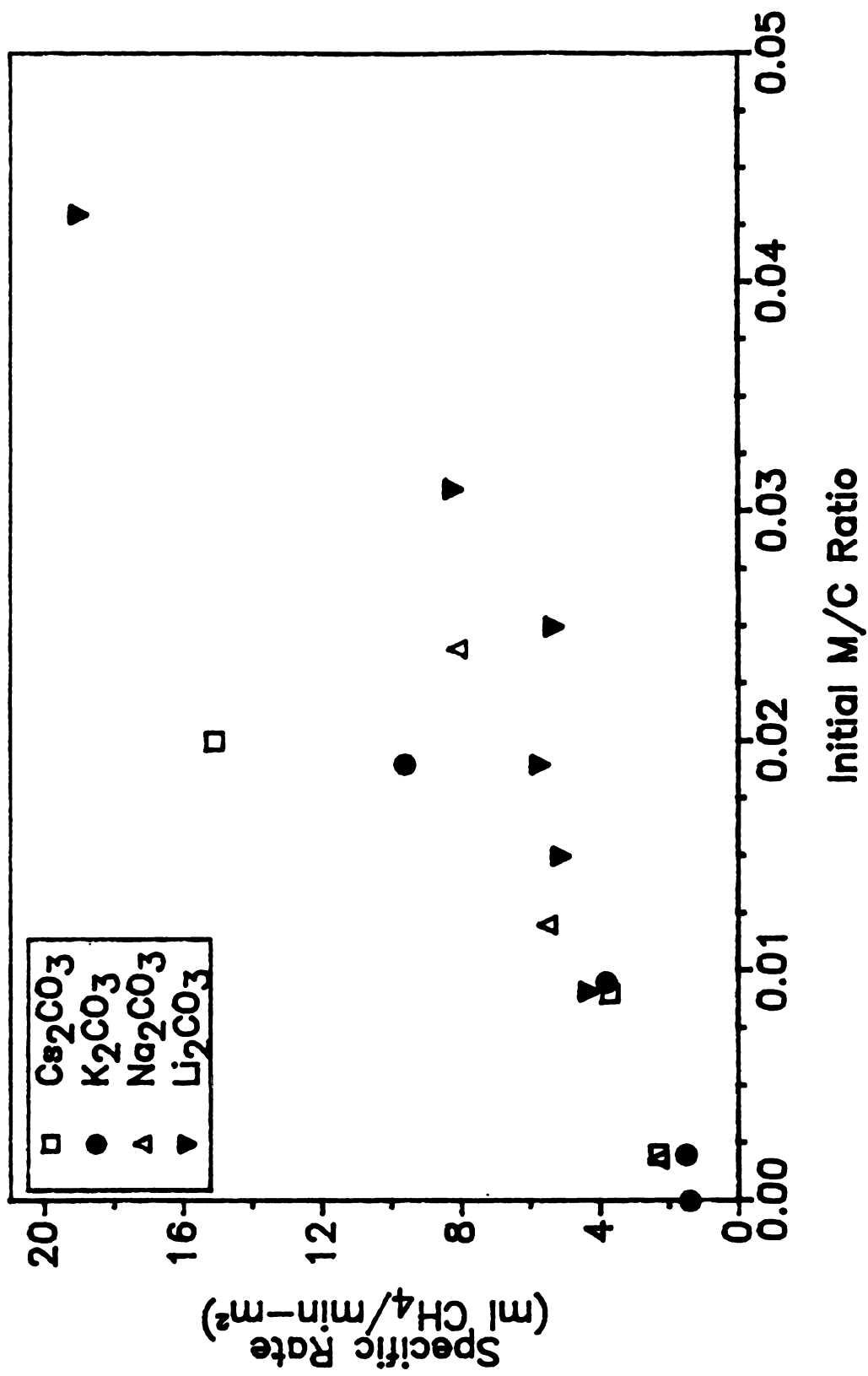


Figure 3.1. Specific rate versus catalyst loading for carbon black at 865° C, 500 psig H_2 .

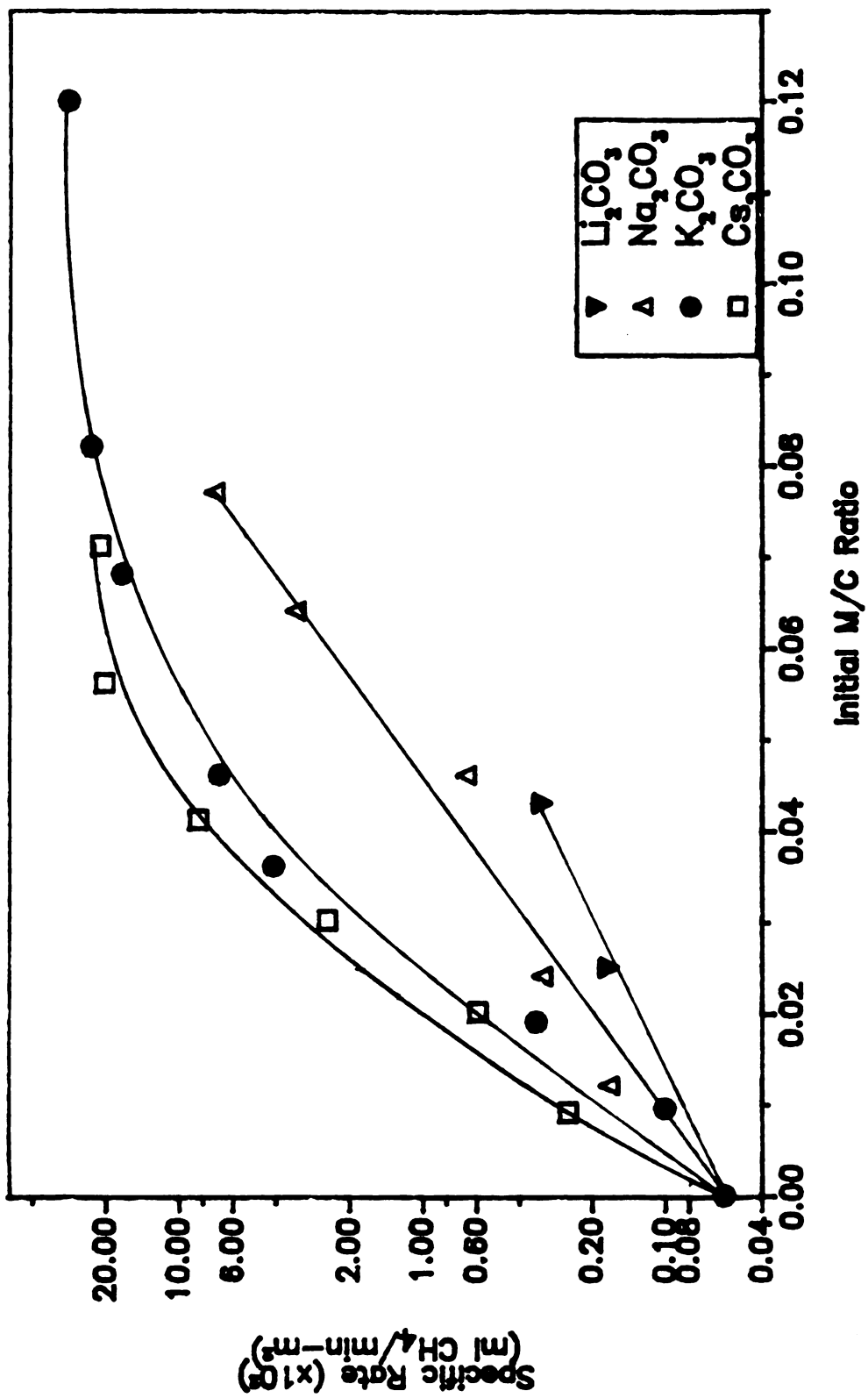


Figure 3.2. Specific rate versus catalyst loading for carbon black at 725° C, 500 psig H₂.

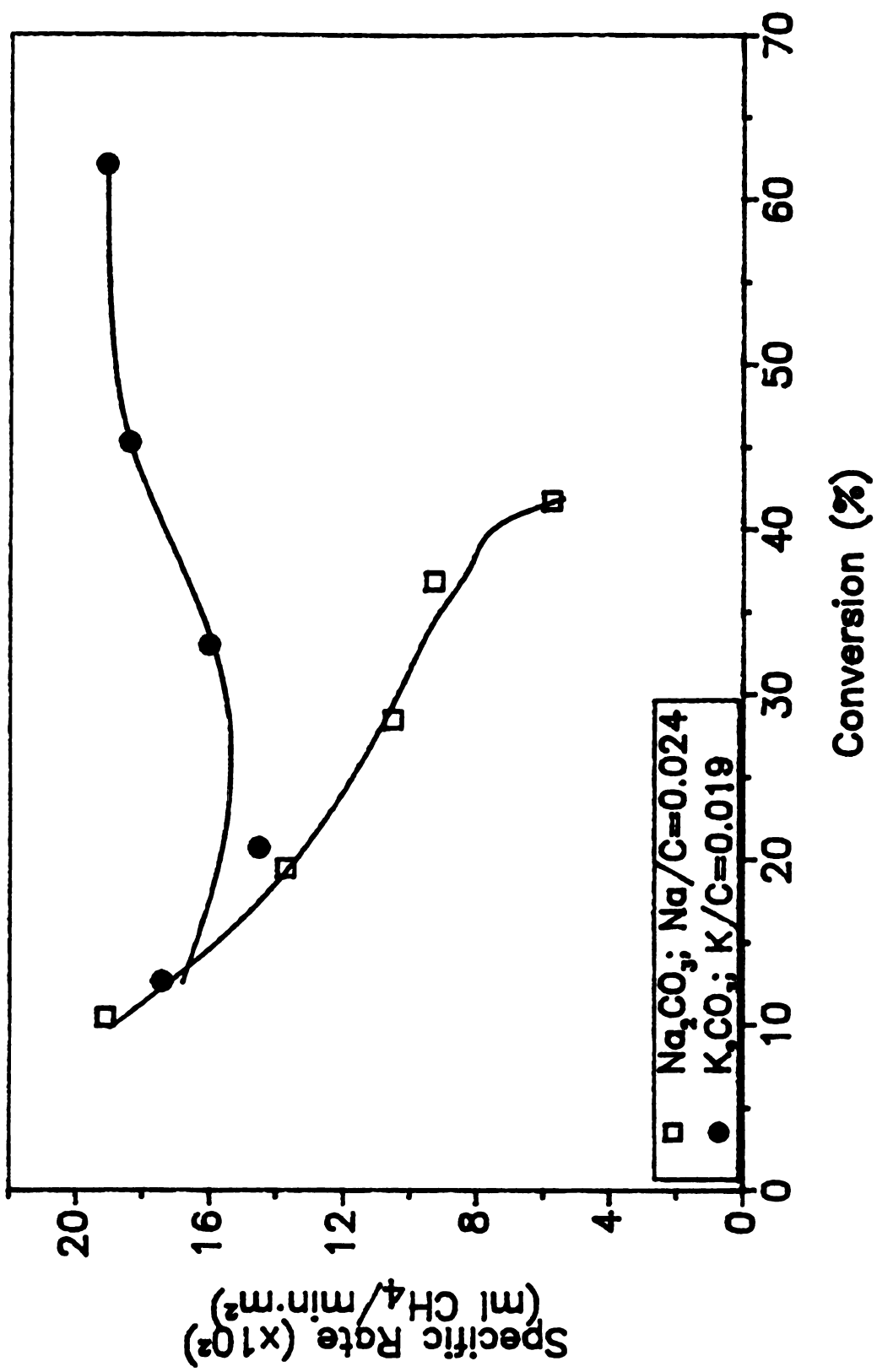


Figure 3.3. Comparison of K₂CO₃ and Na₂CO₃-catalyzed carbon black at 865° C, 500 psig H₂.

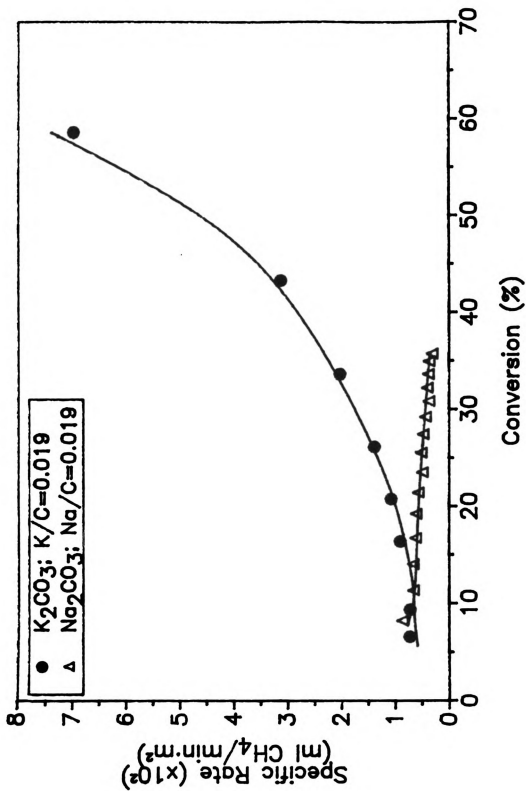


Figure 3.4. Comparison of K_2CO_3 and Na_2CO_3 -catalyzed coconut charcoal at 775°C, 500 psig H_2 .

The activity of a given alkali carbonate catalyst had a strong effect on the characteristics of the residual sample after gasification. For the most active catalysts, Cs_2CO_3 and K_2CO_3 , any visible catalyst residue on the sample holder was spread out in a thin wet film which was highly soluble in water. In some cases, the residual sample began burning upon exposure to air. The less active catalysts, on the other hand, showed visible signs of catalyst agglomeration in the form of white spots on the residual sample. For the case of Li_2CO_3 , with a melting point of 723°C , the catalyst flowed off the sample and formed a solidified pool of material on the ceramic sample holder.

3.2 Anion Effects

In addition to the alkali carbonate catalysts, KOH and NaOH were used to determine the effect of the anion on catalytic activity. Carbon black was impregnated to a loading of $M/C = 0.01$, and the gasification activity was compared to the activity of K_2CO_3 and Na_2CO_3 at the same metal/carbon ratio. Figures 3.5 and 3.6 show that the hydroxide form of the catalyst has a higher activity than the carbonate form for both potassium and sodium as the cation. Sams, *et al.* [63] concluded that K_2CO_3 and KOH had the same CO_2 gasification activity at a given loading, but that KOH was lost from the surface at a faster rate due to vaporization of bulk KOH.

One possible explanation for the observed difference in activity is that formation of the catalytically active species in hydrogen is slower for the carbonate form than for the hydroxide form of the catalyst. Zoheidi [16] showed that initial activation of the catalyst is not the limiting factor in determining the activity of K_2CO_3 . This result alone, however, does not preclude the possibility

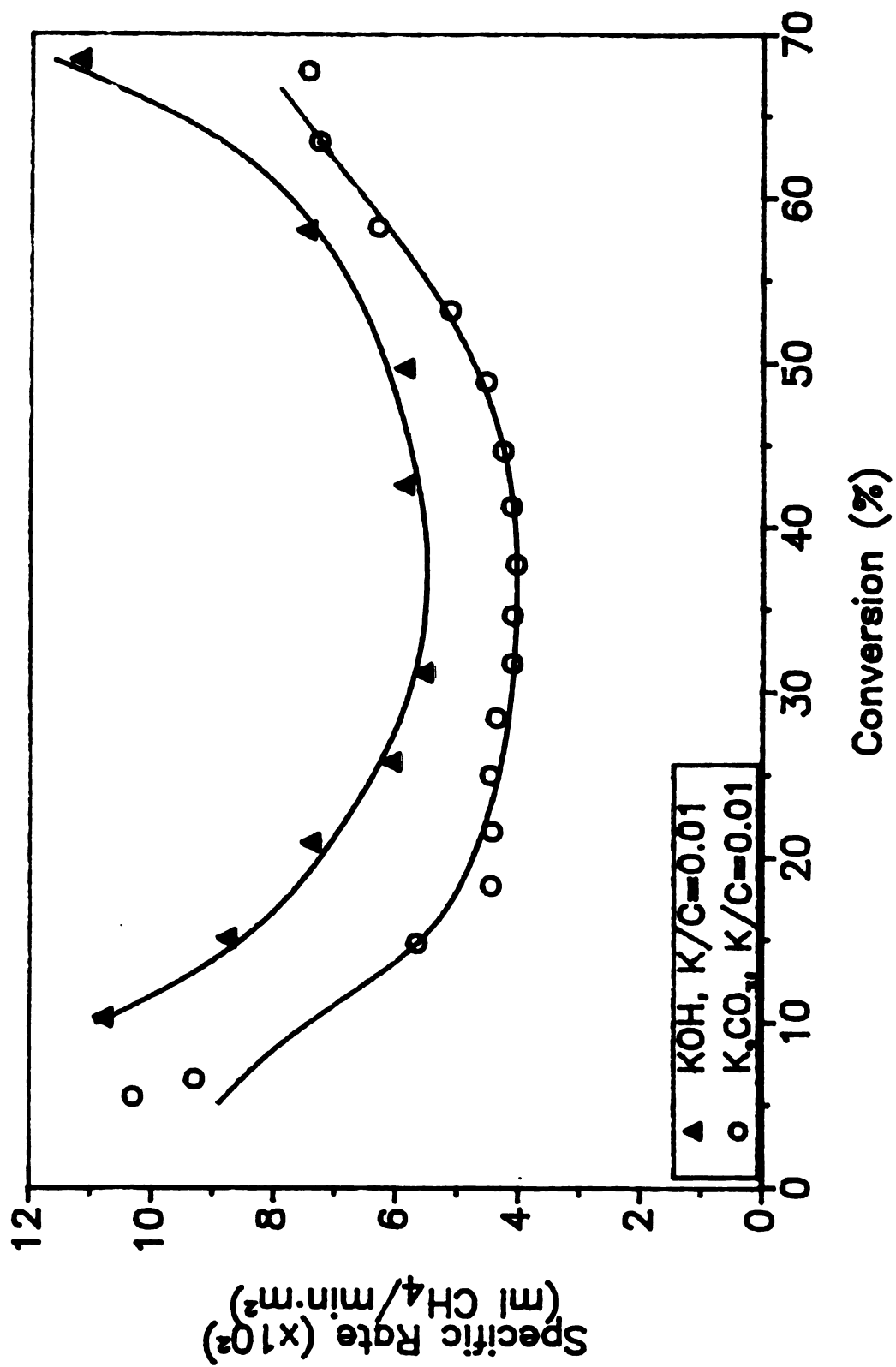


Figure 3.5. Comparison of K₂CO₃ and KOH-catalyzed carbon black at 865° C, 500 psig H₂.

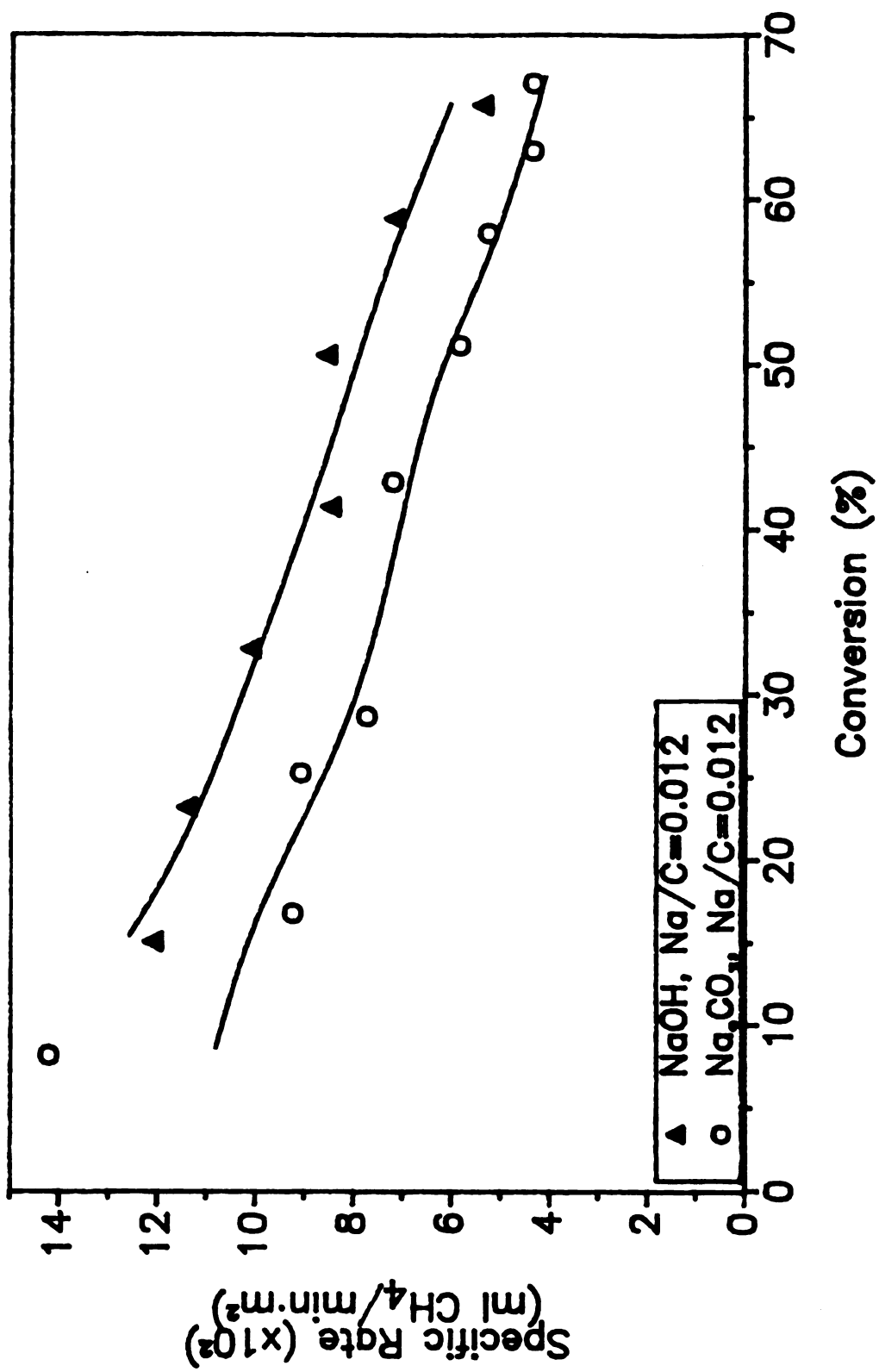


Figure 3.6. Comparison of Na₂CO₃ and NaOH-catalyzed carbon black at 865° C, 500 psig H₂.

that active site generation is faster yet for KOH. It is possible that the hydroxides simply interact more strongly with the carbon or have better dispersion characteristics than the corresponding carbonates.

3.3 Catalyst Dispersion

One of the factors which may cause some of the differences noted between the various alkali carbonate catalysts is the ability of the catalyst to achieve and maintain a highly dispersed state on the carbon surface. To test whether the method of catalyst impregnation has any effect on catalyst dispersion, gasification experiments were performed on samples where the catalyst was added by simply physically mixing with carbon black rather than by wet impregnation. This would be expected to result in substantially lower initial catalyst dispersion. Figures 3.7 and 3.8 show that for two catalysts varying considerably in activity (*i.e.* K_2CO_3 and Na_2CO_3), the reaction rate of the physically mixed sample was higher than for the impregnated sample in each case. It is not clear why this occurred, since the maximum reactivity of a physically mixed sample would be expected to be that of an impregnated sample. The most likely explanation is experimental error in matching the actual catalyst loading of the physically mixed sample to that of the impregnated sample. Another possibility is that locally high concentrations of catalyst in the physically mixed sample result in a higher overall reaction rate than in the impregnated sample.

Taken alone, these results would suggest that initial catalyst dispersion is high for all alkali carbonate catalysts and has no bearing on the differences in activity of the various compounds. Hüttinger and Minges [64] showed that both K_2CO_3 and Na_2CO_3 wet carbon at the temperatures used in these experiments.

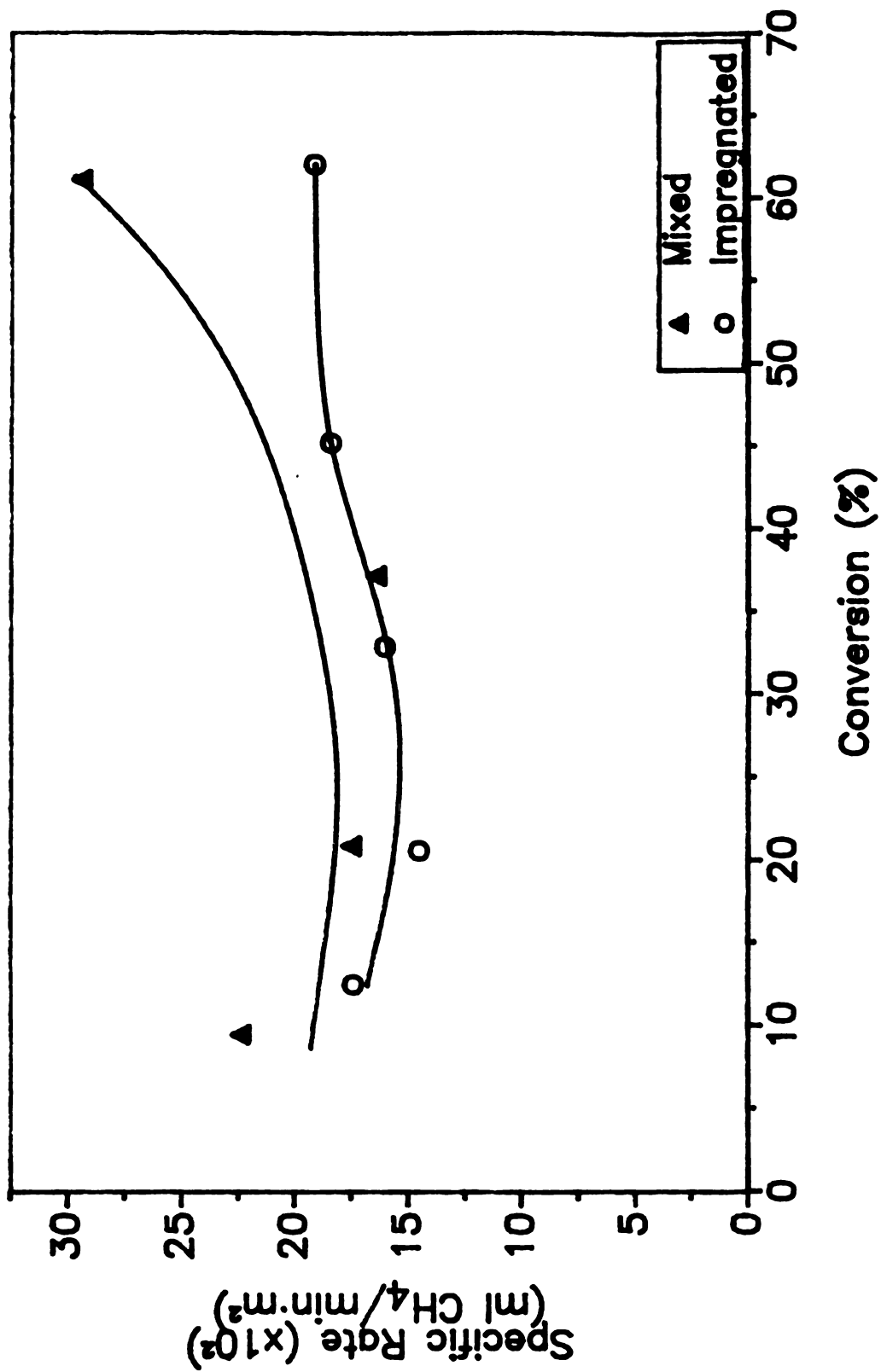


Figure 3.7. Comparison of impregnated and physically mixed K_2CO_3 on carbon black at $865^\circ C$, 500 psig H_2 , $K/C = 0.019$.

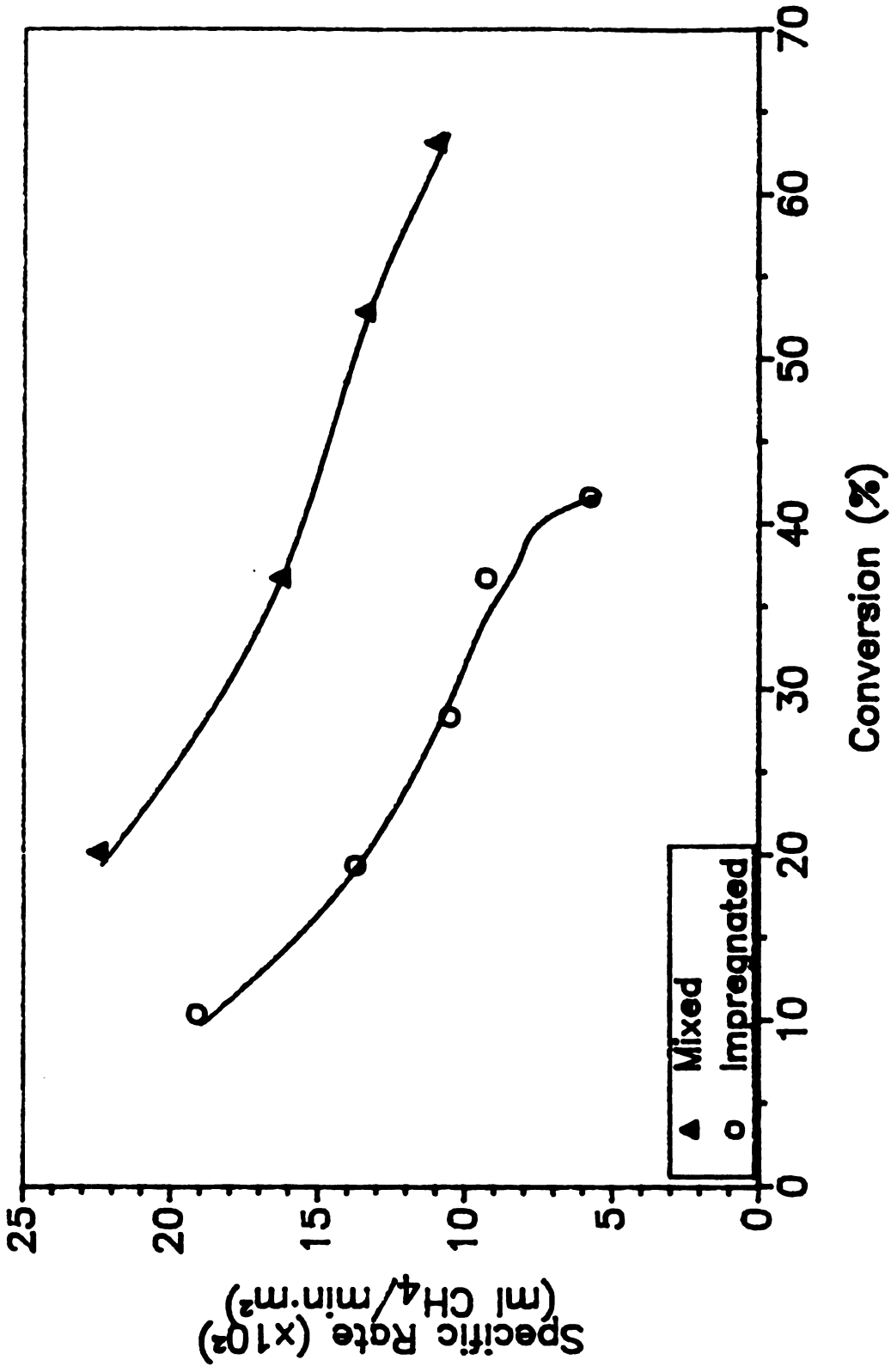


Figure 3.8. Comparison of impregnated and physically mixed Na₂CO₃ on carbon black at 865° C, 500 psig H₂, Na/C= 0.024.

The appearance of the residual samples, as discussed in Section 3.1, suggests that differences do exist at higher conversions. One possible explanation is that the difference in initial dispersion on the initially nonporous carbon black does not strongly affect the reaction rate. It is possible that the results could be quite different if the same experiments were performed on highly porous coconut charcoal; however, this was not done.

3.4 Catalyst Loss

Another parameter affecting catalytic activity is the rate of catalyst loss from the sample. Two catalysts may have the same initial activity for a given initial loading, but if one catalyst is lost much faster from the sample, it may exhibit much lower overall activity. Tables 3.1-3.4 summarize the catalyst loss measurements made, and Figures 3.9-3.11 show that over a wide range of catalyst loadings, pretreatment procedures, and temperatures, loss of Na_2CO_3 and NaOH is generally much greater than for K_2CO_3 or KOH on both carbon black and coconut charcoal. The difference in catalyst loss between cesium and potassium carbonate is not as dramatic, but it does appear that the trend is for K_2CO_3 to be lost at a slightly faster rate than Cs_2CO_3 on carbon black at 725°C . There is insufficient data at 865°C to discern whether this trend holds at higher temperatures.

It is interesting to note that the fraction of catalyst lost does not appear to depend strongly on catalyst loading, but rather only on conversion. This means that the absolute amount of catalyst lost at high loadings is much greater than at low loadings, directly corresponding to the fact that reactivity increases with loading. Thus it appears that absolute catalyst loss is not only a function

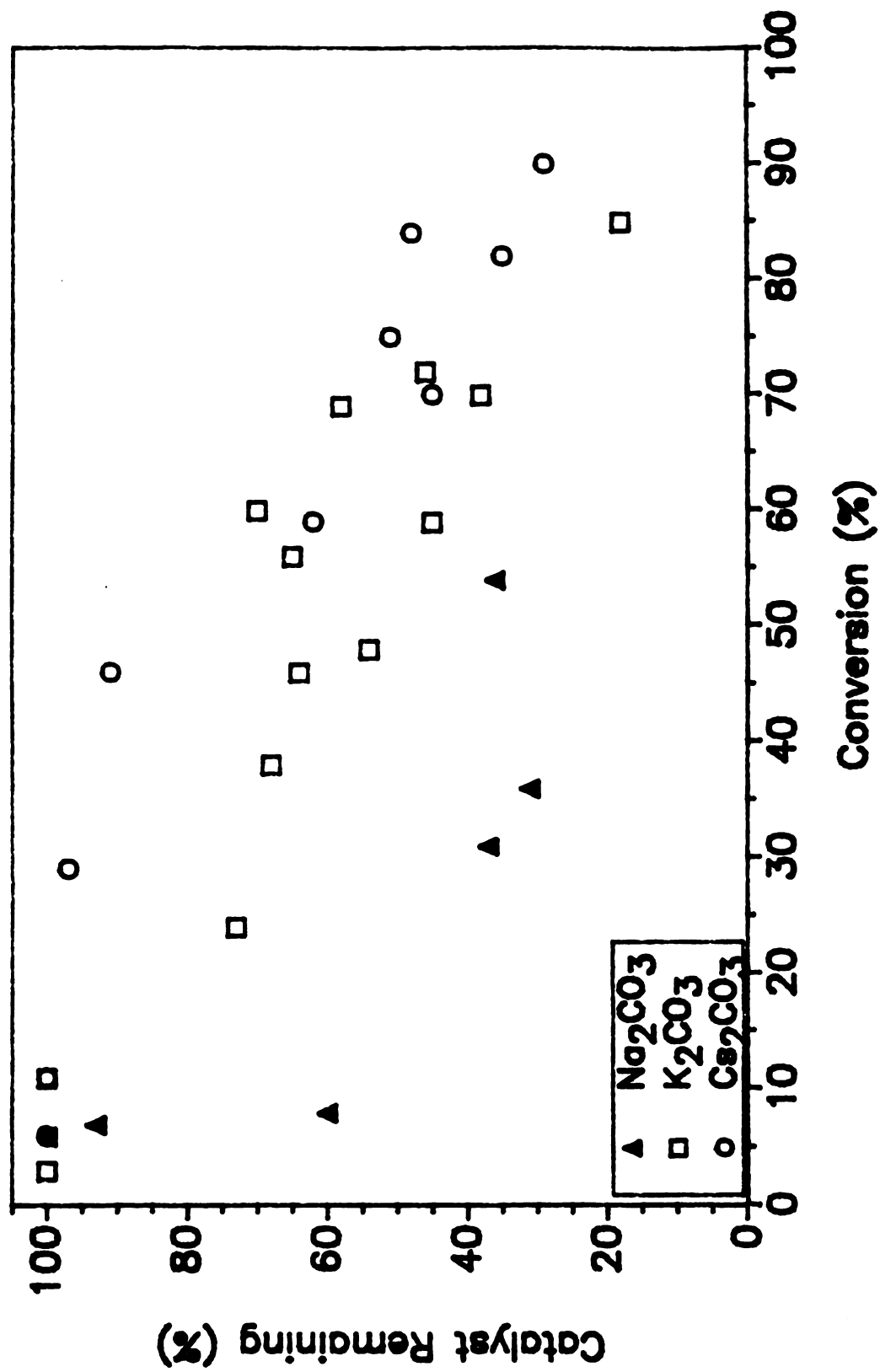


Figure 3.9. Catalyst loss from carbon black at 725° C, 500 psig H₂.

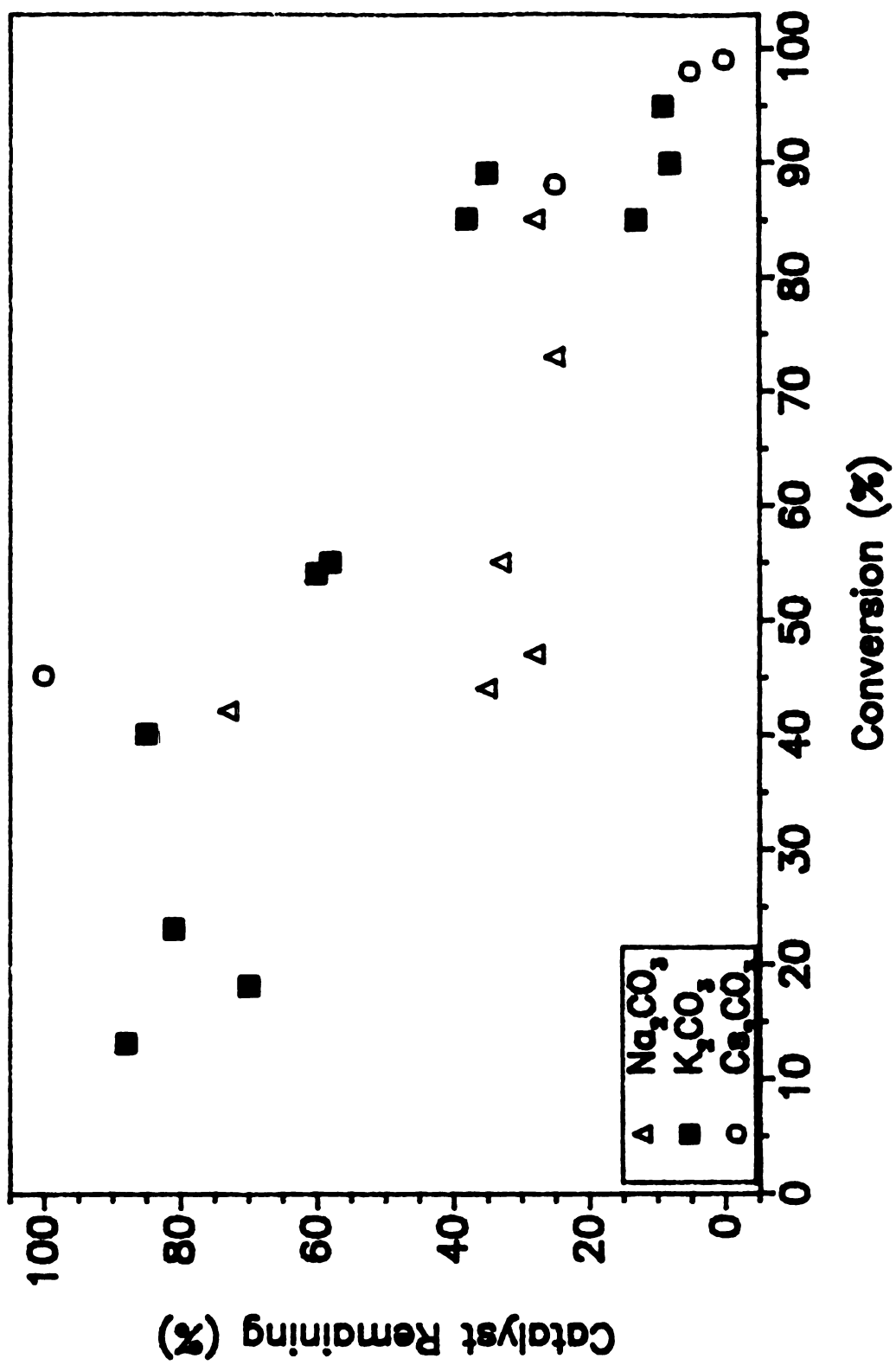


Figure 3.10. Catalyst loss from carbon black at 865° C, 500 psig H_2 .

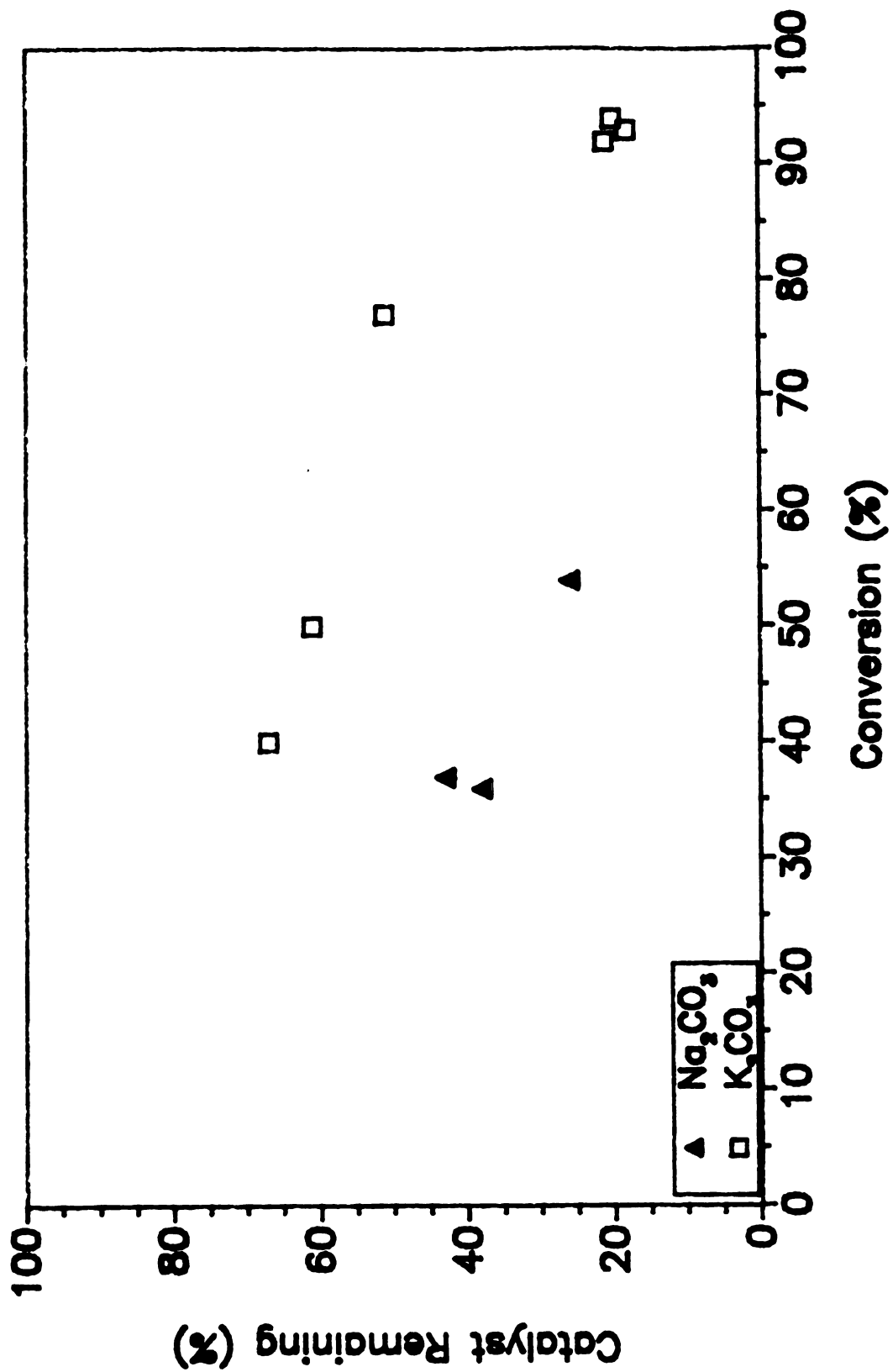


Figure 3.11. Catalyst loss from coconut charcoal at 775° C, 500 psig H₂.

Table 3.1. Catalyst Loss at 725° C on Carbon Black.

Catalyst	Loading (M/ C)	Conversion (%)	Catalyst Remaining (%)
Cs_2CO_3	0.009	6	100
"	0.019	11	100
"	0.031	29	97
"	0.031	84	48
"	0.043	46	91
"	0.043	90	29
"	0.058	75	51
"	0.058	70	45
"	0.074	59	62
"	0.074	82	35
K_2CO_3	0.009	3	100
"	0.019	11	100
"	0.031	60	70
"	0.043	56	65
"	0.043	69	58
"	0.058	70	38
"	0.058	72	46
"	0.074	24	73
"	0.074	46	64
"	0.074	85	18
"	0.116	48	54
"	0.116	59	45
"	0.174	38	68
Na_2CO_3	0.012	6	100
"	0.024	7	93
"	0.043	8	60
"	0.058	31	37
"	0.074	36	31
"	0.074	54	36

Table 3.2. Catalyst Loss at 865° C on Carbon Black.

Catalyst	Loading (M/C)	Conversion (%)	Catalyst Remaining (%)
Cs ₂ CO ₃	0.002	45	100
"	0.009	98	5
"	0.019	88	25
"	0.019	99	0
K ₂ CO ₃	0.009	85	38
"	0.019	13	88
"	0.019	23	81
"	0.019	54	60
"	0.019	89	35
KOH	0.009	40	85
"	0.009	85	13
Na ₂ CO ₃	0.024	42	73
"	0.024	85	28
NaOH	0.012	44	35
"	0.012	73	25

Table 3.3. Catalyst Loss at 775° C on Coconut Charcoal (M/C= 0.02).

Catalyst	Pretreatment	Conversion (%)	Catalyst Remaining (%)
K ₂ CO ₃	None	50	61
"	"	94	20
"	Degassed	40	67
"	"	92	21
"	Deg. Oxidized	77	51
"	"	93	18
Na ₂ CO ₃	None	36	38
"	Degassed	37	43
"	Deg. Oxidized	54	26

Table 3.4. Effect of Pretreatment on Catalyst Loss at 865° C on Carbon Black (M/C= 0.02).

Catalyst	Pretreatment	Conversion (%)	Catalyst Remaining (%)
K ₂ CO ₃	Degassed	18	70
"	"	90	8
"	Deg. Oxidized	55	58
"	"	95	9
Na ₂ CO ₃	Degassed	47	28
"	Deg. Oxidized	55	33

of the cation, but also depends on the loading and hence the reaction rate. One possible explanation is that the high absolute loss at high loadings could be due to a physical process rather than an intrinsic process related to catalyst activity. For instance, at high catalyst loadings, excess catalyst may flow onto the sample holder in greater amounts than at lower loadings.

3.5 Evolution of CO and CO₂

Since one of the primary pieces of evidence demonstrating the strong interaction between the catalyst and carbon is the evolution of large quantities of CO and CO₂ as the temperature is raised, an attempt was made to perform crude TPD experiments in the gasification reactor. Instead of raising the temperature as quickly as possible in a vacuum to 500° C and then starting the hydrogen flow, the temperature was raised slowly in flowing hydrogen while all product gases were collected. The results of these experiments are summarized in Table 3.5.

As expected, large amounts of CO and CO₂ were evolved from the catalyzed samples from 300-700° C. Expressed as a fraction of oxygen present in the catalyst, evolution of CO and CO₂ from the K₂CO₃-catalyzed sample is greater than from the Na₂CO₃-catalyzed sample, while the results from the Cs₂CO₃-catalyzed sample fall in between. The primary gas evolved from K₂CO₃ is CO₂, which appears in the temperature range of 300-500° C, while Na₂CO₃ releases primarily CO at 400-700° C. Cesium carbonate releases approximately equal amounts of CO and CO₂. The bulk of the CO₂ is released from 350-400° C, while CO is released fairly uniformly from 300-700° C.

These results demonstrate the strong interactions occurring between the catalyst and carbon, but the trends in gas evolution with catalyst activity are somewhat unexpected. Since Cs₂CO₃ is the most active catalyst and decomposes at 610° C, it was expected that gas evolution would be at least as high as for K₂CO₃. It is possible that experimental error could explain the apparent discrepancies, since the reactor system is not suited for generating reproducible temperature ramps or for collecting the product gas at arbitrary temperature intervals.

Table 3.5. Gas Evolution During Sample Heatup (M/ C= 0.02).

Catalyst	CO (mg)	CO ₂ (mg)	Total Oxygen (mg)	Fraction of Oxygen in Catalyst Evolved	
				as CO	as CO ₂
None	0.025	0.083	0.075	--	--
Cs ₂ CO ₃	0.46	0.42	0.57	0.13	0.15
K ₂ CO ₃	0.52	1.06	1.07	0.12	0.32
Na ₂ CO ₃	1.02	0.21	0.74	0.22	0.06

3.6 Discussion

It has been well established that the active form of catalyst in steam and carbon dioxide gasification is not the bulk carbonate, but rather a product of the interaction of the catalyst with the carbon. The same is undoubtedly true for hydrogen gasification as well, since these interactions have been shown to take place well below the temperatures required for hydrogen gasification to proceed at an appreciable rate. The fact that Cs_2CO_3 has slightly higher activity than K_2CO_3 even though it decomposes at 610°C indicates that the carbon is acting to retain the alkali metal in some form on the surface. The remaining results in this chapter can also be interpreted on the basis of this assumption. In other words, the activity of a given catalyst depends on how strongly it interacts with the carbon surface and on the stability of these groups once they are formed. Lithium carbonate apparently either interacts very weakly or very slowly with the carbon, producing few additional active sites. Since its melting point is 723°C , the excess carbonate flows off the sample before it has a chance to interact with the carbon.

Sodium carbonate, on the other hand, has initial activity comparable to K_2CO_3 , but it then deactivates rapidly at higher conversion. It apparently does not interact strongly enough with the carbon surface to produce additional active sites as more surface area becomes exposed. Instead, the excess carbonate tends to agglomerate before it is able to interact with the newly exposed surface area, and the active species are apparently vaporized more rapidly than in the case of K_2CO_3 . Deactivation by agglomeration of the Na_2CO_3 has been postulated by several investigators [30-32] to occur in steam and carbon dioxide gasification.

Finally, Cs_2CO_3 and K_2CO_3 produce active sites which are stable enough to propagate as new surface area is formed. In addition, any excess carbonate is able to remain highly dispersed until it is able to interact with the newly formed surface area. Catalyst loss is still significant, suggesting that it may play an important part in the catalytic process. Many of the proposed catalytic mechanisms for steam gasification involve cyclic formation of active sites by a redox process involving the catalyst and the reactant gas. Since such a cycle is not likely to exist in hydrogen, it seems logical that an active catalyst would tend to be reduced to the free metal and subsequently vaporized more rapidly in hydrogen than in an oxidizing environment, resulting in the high rates of catalyst loss observed here and by Zoheidi [16]. The active form of the catalyst and the mode by which the catalyst increases the number of active sites is postulated to be very similar, if not the same, as in steam or carbon dioxide gasification. The similarity of catalyst behavior observed in this chapter to that observed in steam and carbon dioxide gasification supports this postulate.

Chapter 4

Effect of Pretreatment on Uncatalyzed Gasification

The role of oxygen in uncatalyzed hydrogen gasification is examined in this chapter. Gasification of carbon oxidized with liquid HNO_3 is compared to experiments performed by Zoheidi [16], who showed that partial combustion enhances the reactivity of both fresh and degassed carbon black by fixing acidic groups on the surface. In addition, activated coconut charcoal is used to aid in clarifying the role of carbon structure and composition in gasification and oxidation. The surface oxygen content of samples treated in the vacuum pretreatment reactor was measured by XPS, and the results are interpreted in relation to the kinetic results obtained in the high pressure gasification reactor.

4.1 Carbon Black

4.1.1 Pretreatment and Gasification

The effects of pretreatment and HNO_3 oxidation on the reactivity of fresh and degassed carbon black are shown in Figures 4.1 and 4.2. Oxidation of fresh carbon black results in approximately a 30% increase in the reaction rate. Degassing reduces the rate approximately six-fold, and subsequent HNO_3 oxidation results in only a slight rate enhancement (5-10%), if any. In contrast, Zoheidi [16] showed that partial combustion prior to gasification results in approximately a two-fold increase in the reaction rate for both fresh and degassed carbon black. The results of Zoheidi are shown in Figure 4.3 for comparison.

4.1.2 Surface Analysis

The results of XPS measurements showing the effect of various treatment procedures on the surface oxygen content of carbon black are shown in Table 4.1. The values for oxygen content are normalized to the area of the C(1s) peak for consistency, and are expressed as oxygen atoms per 100 carbon atoms. This was accomplished by simply dividing the oxygen surface content by the carbon surface content as calculated by Equation 3-1 and multiplying by 100. Normalized values are used because absolute surface concentration measurements using XPS are not as accurate and depend on many factors. Relative measurements are more accurate, and the relative differences in surface oxygen noted in these experiments are significant and reproducible.

An attempt was made to correct for inorganic oxygen present in the ash by assuming the ash is SiO_2 . This results in an inorganic oxygen content of approximately 0.1 oxygen atoms per 100 carbon atoms for carbon black, and 0.6

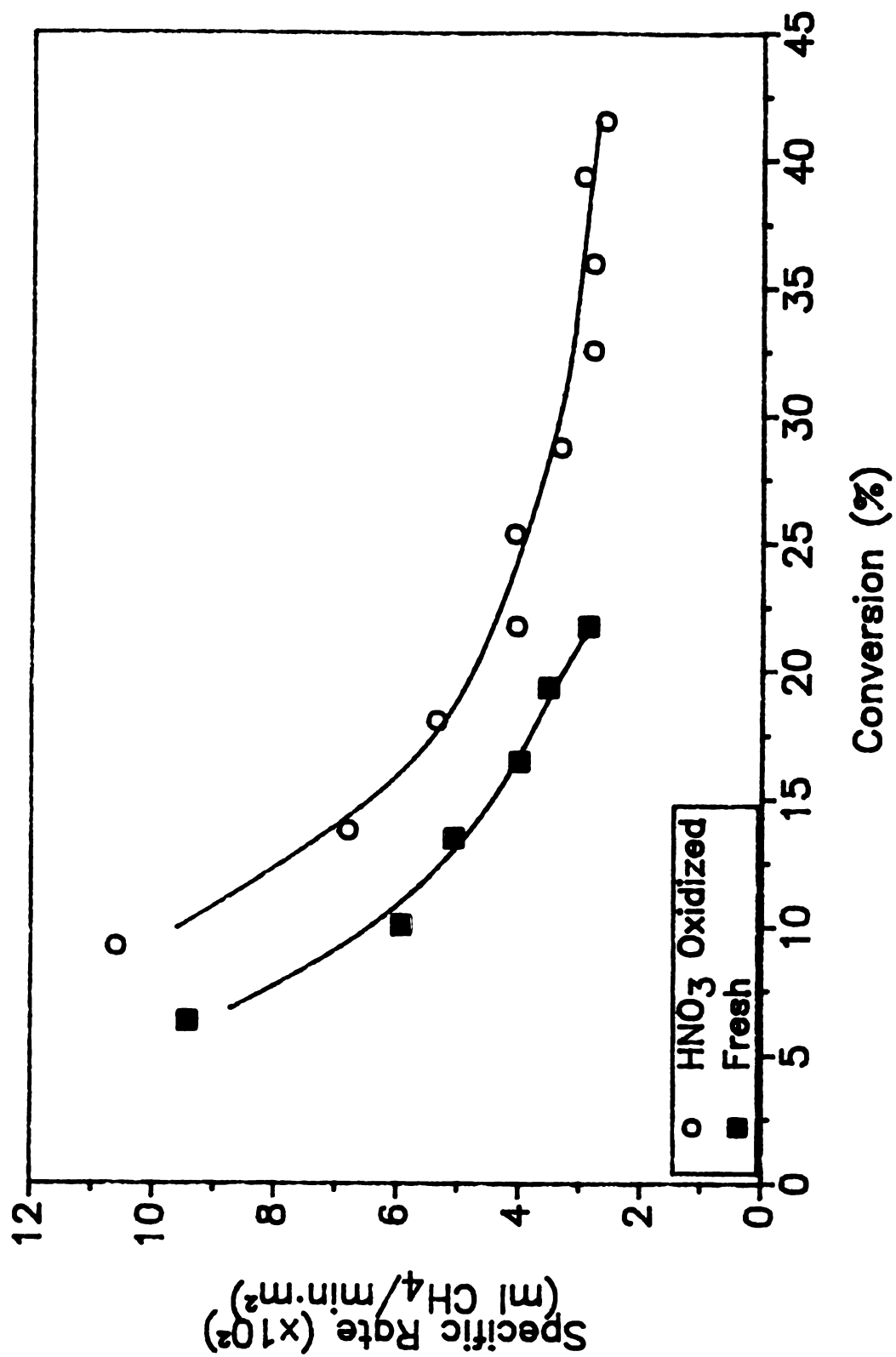


Figure 4.1. Effect of HNO_3 oxidation on reactivity of fresh carbon black at 865°C , 500 psig H_2 .

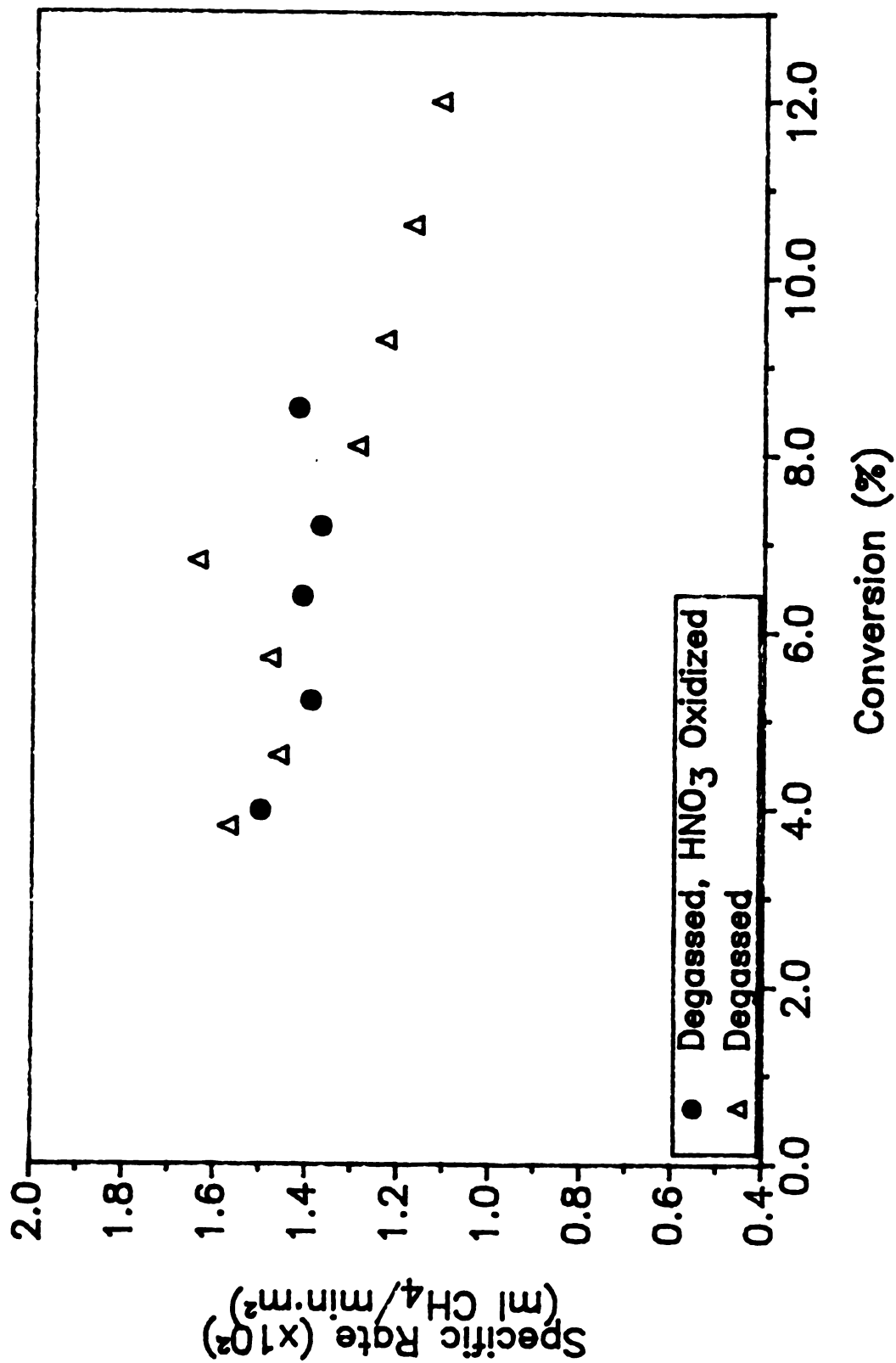


Figure 4.2. Effect of HNO₃ oxidation on reactivity of degassed carbon black at 865° C, 500 psig H₂.

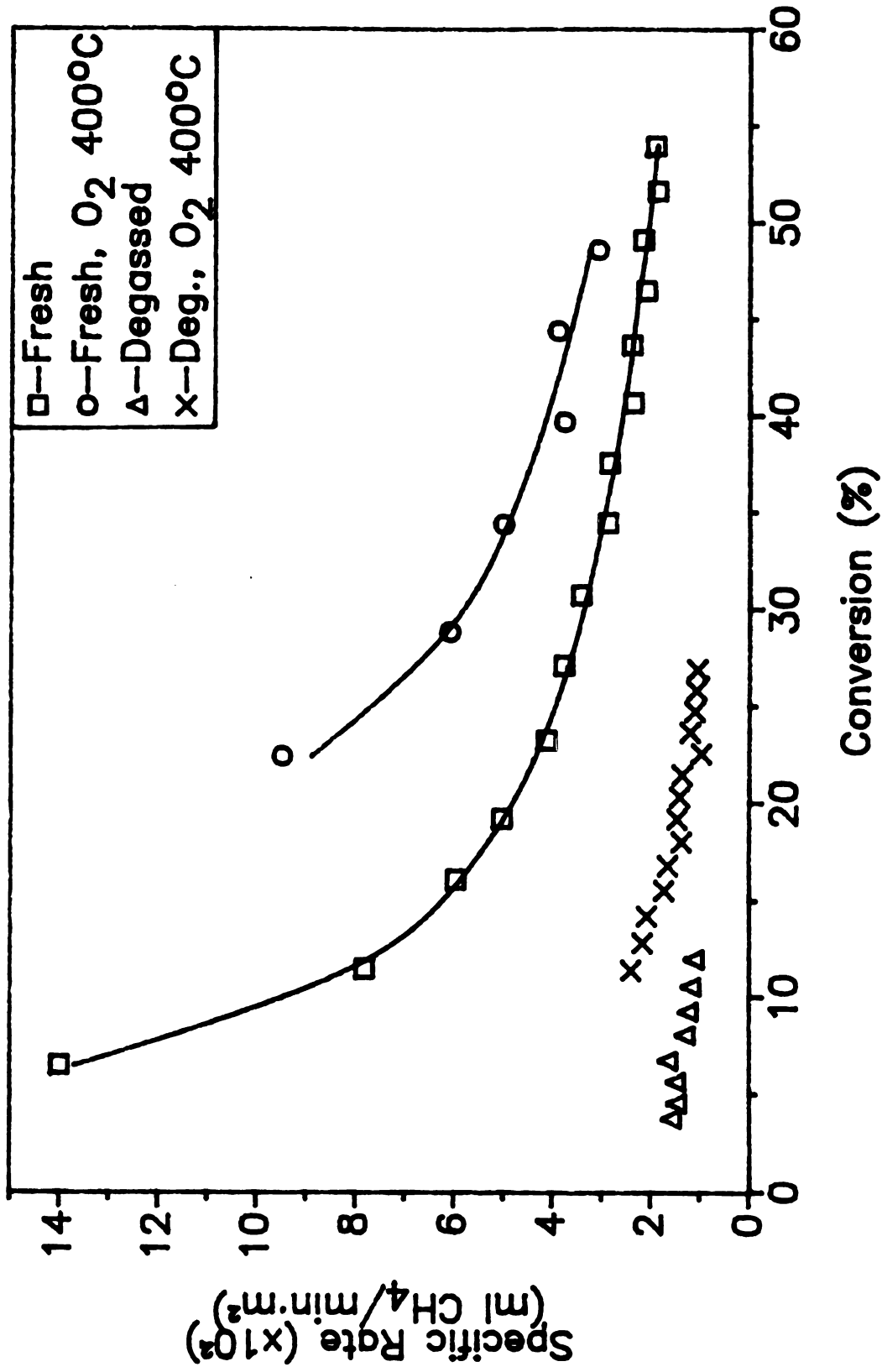


Figure 4.3. Effect of partial combustion at 400° C on reactivity of carbon black at 865° C, 500 psig H₂ (from Zoheidi [16]).

oxygen atoms per 100 carbon atoms for coconut charcoal. No correction was made for inorganic oxygen associated with sulfur. The presence of an S(2p) peak at 170 eV on oxidized carbon black in addition to the usual peak at 164 eV suggests that some of the sulfur is being oxidized. The total amount of sulfur is small, however, and the amount oxidized is only a small fraction of the total amount.

Table 4.1. Surface Oxygen Content of Carbon Black.

Treatment	Oxygen Atoms per 100 Carbon Atoms	High/Low B.E. Ratio
None	2.5	1.6
Heated to 200° C in Vacuum	2.0	1.6
Heated to 400° C in Vacuum	1.2	1.3
Heated to 600° C in Vacuum	0.4	1.5
H ₂ 750° C	0.1	--
65% Gasified	0.2	--
Degassed	0.3	--
HNO ₃ Oxidized	7.7	1.3
HNO ₃ Oxidized, Heated to 200° C	5.7	1.5
HNO ₃ Oxidized, Heated to 400° C	3.4	1.2
HNO ₃ Oxidized, Heated to 600° C	1.8	--
HNO ₃ Oxidized, H ₂ 750° C	0.5	--
Degassed, HNO ₃ Oxidized, Heated 200° C	2.3	1.5
Degassed, HNO ₃ Oxidized, Heated 400° C	1.4	3.0
O ₂ Oxidized at 400° C	4.5	1.5
O ₂ Oxidized, Heated to 600° C	3.4	--
O ₂ Oxidized, H ₂ 750° C	0.1	--

Degassing at 1000° C for seven hours at 10^{-4} torr reduces the surface oxygen/carbon ratio to approximately 0.3 oxygen atoms per 100 carbon atoms from an initial value of about 2.5. The residual surface oxygen concentration thus approaches the bulk oxygen content of approximately 0.2 oxygen atoms per 100 carbon atoms as measured by ultimate analysis. At the relatively short

counting times used in these experiments, however, the signal-to-noise ratio is quite low, and thus the low residual oxygen values have a relatively high level of uncertainty.

Treatment for one hour in a vacuum at successively higher temperatures reduces the oxygen content gradually, and once the sample is treated at 750° C in the presence of hydrogen, the oxygen content has essentially reached the residual level. The same is true for a sample that was gasified to 65% conversion, transferred to the vacuum pretreatment reactor, and reexposed to hydrogen at 750° C.

Oxidation with HNO₃ approximately doubles the surface oxygen content once the sample is heated to 200° C in a vacuum to remove weakly bound oxygen. Oxidation by partial combustion in air at 400° C and a pressure of 15 inches Hg for one hour increases the oxygen content approximately the same amount as HNO₃ oxidation, but the resulting groups are stable to higher temperatures since they were formed at 400° C.

In addition to quantitative information, the position of the O(1s) peak can also provide information on the surrounding electronic environment. Since oxygen is more electronegative than carbon, it withdraws electron density from the carbon atom, thus increasing the electron density around the oxygen atom and reducing its core electron binding energies. Thus oxygen with more bonds to carbon would be shifted to lower binding energies. In practice, however, the O(1s) peak envelope from oxygen on the surface of carbon is not as easily resolvable as in the case of more clearly defined molecules. Proctor and Sherwood [65] noted that the O(1s) peak is usually broad and difficult to resolve into unique components. Some investigators have distinguished between high and low binding energy oxygen, and have assigned the peaks to oxygen with one and two bonds to carbon, respectively [66,67].

An attempt was made to resolve the O(1s) peak envelopes of the data in Table 4.1 into unique components. It was found that two peaks located at 531.9 ± 0.2 eV and 533.9 ± 0.2 eV with a full-width at half-maximum (FWHM) of 2.3 ± 0.1 eV provided an adequate fit of the data. A 90% Gaussian, 10% Lorentzian peak shape was assumed. In addition to the two main peaks, a small peak at about 536 eV improved the fit considerably. This peak, however, usually comprised less than 10% of the total oxygen peak area, and has been attributed to oxygen not chemically bound to the carbon [67], although it is not clear how such species could persist at higher temperatures. The O(1s) peaks from which the information in Table 4.1 was obtained are presented in Appendix B.

The ratio of high to low binding energy oxygen is presented in Table 4.1. Since oxygen with fewer bonds to carbon should be removed at lower temperatures, this ratio should drop as the treatment temperature is increased. This may be the case for fresh and HNO₃ oxidized carbon black, but the results are inconclusive for degassed and O₂-oxidized carbon black. Figure 4.4 shows the change in the O(1s) peak of fresh carbon black with increasing treatment temperature. While it clearly demonstrates the gradual removal of oxygen from the surface with increasing temperature, the proportion of high and low binding energy oxygen does not change visibly. Below about 1% oxygen, it was usually not possible to perform a meaningful curve fit because of noise in the oxygen peak even after performing a 25-point smooth. It was concluded that the relative changes in the small amounts of oxygen on the surface were too small to be measurable as unique changes in the O(1s) peak envelope without performing a significant number of replicates to determine the statistical significance of the observed changes.

In addition to shifts in the binding energy of the O(1s) peak, the presence of oxygen bound to carbon should also affect the position of the C(1s) peak.

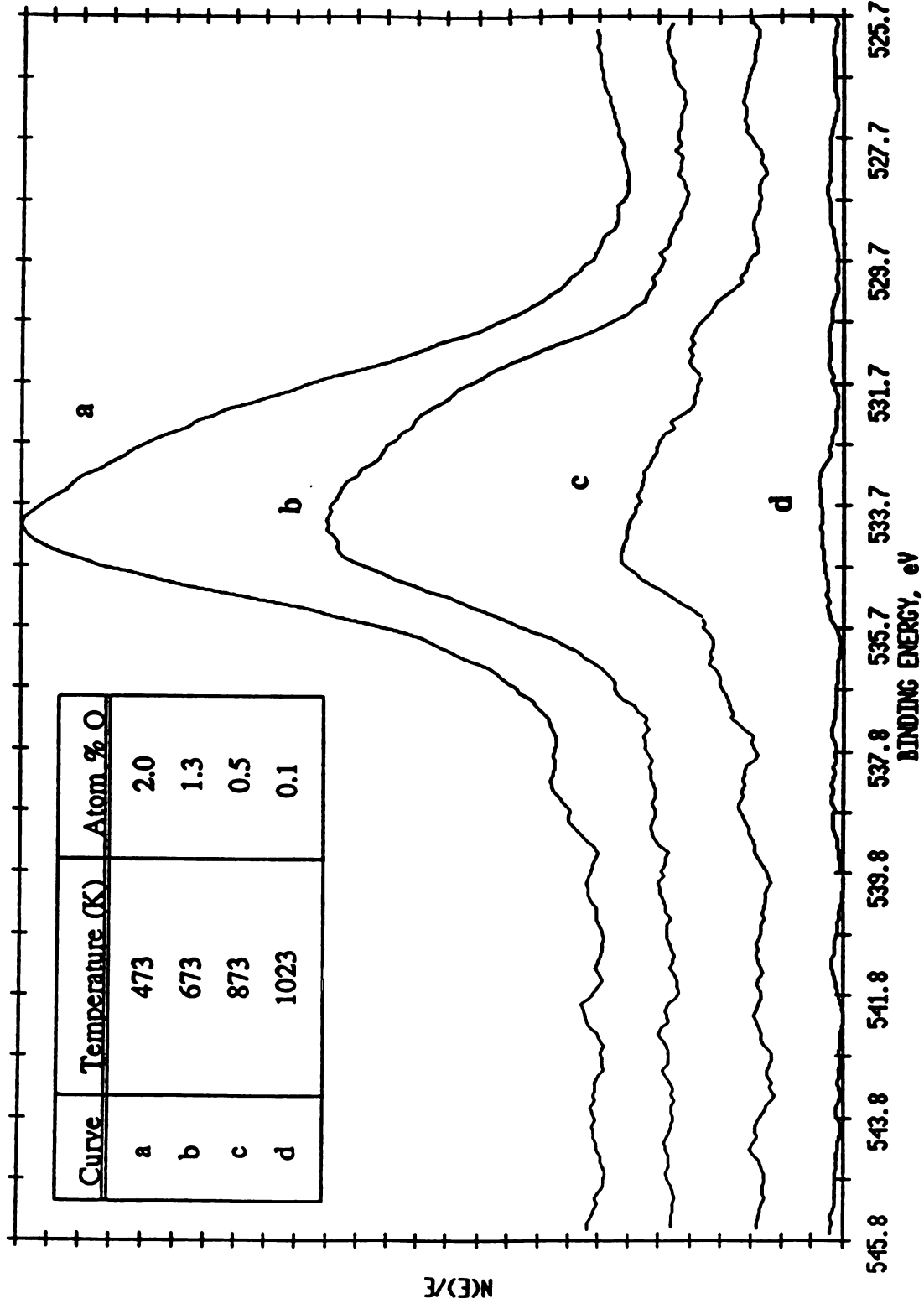


Figure 4.4. Change in the O(1s) peak of carbon black with temperature.

Oxygen bound to carbon withdraws electron density from the carbon atom, resulting in an increase in the core electron binding energy relative to a carbon atom with no oxygen bound to it. Investigators studying oxygen groups on coal [68,69] and carbon fibers [66,67] have shown that a good fit can be obtained by assuming a 1.5 ± 0.1 eV shift from the bulk carbon peak for each bond from oxygen to carbon, plus a component shifted ~ 7 eV to fit a plasmon or a shakeup peak, if present. There is discrepancy in the literature as to whether a peak at this location is a plasmon caused by interaction of the photoelectron with the conduction band, or a shakeup peak caused by energy loss due to $\pi-\pi^*$ transitions in a conjugated structure.

The aforementioned curve fitting procedure was used here, and a good fit was obtained with a FWHM of 1.7 ± 0.1 eV for the main peak and 2.1 ± 0.1 eV for the remaining peaks. As with the oxygen peak, a 90% Gaussian, 10% Lorentzian peak shape was assumed. A component for β -shifted carbon was not used.

Figure 4.5 shows a typical C(1s) peak and the corresponding components of the curve fit. The remainder of the curve fits are summarized in Table 4.2 along with the corresponding values for total oxygen, since the shape of the C(1s) peak did not vary visibly as the oxygen content was varied. Although the differences are small, on the order of 10%, the amount of the carbon peak shifted to higher binding energy does increase as the oxygen content increases. There is a significant amount of scatter, however, so any further interpretation of the data would require many replicates to determine the statistical significance of the small differences.

This was done in a crude sense by dividing the data into three categories: samples with an O/C ratio of less than one oxygen atom per 100 carbon atoms, those with between one and three, and those with greater than three oxygen

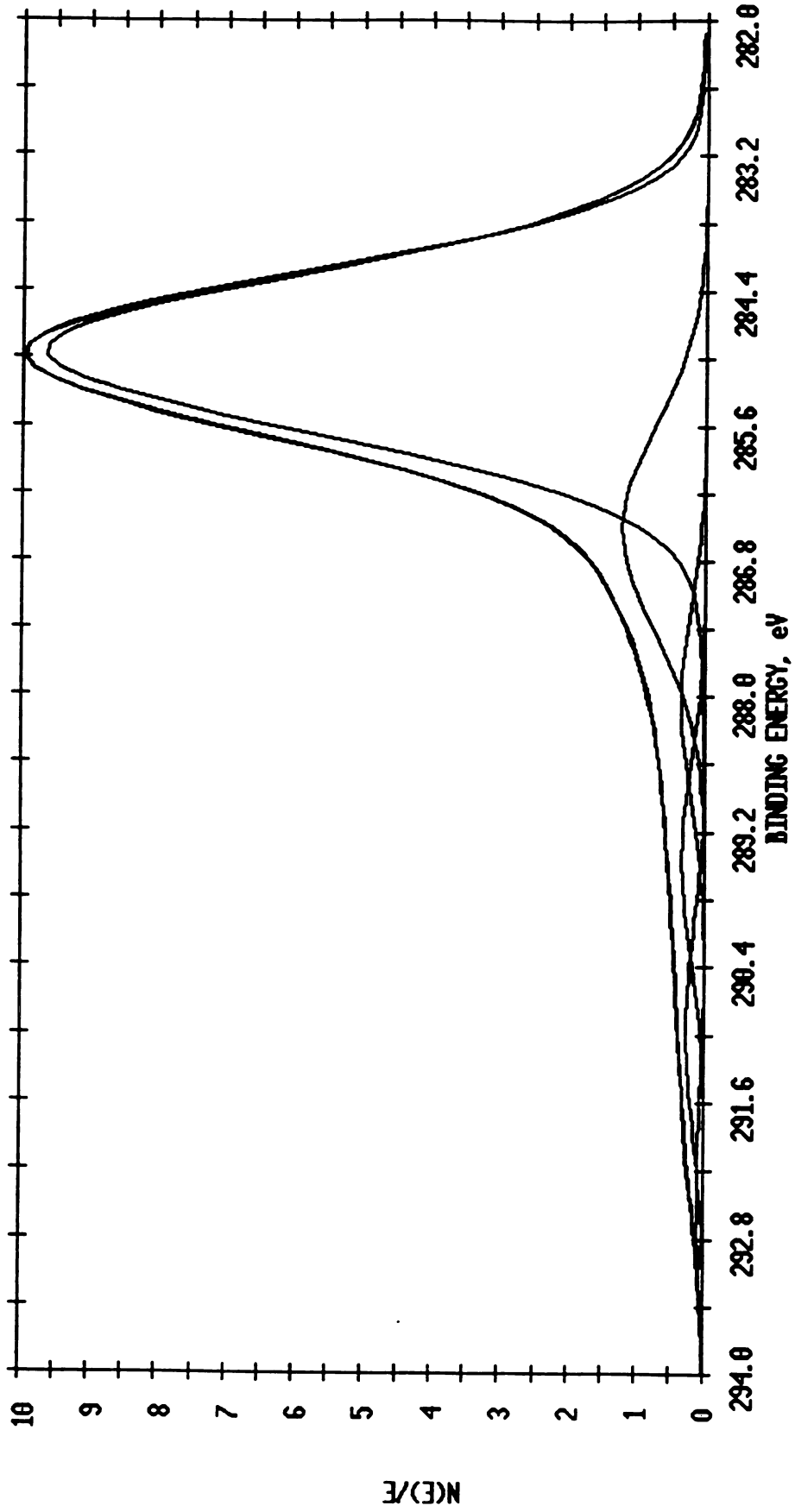


Figure 4.5. C(1s) peak and curve fit components of untreated carbon black.

atoms per 100 carbon atoms. The average unshifted carbon peak was 75.8% of the total peak for samples with a low oxygen content, 73.8% for the samples with intermediate oxygen content, and 71.4% for samples with the lowest oxygen content. Correspondingly, the average areas of the peaks shifted 1.5, 3, and 5 eV increase with increasing oxygen content. The peaks shifted 6 and 7.3 eV fluctuate randomly, as expected, since no carbonate groups are expected to be present and a plasmon or shakeup peak would not be expected to change with oxygen content.

Table 4.2. Summary of curve fits for the C(1s) peak of carbon black.

Treatment	O/C (x100)	Shift (eV)					
		0	1.5	3	4.5	6	7.3
None	2.3	75.9	12.5	4.2	3.4	2.6	1.4
None	3.0	73.9	14.0	4.1	3.7	3.3	0.9
Heated 200° C	2.1	73.8	12.2	4.2	3.5	4.2	2.2
Heated 400° C	1.3	74.4	12.8	4.6	3.8	3.2	1.3
Heated 600° C	0.5	76.4	11.9	4.2	3.2	3.1	1.1
H ₂ 750° C	0.1	74.6	10.9	4.3	4.5	3.4	2.3
Degassed	0.5	74.8	10.4	4.2	4.2	3.7	2.7
HNO ₃ Oxidized	7.8	73.5	13.8	4.3	4.1	2.8	1.6
HNO ₃ Oxidized	8.5	68.6	15.0	6.8	4.1	3.0	2.4
HNO ₃ Ox., 200° C	5.8	68.0	16.9	4.7	4.7	3.1	2.6
HNO ₃ Ox., 400° C	3.5	74.7	12.3	4.5	3.5	3.4	1.6
HNO ₃ Ox., 600° C	1.9	72.1	13.6	5.1	3.2	3.4	2.6
HNO ₃ Ox., H ₂ 750° C	0.9	77.2	11.3	3.9	3.3	3.1	1.2
HNO ₃ Ox., H ₂ 750° C	0.4	76.2	11.6	4.1	3.7	2.7	1.6
Deg., HNO ₃ Ox., 200° C	2.4	71.6	13.5	4.4	4.1	3.9	2.5
Deg., HNO ₃ Ox., 400° C	1.5	74.8	14.0	3.4	2.8	4.0	1.2
O ₂ Oxidized	5.0	70.7	13.9	5.8	3.9	3.2	2.6
O ₂ Oxidized	4.2	70.2	14.5	4.6	5.3	3.2	2.1
O ₂ Ox., Heated 600° C	3.5	73.9	13.3	4.6	3.5	3.5	1.2

These results do not have a great deal of significance in relation to the other results presented in this work when it is realized that these small changes were detected in samples that covered a range of almost two orders of magnitude in oxygen content. It was concluded that the majority of the high binding energy component of the C(1s) peak is due to asymmetric tailing of the peak due to conduction band interactions arising from the graphitic nature of the carbon [70].

Although the XPS spectra did not provide any specific information on the nature of the oxygen groups on the surface of the carbon, the variation in total surface oxygen with pretreatment does provide some insight into the role of surface oxygen in hydrogen gasification. Figure 4.6 shows a plot of the initial reaction rate as measured in the high pressure gasification reactor versus the initial surface oxygen content of the carbon after removal of weakly bound oxygen at 200° C in the vacuum pretreatment reactor. A strong correlation does appear to exist between reactivity and initial surface oxygen content. This is one of the most important findings of this work, and it agrees with the work done in steam and carbon dioxide gasification that demonstrates the effect of surface oxygen content on reactivity.

The surface oxygen content and reactivity did not correlate, however, in every case. Degassed, HNO₃ oxidized carbon black had about the same oxygen content after heating to 200° C and 400° C as fresh carbon black. Since the reactivity of the degassed, oxidized sample is only slightly higher than the degassed sample, it was expected that most of the oxygen was weakly bound and would be removed at 200° C. The oxygen is relatively strongly bound, yet it does not appear to significantly enhance the reaction rate. Obviously, the situation is somewhat more complicated than a simple correlation between reactivity and initial surface oxygen content. Apparently, oxygen is strongly bound to the

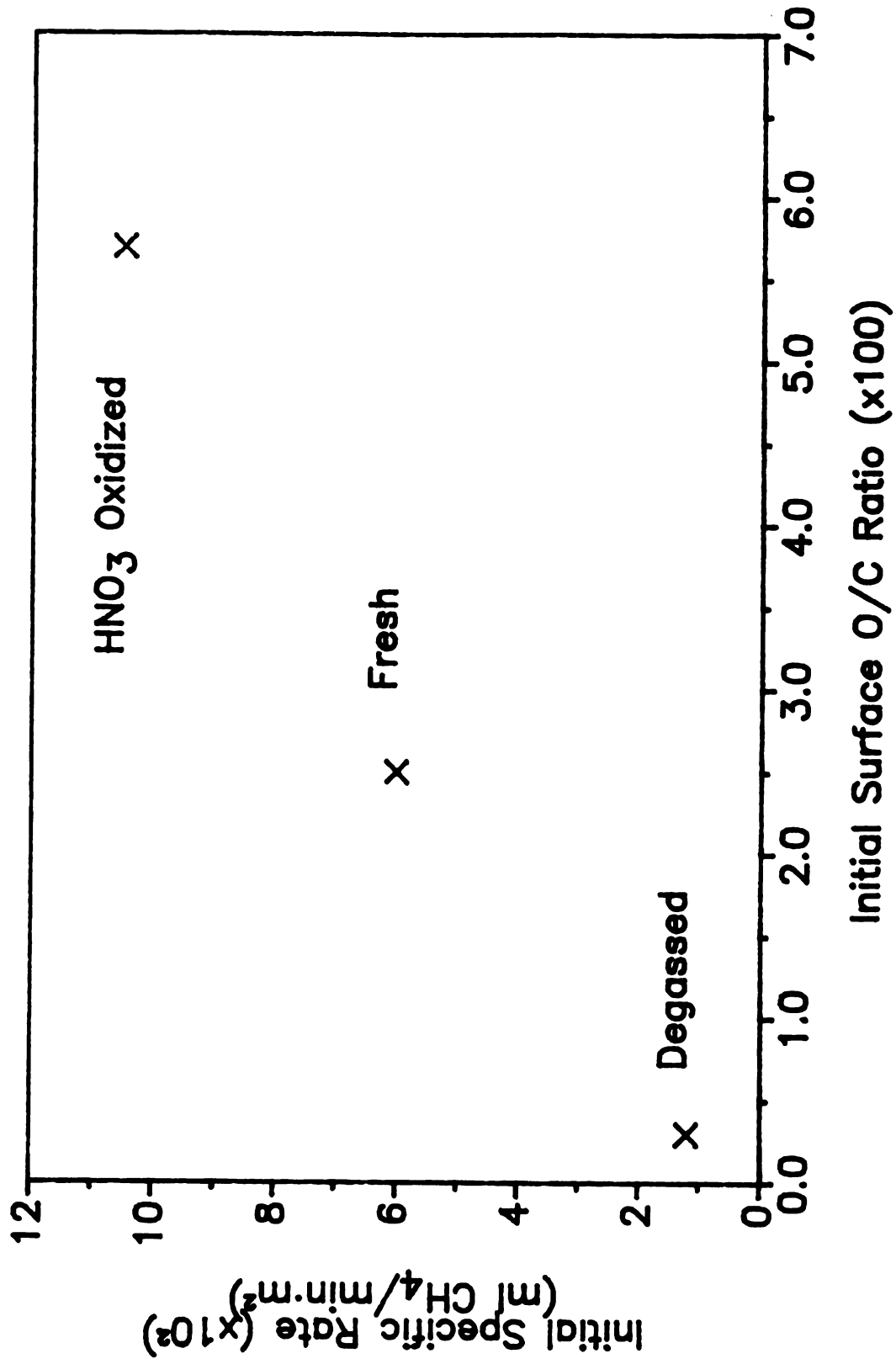


Figure 4.6. Initial rate versus initial surface oxygen content for carbon black.

annealed surface, but active sites are not regenerated to any great extent under reaction conditions. This particular sample was quite old when the XPS analysis was performed, so the possibility of slow oxidation at room temperature must also be taken into consideration.

4.2 Coconut Charcoal

4.2.1 Pretreatment and Gasification

The effects of degassing and HNO_3 oxidation on the reactivity of uncatalyzed coconut charcoal at 865°C are shown in Figure 4.7. In contrast to carbon black, degassing only reduces the reaction rate by less than a factor of two. Nitric acid oxidation, on the other hand, increases the rate of both the fresh and degassed samples. For the degassed sample, oxidation increases the rate almost to the value of that for fresh char. At high conversion, the rates of all samples converge; the effects of surface treatments thus decay as carbon is consumed. In addition, the specific reaction rate of fresh coconut charcoal is approximately constant with conversion, in contrast to fresh carbon black, for which the specific reaction rate decreases drastically with conversion.

Comparison of Figure 4.1 with Figure 4.7 reveals that the specific rate of fresh coconut char is approximately the same as that of degassed carbon black. This was unexpected, since the amorphous coconut charcoal would be expected to have a much higher ratio of ASA to TSA than graphitic carbon black that had been degassed at 1000°C . One possible explanation for the lower specific reactivity would be mass transfer resistances within the micropores of the char particles. Although Zoheidi [16] showed both experimentally and theoretically that internal and external mass transfer resistances are negligible in uncatalyzed

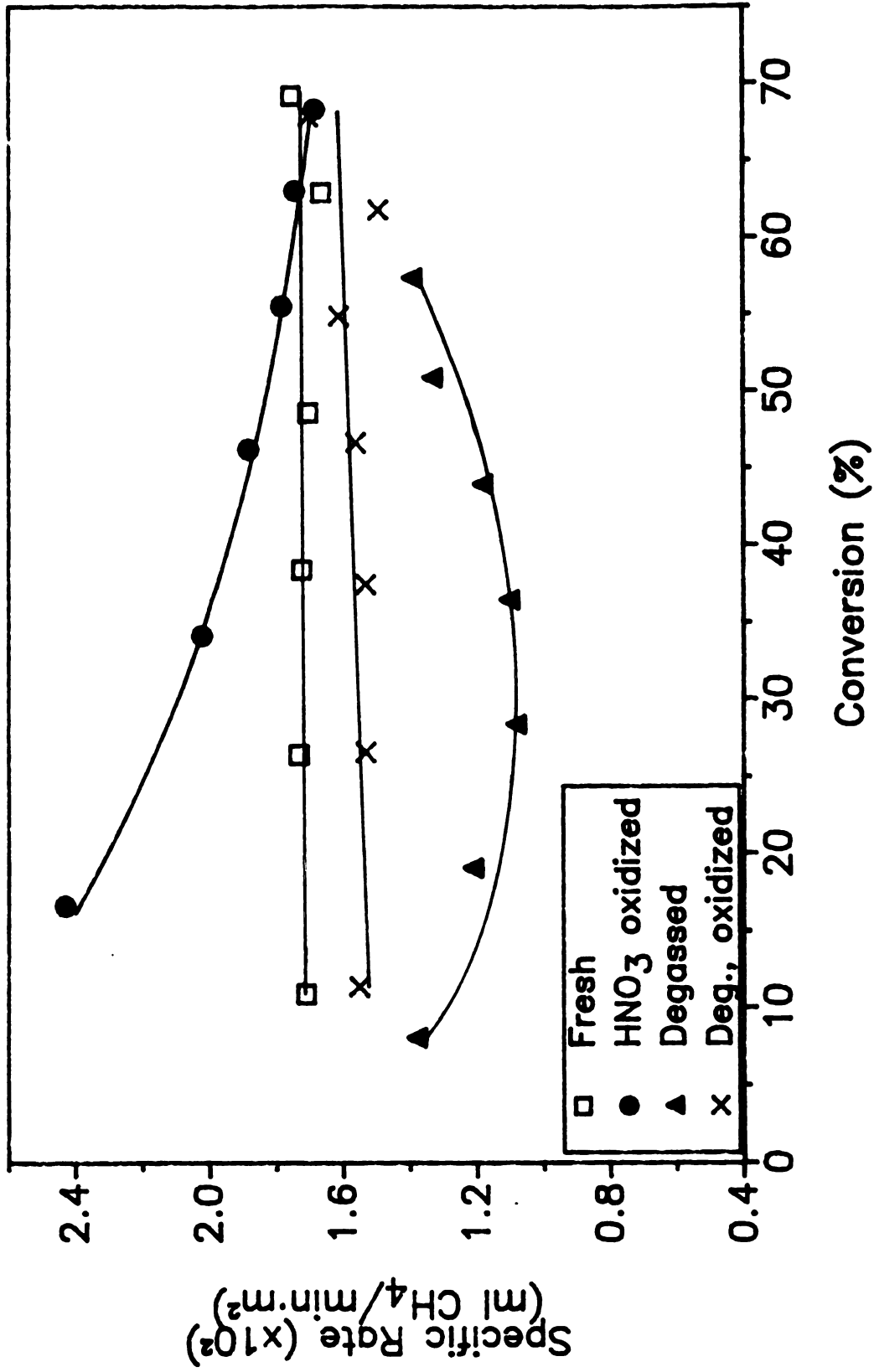


Figure 4.7. Effect of HNO_3 oxidation on reactivity of uncatalyzed coconut charcoal at 865°C , 500 psig H_2 .

carbon black, the char particles are considerably larger and more porous, a combination which could result in significant internal resistances. The possibility of significant mass transfer resistances is even greater in the case of catalyzed coconut charcoal, where reaction rates are significantly higher.

Since one indication of mass transfer resistances is a reduction in the apparent activation energy, an estimate was made for coconut charcoal based on the rates at 865° C and 775° C at 20% conversion. Based on these two points, the activation energy was calculated to be 70 kcal/mol-K, approximately the same value calculated by Zoheidi [16] for carbon black. The uncertainty in this value is fairly large since only two points were used, and the possibility of curvature in the Arrhenius plot, another indicator of mass transfer resistances, cannot be ruled out. While mass transfer resistances would mask the intrinsic kinetics of coconut charcoal gasification somewhat, determination of gross differences in gasification behavior between carbon black and coconut charcoal in relation to oxidation and degassing should still be valid.

4.2.2 Surface Analysis

Pretreatment followed by XPS analysis was performed on uncatalyzed coconut charcoal using the experimental procedure described in Chapter 2. Table 4.3 summarizes the XPS results of surface oxygen content for various pretreatment procedures. Severe charging of the sample was noted in many cases, resulting in distortion of the peak shapes. Measurement of total oxygen, however, is unaffected by peak broadening as long as a portion of the peak does not move completely out of the analysis window.

The results in Table 4.3 demonstrate distinct differences between the behavior of oxygen groups on carbon black and coconut charcoal. The initial surface oxygen/carbon ratio of the char is about 7 oxygen atoms per 100 carbon

Table 4.3. Surface Oxygen Content of Coconut Charcoal.

Treatment	Oxygen Atoms per 100 Carbon Atoms
None	7.0
Heated to 200° C in Vacuum	7.9
H ₂ 750° C	0.8
Degassed	1.7
HNO ₃ Oxidized	12.2
HNO ₃ Oxidized, Heated to 200° C	10.1
HNO ₃ Oxidized, H ₂ 750° C	0.9
Degassed, HNO ₃ Oxidized, Heated to 200° C	6.1

atoms, more than double the value of 2.8 oxygen atoms per 100 carbon atoms for the bulk char as measured by ultimate analysis. Degassing reduces the surface oxygen/carbon ratio to a value of 1.7, below the value for the bulk char, and exposure to hydrogen for 30 minutes at 750° C reduces it to 0.8. Oxidation with HNO₃ increases the surface oxygen/carbon ratio to about 10, even after heating to 200° C. Oxidation of the degassed char also increases the oxygen content considerably. As in the case of carbon black, the initial reaction rate correlates very well with the initial surface oxygen content. Figure 4.8 shows a plot of this relationship.

As in the case of carbon black, variation in the oxygen content of the char could be seen as shifts in the C(1s) peak, but not in the O(1s) peak. Table 4.4 shows the results of the C(1s) curve fits for the samples which did not show any evidence of differential charging. Again, a large portion of the shift is likely due to the asymmetric nature of the bulk C(1s) peak.

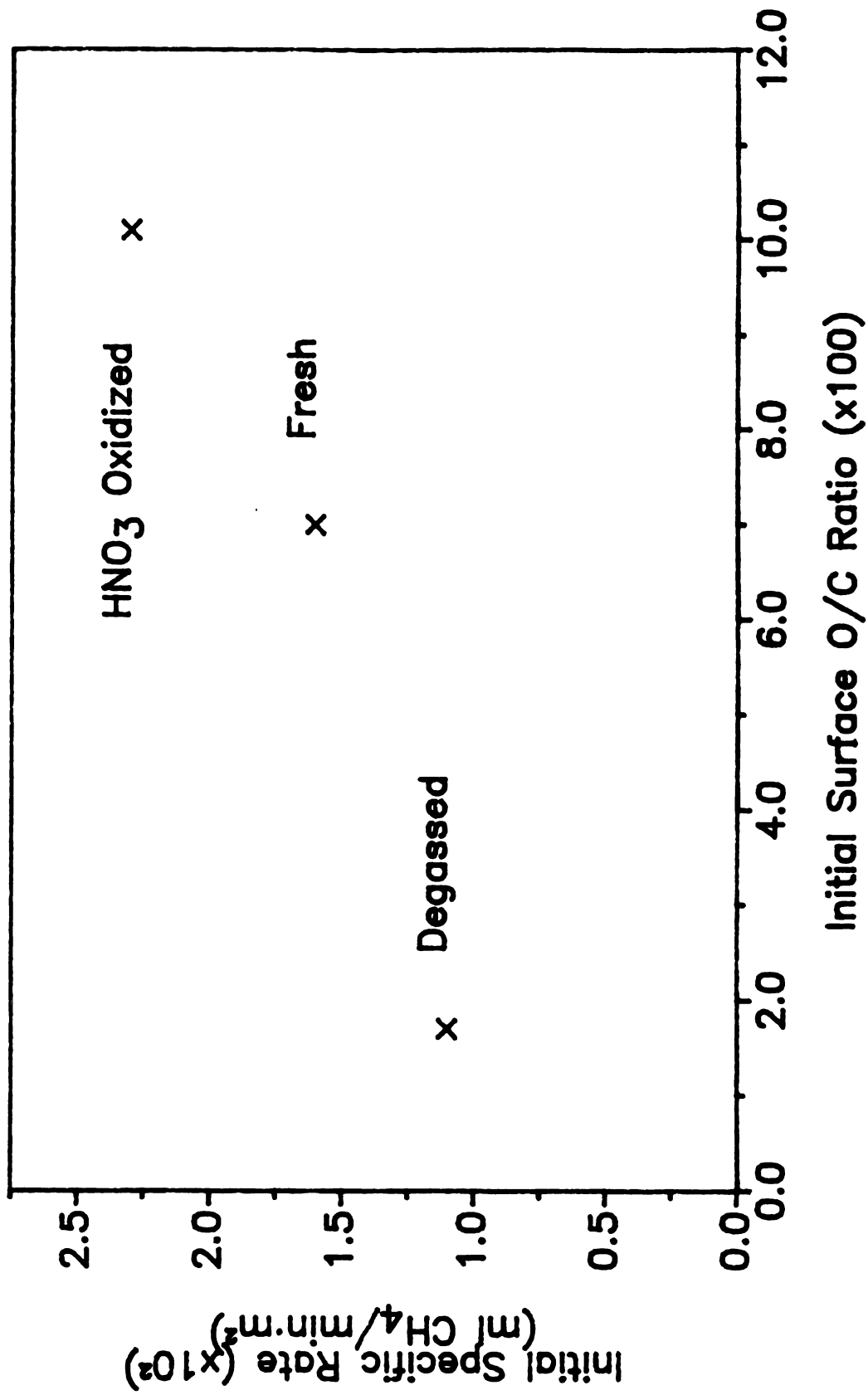


Figure 4.8. Initial rate versus initial surface oxygen for coconut charcoal.

Table 4.4. Curve fit results for the C(1s) peak of coconut charcoal.

Treatment	O/C (x100)	Shift (eV)					
		0	1.5	3	4.5	6	7.3
None	7.6	67.4	15.6	5.8	6.2	4.3	0.8
None	7.6	69.1	13.2	7.0	4.7	4.2	1.9
Degassed	2.3	76.7	7.9	6.2	4.1	3.9	1.2
HNO ₃ Oxidized	13.8	67.7	14.9	6.9	5.4	4.1	1.0
HNO ₃ Oxidized	11.9	58.0	20.0	8.2	7.1	3.5	3.2

4.3 Discussion

4.3.1 Carbon Black

The results presented in this chapter support the conclusions of Zoheidi [16], who postulated that acidic groups on the surface of carbon black decompose to form nascent active sites which facilitate hydrogen gasification. These nascent sites are consumed as the carbon reacts, resulting in the observed decrease in gasification rate of fresh carbon black with conversion. Thermal degradation of nascent sites does not occur at gasification temperatures, as evidenced by an experiment in which carbon black was heated to 865° C for four hours in helium. Upon exposure to hydrogen, the reaction rate was the same as that of a sample directly heated to 865° C in hydrogen. The XPS results indicate that desorption of the oxygen groups is essentially complete once gasification conditions are reached, but that the reactivity still strongly depends on the initial surface oxygen content. This supports the postulate that the oxygen groups do not participate directly in the reaction mechanism, but rather desorb to form the active sites where gasification occurs (Reactions 1-6 and 1-7).

High temperature degassing, however, thermally anneals the nascent sites formed, resulting in a much lower gasification rate. The XPS results show that essentially all excess surface oxygen is removed. Gasification activity following degassing, which remains constant with carbon conversion, is attributed to the residual basic oxygen groups in the bulk carbon which are exposed as carbon is gasified. These groups apparently also facilitate gasification, although at a much slower rate. The x-ray diffraction patterns are identical for fresh and degassed carbons [16], indicating that no bulk changes in the carbon structure occur during the degassing process, and thus annealing is a surface process only.

Partial combustion in oxygen at 400° C produces significant new surface area in carbon black, as about 10% of the solid was gasified by the oxygen in Zoheidi's experiments. More importantly, partial combustion fixed acidic oxygen groups on the surface. Under reaction conditions, these acidic groups decompose to give substantially more active gasification sites than would be present at 10% conversion of fresh carbon black. Thus partial combustion enhances methane formation for both fresh and degassed carbon black by the creation of active sites from acidic surface groups on newly formed surface area.

Nitric acid oxidation produces both acidic and basic groups on carbon [8] and is unable to expose fresh surface area as partial combustion can. Thus HNO₃ oxidation gives different results than partial combustion. Oxidation of fresh carbon black somewhat enhances the methane formation rate; acidic groups formed in oxidation again form active sites upon heating to reaction conditions. Upon degassing, however, the carbon surface is no longer susceptible to liquid HNO₃ oxidation, and only slight rate enhancement is observed following oxidation of the degassed carbon. The XPS results indicate that partial combustion is able to fix more oxygen groups on the surface, and that they are stable to higher temperatures than groups produced by HNO₃ oxidation. This suggests that the

fraction of oxygen groups which produce active sites is higher for partial combustion than for HNO_3 oxidation. This supports the postulate that acidic groups are responsible for rate enhancement of uncatalyzed carbon.

In summary, the carbon black gasification rate depends on a number of factors, including the extent of surface oxidation and annealing, and the ability of an oxidizing agent to remove annealed sites and oxidize fresh surface area. The type of oxygen groups formed on the surface also plays a role, since it is postulated that acidic groups are responsible for rate enhancement in the uncatalyzed case.

4.3.2 Coconut Charcoal

The coconut char studied has significantly different structure and composition than carbon black. The nearly constant gasification rate with conversion suggests that the high bulk oxygen content and amorphous structure of the char provide new active sites for gasification as carbon is consumed. In contrast to carbon black, the XPS results show that a significant amount of oxygen is present on the char after exposure to reaction conditions or even degassing conditions. As in the case of carbon black, the surface oxygen content is reduced to approximately the same level as the bulk oxygen content.

The effect of degassing on gasification is much less for the char than for carbon black, and the XPS results are consistent with this effect. It is proposed that this also results from the amorphous nature and high bulk oxygen content of the char. Degassing only removes surface-adsorbed groups and apparently does not affect bulk oxygen, which is present in much higher levels than in carbon black. Because the char is amorphous, and thus so many carbon atoms are potential reactive sites, thermal annealing apparently does not destroy as large a fraction of active sites in the char as in carbon black. Thus, while acidic surface

groups are still desorbed during degassing, and the active sites associated with them are likely annealed, there are enough reactive sites and bulk oxygen remaining that char reactivity is only moderately reduced. Another possible explanation is that the active sites removed by degassing carbon black are not present in coconut charcoal. The reactivity of uncatalyzed carbon black is initially very high and drops rapidly to nearly the same rate as degassed samples. This suggests that the surface of carbon black particles is much more reactive than the bulk, possibly due to a higher degree of disorder at the surface. Degassing thus has more of an effect on carbon black than on coconut charcoal.

Both fresh and degassed char show significant gasification rate enhancement upon oxidation in HNO_3 . The large quantity of gas evolved during the oxidation procedure indicates extensive oxidation of the surface, and the XPS results support this conclusion. These results can again be attributed to the noncrystalline nature of the char, resulting in a much higher ASA/TSA ratio for oxidation. The increase in acidic group concentration from oxidation results in accelerated methane formation following oxidation.

These results demonstrate the strong correlation between reactivity and surface oxygen content for both carbon black and coconut charcoal. A simple 1:1 correspondence was not observed, nor was it expected, since not every oxygen group necessarily desorbs to form an active site, and differences in the energetics of various sites formed would also be expected to play a role.

In addition, the results of coconut charcoal gasification demonstrate the importance of carbon structure in determining the effect of various pretreatment procedures. They also point out the necessity for thorough carbon characterization in order to distinguish effects related to structure and impurity content.

Chapter 5

Effect of Pretreatment on Catalyzed Gasification

Hydrogen gasification and XPS experiments were carried out on carbon black and coconut charcoal samples treated by degassing and/or HNO_3 oxidation prior to catalyst impregnation using similar procedures as in the uncatalyzed case. Both K_2CO_3 and Na_2CO_3 were used to determine whether catalyst activity influences the ability of HNO_3 oxidation to enhance the catalyzed reaction rate.

5.1 Carbon Black

The effects of degassing and HNO_3 oxidation on the reactivity of K_2CO_3 and Na_2CO_3 -catalyzed carbon black at 865°C are shown in Figures 5.1 and 5.2, respectively. Catalysts were impregnated to a loading of $M/C = 0.02$ in all cases. The catalysts strongly enhance the reactivity of both fresh and degassed carbon black. In contrast with the uncatalyzed case, however, HNO_3 oxidation enhances the reaction rate of both fresh and degassed carbon black impregnated

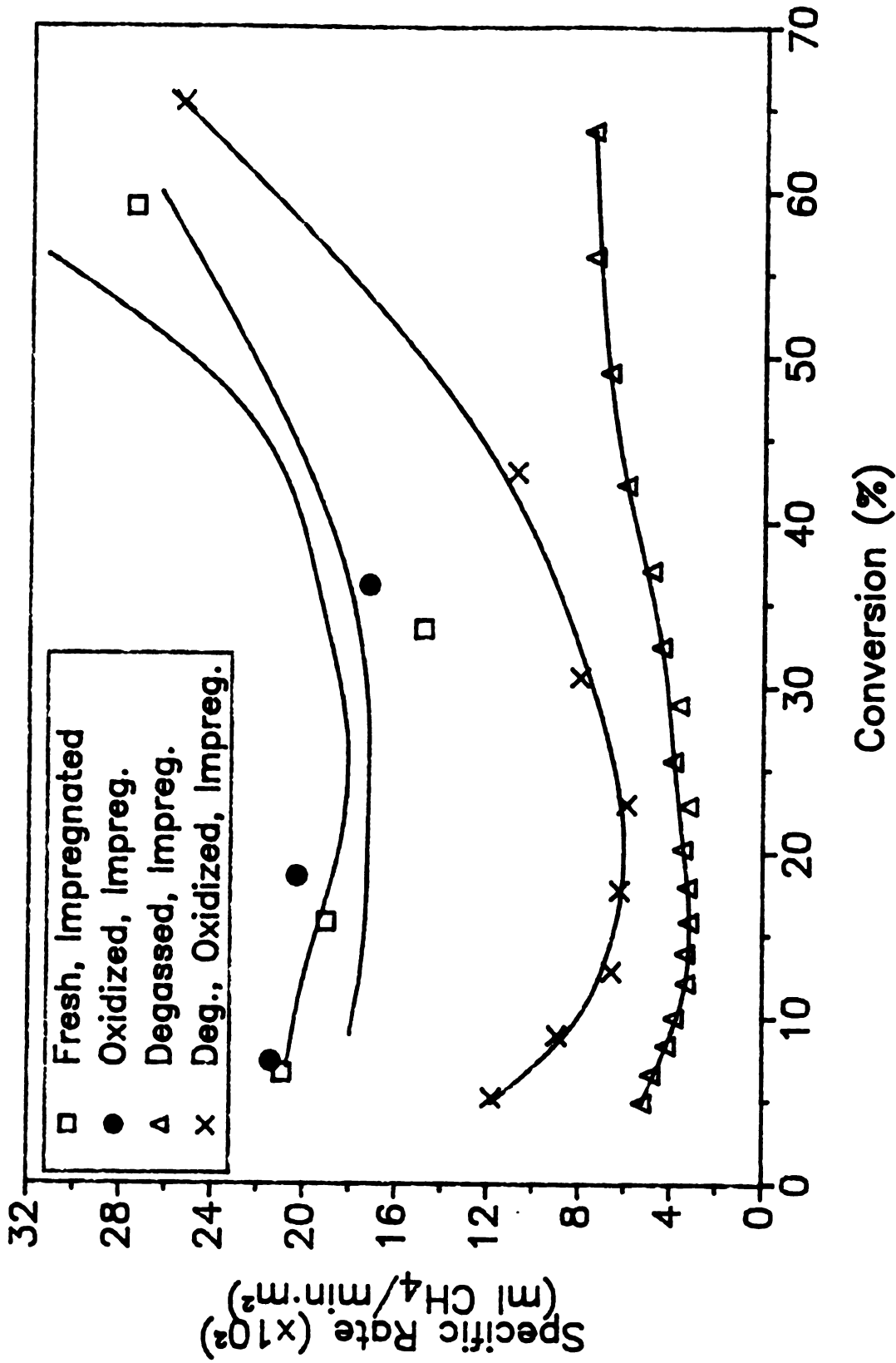


Figure 5.1. Effect of HNO₃ oxidation on reactivity of K₂CO₃-catalyzed carbon black at 865° C, 500 psig H₂, K/C= 0.02.

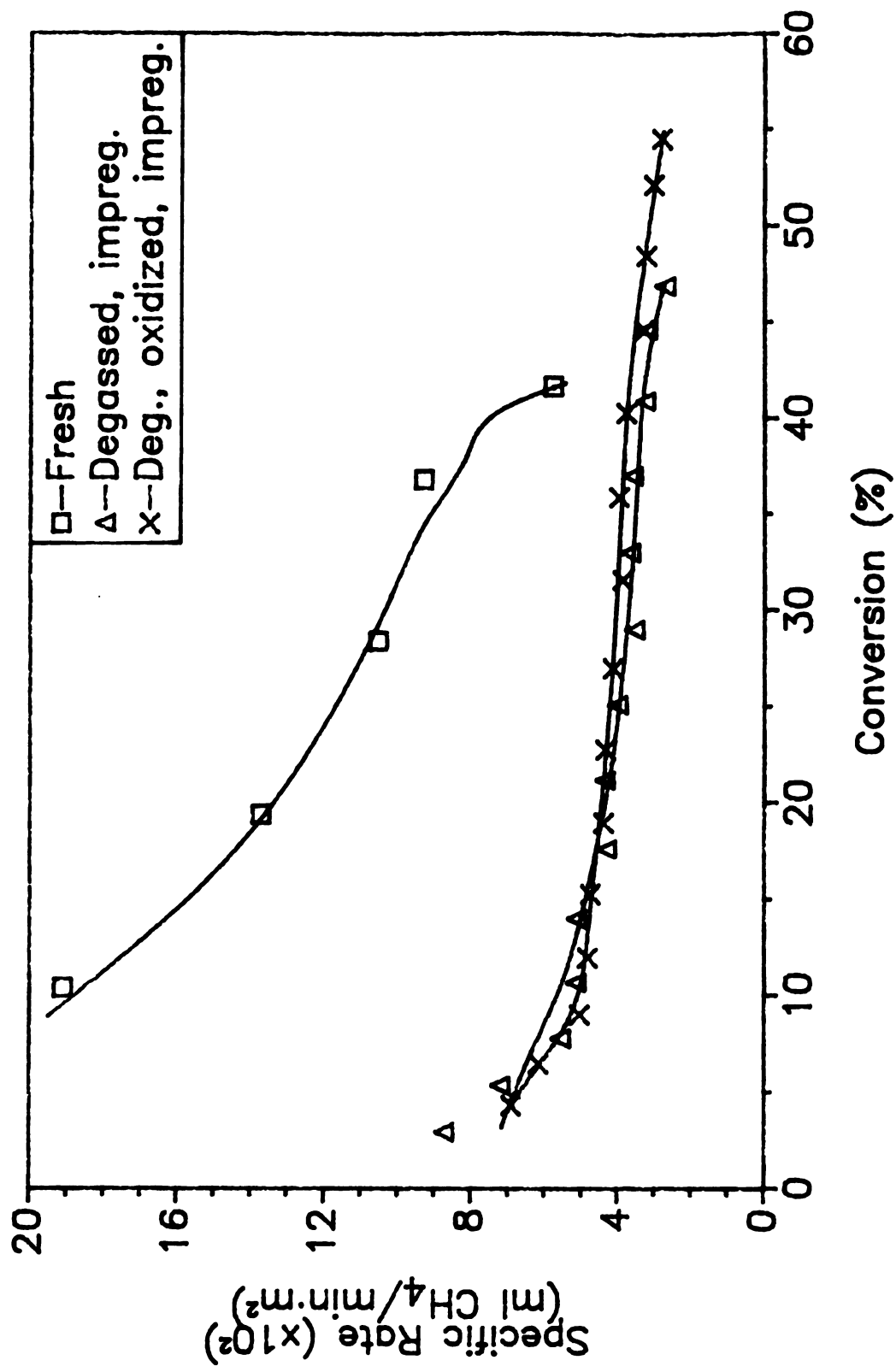


Figure 5.2. Effect of HNO₃ oxidation on reactivity of Na₂CO₃-catalyzed carbon black at 865° C, 500 psig H₂, Na/C= 0.02.

with K_2CO_3 . The rate of a degassed, oxidized sample catalyzed by Na_2CO_3 is enhanced only slightly over that of the degassed sample, similar to the uncatalyzed case. Apparently the less active Na_2CO_3 deactivates before it is able to interact to any great extent with the additional oxygen groups fixed on the surface of the carbon. This is not surprising, since it is postulated that interaction with oxygen groups on the surface of the carbon is a necessary precursor for catalytic activity.

5.2 Coconut Charcoal

The effect of pretreatment procedures on K_2CO_3 and Na_2CO_3 -catalyzed coconut charcoal gasification at $775^\circ C$ are shown in Figures 5.3 and 5.4, respectively. As in the case of carbon black, catalysts were impregnated to a loading of $M/C = 0.02$. The reaction temperature of $775^\circ C$ was chosen because the methane evolution rate was too high to be measured accurately at higher temperatures. In contrast with both carbon black and uncatalyzed coconut charcoal, degassing has no effect on the catalyzed reaction rate. Nitric acid oxidation, on the other hand, enhances the rate of fresh and degassed char catalyzed by both K_2CO_3 and Na_2CO_3 .

As in the case of carbon black, the Na_2CO_3 -catalyzed reaction rate decreases with conversion, while the K_2CO_3 -catalyzed rate increases even more drastically than for carbon black. Since the uncatalyzed rate for coconut char is constant with conversion while the rate for carbon black decreases, the enhancement factor (*i.e.*, the ratio of the catalyzed rate to the uncatalyzed rate at a given conversion) follows a similar trend with conversion for both K_2CO_3 -catalyzed carbons. In both cases the enhancement factor increases drastically

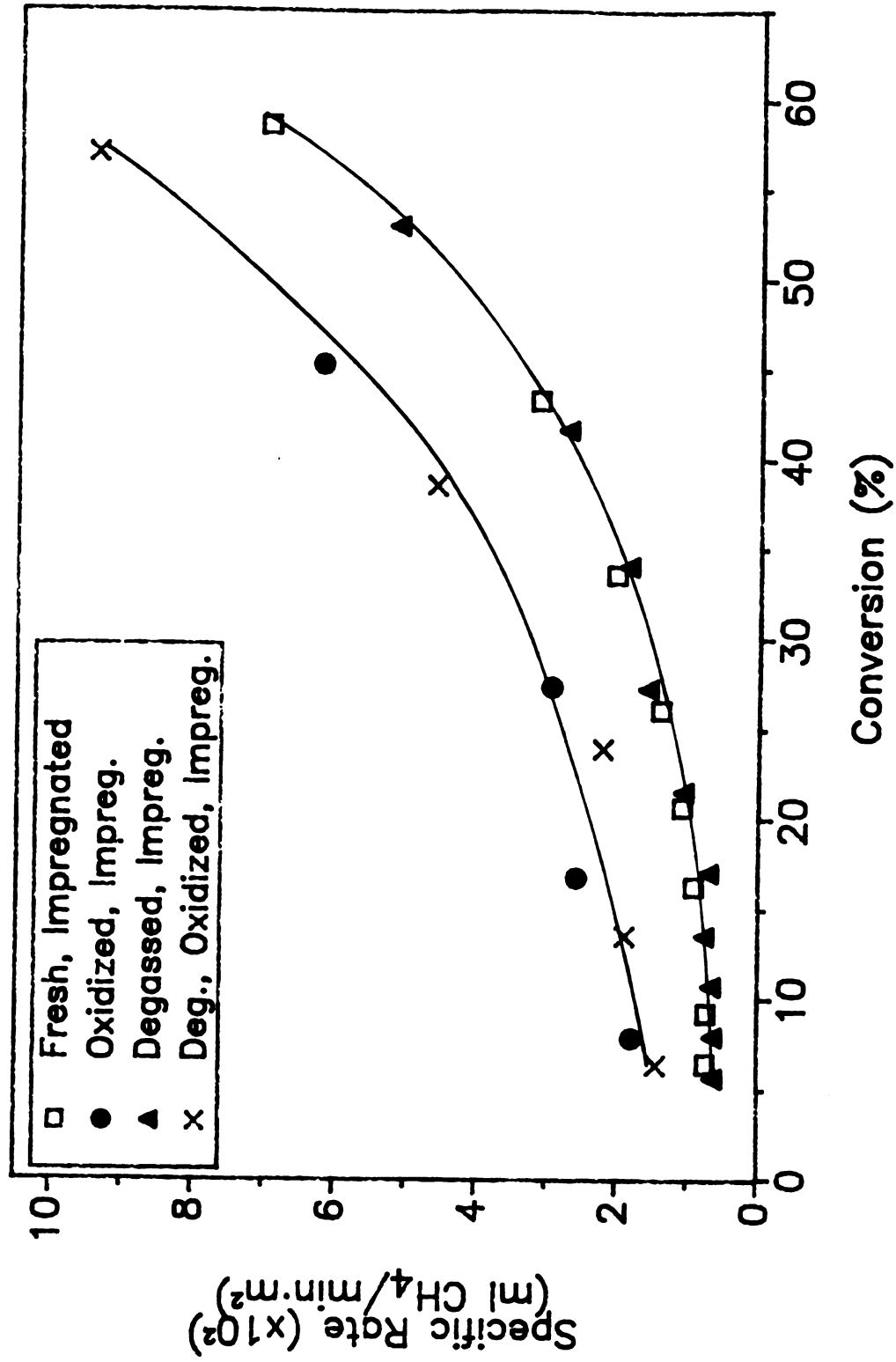


Figure 5.3. Effect of HNO₃ oxidation on reactivity of K₂CO₃-catalyzed coconut charcoal at 775°C, 500 psig H₂, K/C = 0.02.

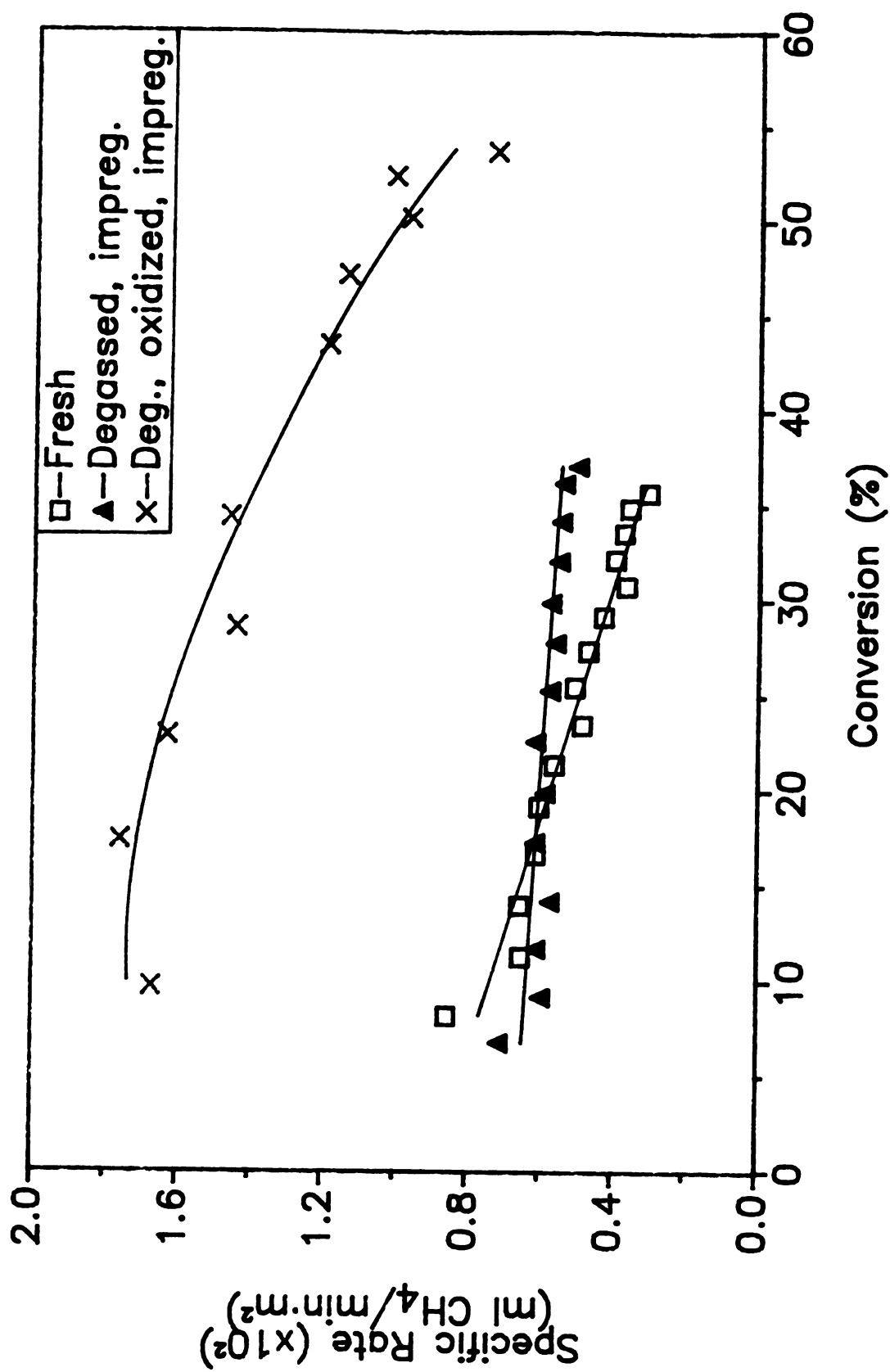


Figure 5.4. Effect of HNO₃ oxidation on reactivity of Na₂CO₃-catalyzed coconut charcoal at 775° C, 500 psig H₂, Na/C = 0.02.

with conversion, but it is not clear why this occurs. Zoheidi [16] discussed this phenomenon in considerable detail, and concluded that interaction of the catalyst with basic groups in the bulk of the carbon black caused the catalyst to become more active as the groups were exposed during gasification. Measurement of the pH of fresh and gasified coconut charcoal has not been performed, however, so it is not clear whether this explanation makes sense in the case of coconut charcoal.

5.3 Surface Analysis

5.3.1 K₂CO₃ Standard

Analysis by XPS of carbon impregnated with K₂CO₃ is complicated somewhat by the presence of a potassium x-ray satellite peak in the same location as the C(1s) peak. In addition, no information was found in the literature on the XPS spectrum of K₂CO₃. A K₂CO₃ standard was therefore prepared by the same method as carbon black samples and analyzed by XPS after heating to 200° C in the vacuum pretreatment reactor. The white sample turned a light shade of violet during the XPS analysis. The C(1s), O(1s), and K(2p) peaks are shown in Figures 5.5-5.7, respectively. The C(1s) peak clearly shows the presence of carbonate carbon at 288.7 eV and carbon contamination at 285 eV. Since there is no carbon substrate, the contamination was used as the basis for charge referencing. The validity of this assumption will be discussed in the next section when the standard is compared to a K₂CO₃-impregnated sample.

The O(1s) peak is located at 531 eV and has a FWHM of 1.9 eV, and the K(2p) peaks are located at 292.6 eV and 295.3 eV. The O/K ratio is 1.54, in good agreement with the expected value of 1.5. The potassium to carbonate

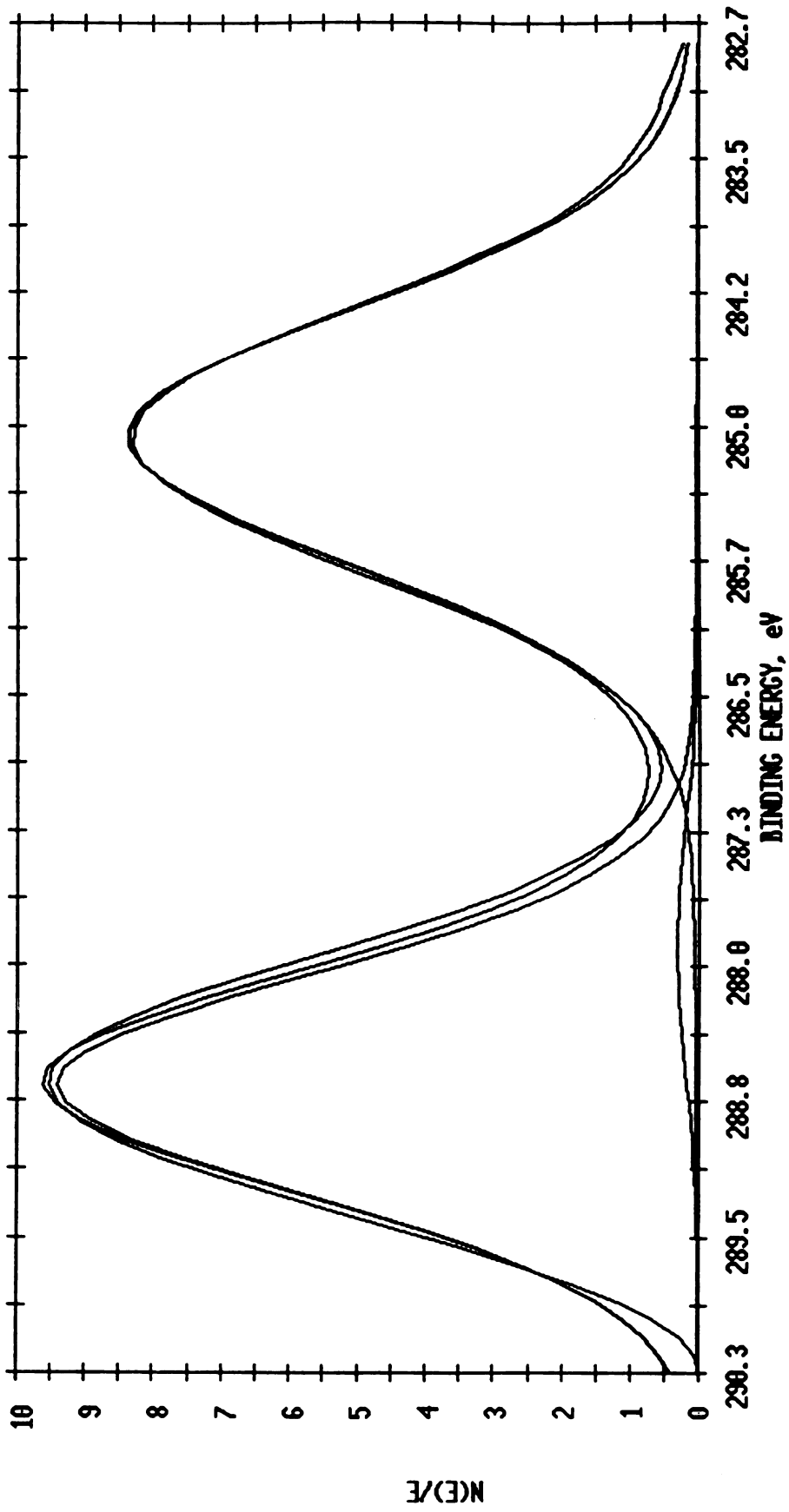


Figure 5.5. C(1s) peak of K_2CO_3 standard heated to $200^\circ C$.

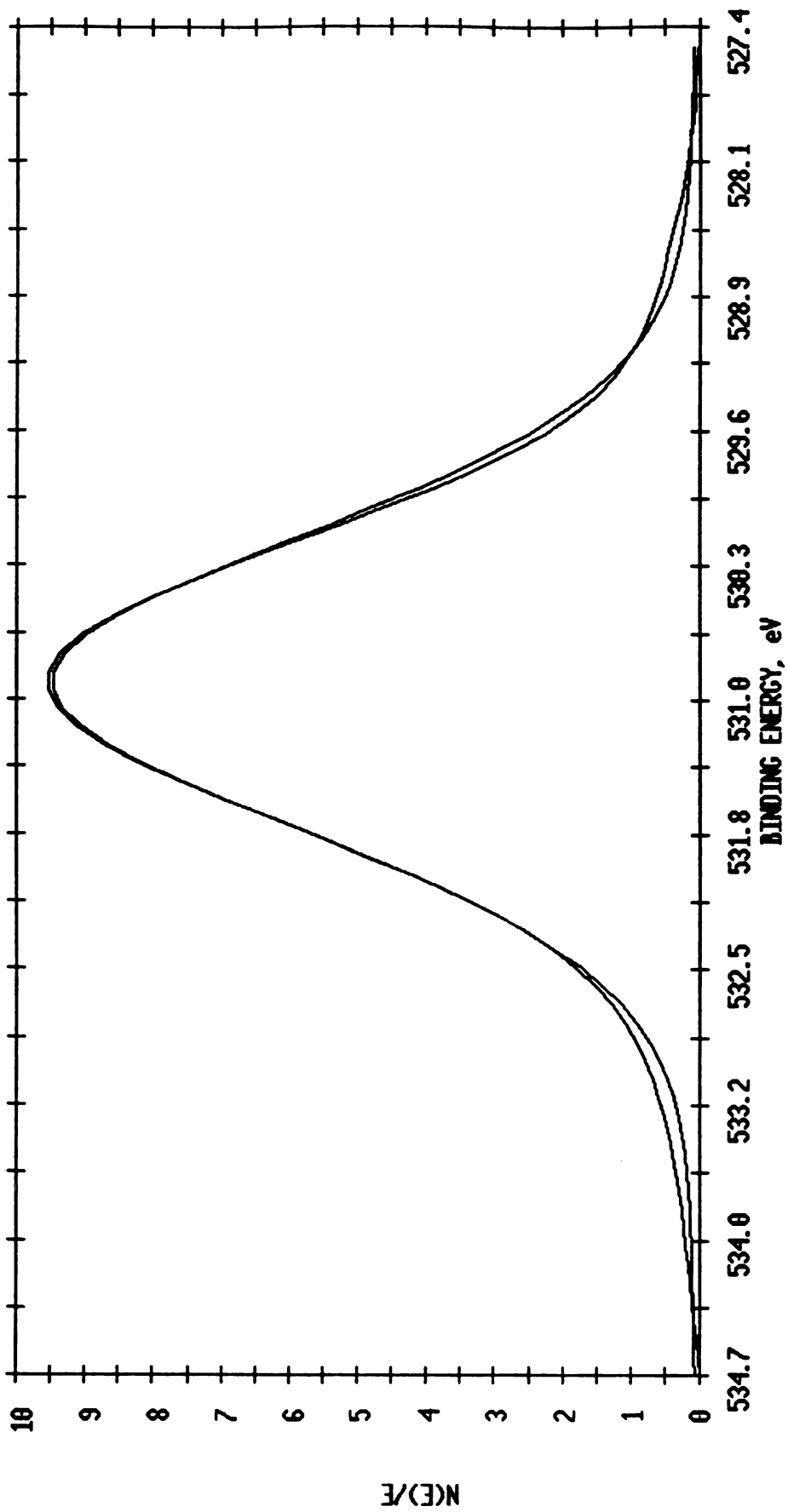


Figure 5.6. O(1s) peak of K_2CO_3 standard heated to $200^\circ C$.

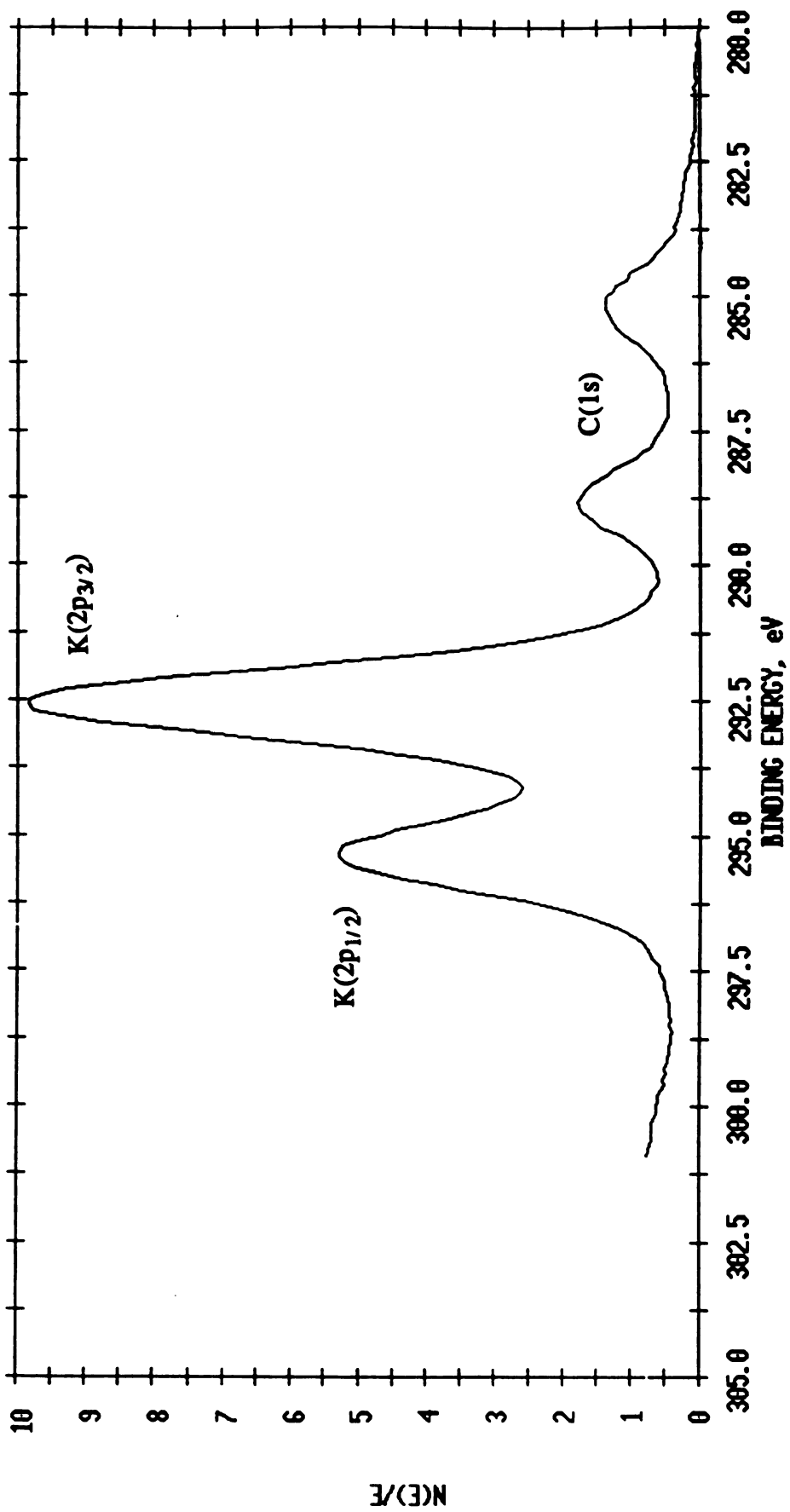


Figure 5.7. K(2p) peak of K_2CO_3 standard heated to 200° C.

carbon ratio, however, is 3.1, a value 50% higher than the expected value of 2. The close proximity of the potassium peak to the carbonate carbon peak, however, makes accurate measurement of the carbonate peak area difficult.

5.3.2 K₂CO₃-Impregnated Carbon Black

Table 5.1 contains the quantitative results from the XPS analysis of K₂CO₃-impregnated carbon black subjected to various treatments in the vacuum pretreatment reactor. Prior to treatment, the sample has an extremely high oxygen content, which suggests that there is a significant amount of adsorbed moisture on the sample. The K/C ratio is 0.01, approximately one-half the bulk value of 0.019. As the sample is heated in a vacuum, both the potassium and oxygen contents drop as the temperature is raised, while the O/K ratio increases somewhat from 2.1 to 3.5. After exposure to hydrogen at 750° C, the potassium, oxygen, and sulfur concentrations jump to levels significantly higher than the bulk concentration, while the O/K ratio drops to about 1.8. At 800° C, the potassium, oxygen, and sulfur concentrations increase by another order of magnitude relative to the carbon signal. In addition, all of the sulfur is present as oxidized sulfur in the samples exposed to hydrogen, as evidenced by a shift in the S(2p) binding energy from 164.4 eV to 170 eV. Figures 5.8 and 5.9 show the sulfur peak before and after exposure to hydrogen at 800° C. This result was not expected in a reducing environment, and suggests that interaction with the catalyst leads to the formation of sulfate groups.

Examination of the K(2p_{3/2}) peak of the catalyzed carbon black after heating reveals that the peak position does not match with that of the K₂CO₃ standard by about 1.9 eV. This suggests the assumption that placement of the carbon contamination peak of the standard at 285 eV is not valid. Therefore, the peaks of the standard are referenced to the K(2p_{3/2}) peak of the catalyzed

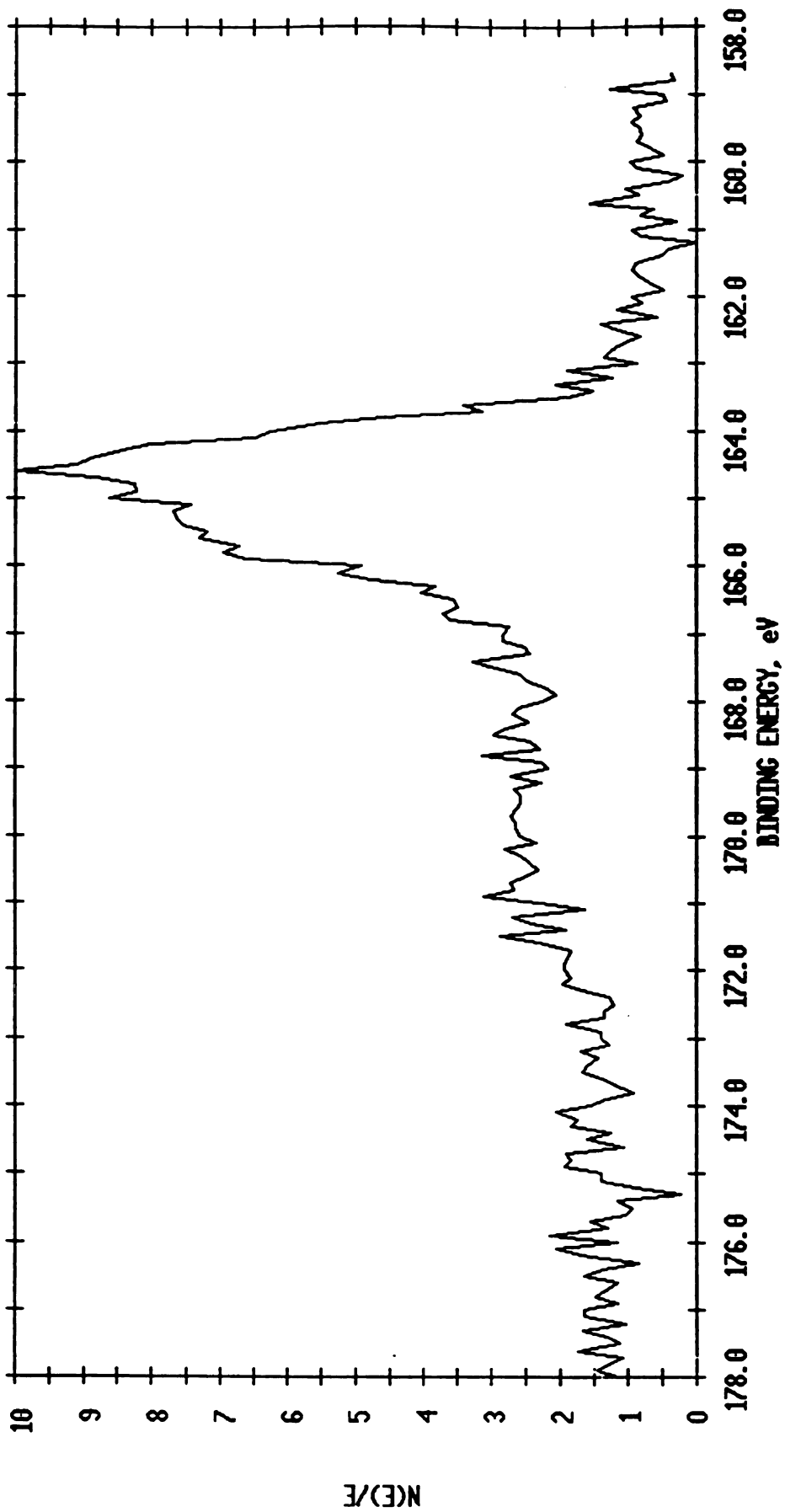


Figure 5.8. S(2p) peak of untreated K_2CO_3 -impregnated carbon black.

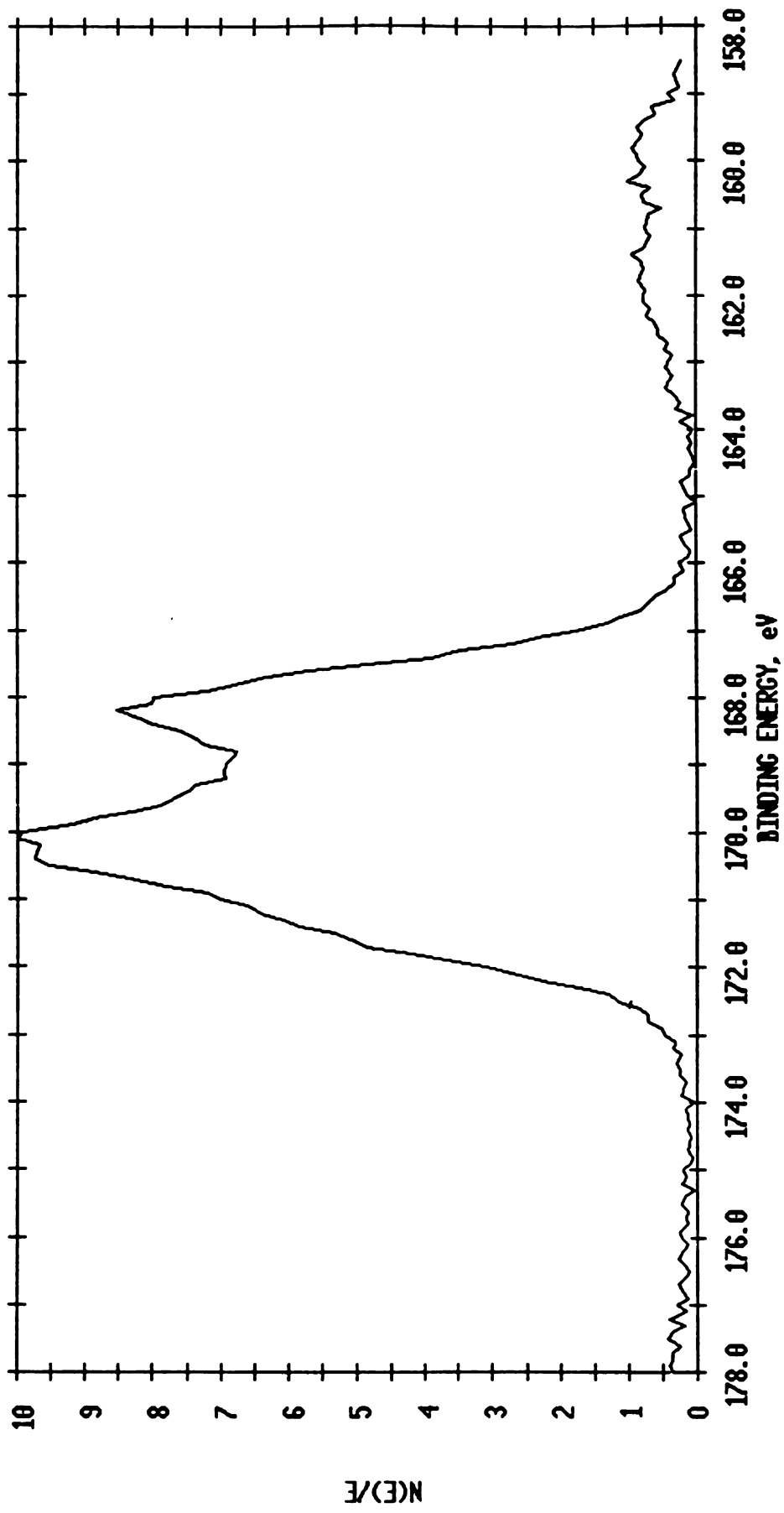


Figure 5.9. S(2p) peak of K_2CO_3 -impregnated carbon black after exposure to H_2 at $800^\circ C$, 1 atm.

Table 5.1. XPS Results for K₂CO₃-impregnated Carbon Black.

Treatment	O/K	O/C (x10)	K/C (x10)	K(2p _{3/2}) (eV)	S/C (x10)
None	9.0	0.94	0.10	293.9	0.087
200° C	2.1	0.48	0.23	294.3	0.085
500° C	2.8	0.23	0.08	294.6	0.077
750° C	3.5	0.19	0.06	294.6	0.071
750° C, H ₂	1.7	2.3	1.4	294.5	0.26
750° C, H ₂	1.9	6.3	3.3	294.3	0.42
800° C, H ₂	1.9	100	54	294.7	22
10% Gasified	4.8	0.57	0.12	294.0	0.015

carbon sample. This means the K(2p_{3/2}) peak of the standard is located at 294.5 eV, the carbonate carbon peak is at 290.6 eV, and the O(1s) peak is at 532.9 eV. The uncertainty in these values is about ±0.2 eV. Based on the assumption of a 1.5 eV shift for each bond to carbon, the carbonate carbon peak should be at 291 eV, in fairly good agreement with the standard.

It is not clear why the potassium peak is located approximately 0.6 eV higher in the samples treated in the vacuum pretreatment reactor compared to untreated samples. Yokoyama, *et al.* [71] attributed a similar shift to the presence of elemental potassium at 650° C, but this would certainly not be expected to happen already at 200° C, or even to any great extent at 500° C. Since water of hydration, if present, would be bound to the potassium, it is possible that the shift is due to the removal of water.

As in the case of uncatalyzed carbon black, the shape and position of the O(1s) peak provides little unambiguous information about the chemical nature of the carbon surface. Since the oxygen peak of the standard was located at 532.9 eV, one component of the curve fit for the catalyzed carbon black oxygen peak was placed there. In addition, peaks at lower and higher binding energies were also required for a good fit. The O(1s) peaks and the results of the curve fits are

shown in Appendix B. Comparison of the oxygen peaks of the catalyzed and uncatalyzed samples shows that oxygen on the uncatalyzed carbon also has a significant component at 532.9 eV. Thus it is impossible to distinguish between carbonate and various other forms of oxygen on the carbon based on the position of the oxygen peak alone.

The large chemical shift of the carbonate carbon peak was evident, however, in the case of catalyzed carbon black exposed to hydrogen at 750° C and 800° C. The C(1s) peak from the 800° C experiment is shown in Figure 5.10. It clearly shows the presence of carbonate carbon at 290 eV, compared to the peak at 290.6 eV for the standard. A significant portion of the C(1s) peak is also shifted 1.5-2 eV, strong evidence of the presence of oxygen singly bonded to the carbon.

These spectra suggest that a large portion of the catalyst is still present in the carbonate form. Saber, *et al.* [27] found that only approximately half of the K_2CO_3 decomposed at 750° C, and that a temperature of about 800° C was required to decompose all of the carbonate. With a compressed carbon black pellet, however, a ten weight percent catalyst loading may provide more catalyst on the pellet surface than there are available carbon sites. Excess catalyst would then remain in the carbonate form.

The presence of a shoulder at 286.5 eV for the 750° C sample and at 287 eV for the 800° C sample indicates the presence of singly bonded oxygen, possibly due to the formation of active K-O-C groups. In both experiments, however, the O/K ratio was greater than the theoretical carbonate ratio of 1.5. One possible explanation is that the catalyst stabilizes the oxygen groups already present on the surface of the carbon that would be desorbed in the absence of catalyst. Another possibility is that a few percent of metal oxides are contaminating the

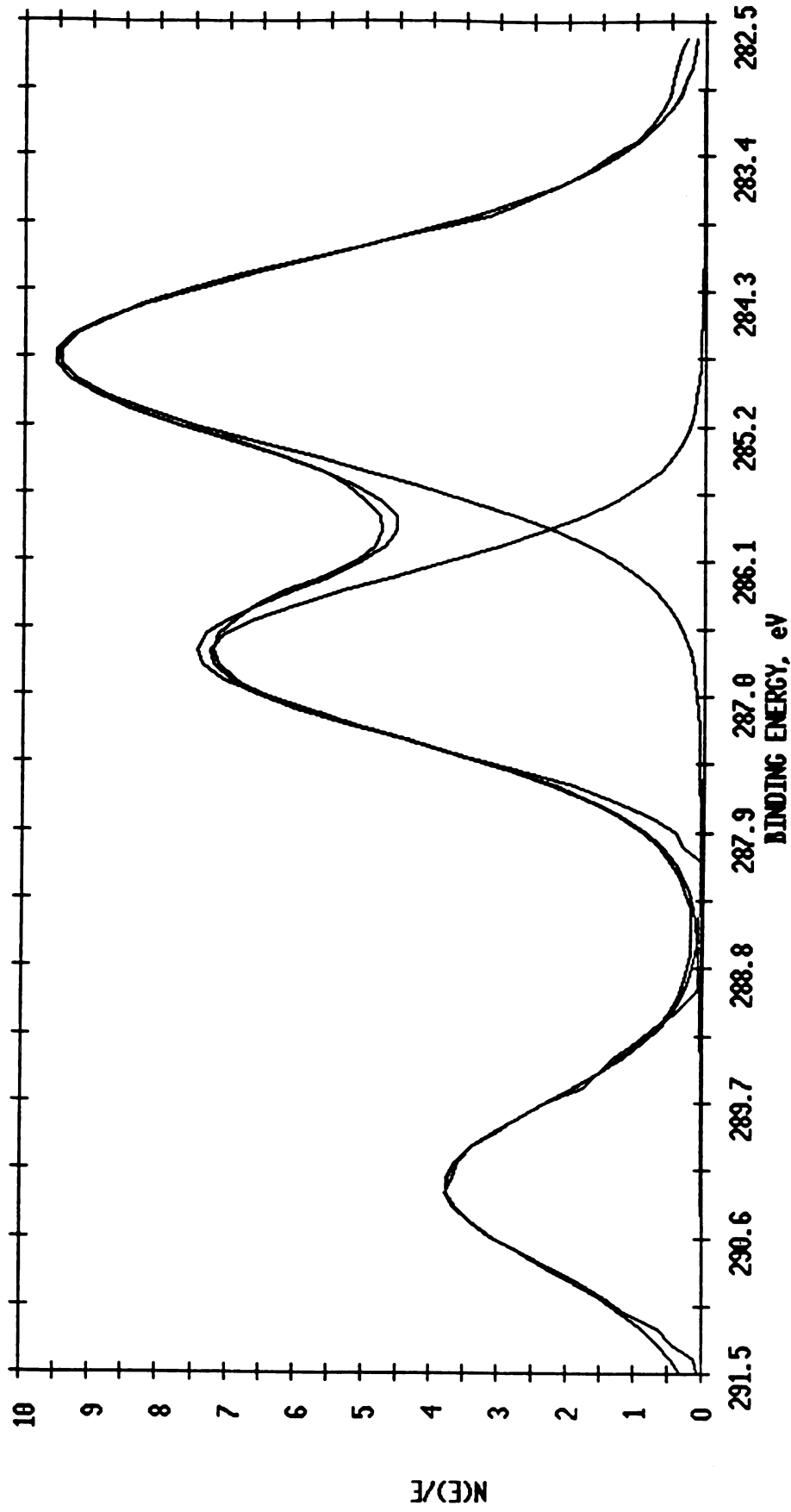


Figure 5.10. C(1s) peak of K₂CO₃-impregnated carbon black exposed to H₂ at 800° C, 1 atm.

surface, resulting in high apparent oxygen contents. No significant metal peaks were seen in the XPS survey scan, however.

The results of most of the investigators mentioned in Chapter 1 have indicated that decomposition of the catalyst to form active groups occurs at relatively low temperatures and should be independent of exposure to hydrogen. This was not observed by XPS in the present experiments because the initial carbonate carbon to bulk carbon ratio is too low to observe any changes in the catalyst prior to exposure to hydrogen and partial gasification of the carbon black pellet.

5.4 Discussion

5.4.1 Gasification Results

The results in Figures 5.1 and 5.2 for carbon black, and Figures 5.3 and 5.4 for coconut char, suggest that neutral and basic groups (carbonyl and pyrone/chromene) interact with K_2CO_3 , and to a lesser extent, Na_2CO_3 , resulting in catalytic enhancement of the reaction rate. This is in contrast to uncatalyzed hydrogen gasification, in which acidic groups are postulated to be responsible for the formation of active sites. Hydrogen gasification of degassed carbon black, which contains only stable basic groups presumably arising from bulk oxygen [16], is strongly catalyzed by both K_2CO_3 and Na_2CO_3 . Oxidation by HNO_3 , which fixes acidic and basic groups in the surface [8], further enhances the catalyst activity. Partial combustion at $400^\circ C$, which fixes acidic groups on the surface, does not enhance the the K_2CO_3 -catalyzed gasification rate of degassed carbon black [16], indicating that nascent sites formed by desorption of acidic groups do not interact with the catalyst to enhance the reaction rate.

Partial combustion at 800° C, which fixes basic groups on the surface, was shown to enhance the catalyzed reaction rate.

For coconut charcoal, there is essentially no difference in the catalyzed gasification rate of fresh and degassed samples. This indicates that acidic surface groups desorbed during degassing are not important for the catalytic reaction. Instead, it appears that basic groups arising from bulk oxygen, which are not affected by degassing, interact with the catalyst. Oxygen provided by the catalyst also undoubtedly plays a role, since degassed carbon black samples with very little bulk oxygen are still strongly catalyzed. Nitric acid oxidation, which results in a significant increase in all types of oxygen groups, also results in a significant enhancement of the catalyzed rate. A set of pH measurements of coconut charcoal similar to those performed by Zoheidi [16] on carbon black would help to support this postulate.

5.4.2 XPS Results

The quantitative XPS results indicate the presence of a catalyst-rich layer with high oxygen content at the surface of the pellet after exposure to hydrogen at atmospheric pressure. As discussed in Chapters 1 and 3, K_2CO_3 agglomeration is not expected under these conditions. Yokoyama, *et al.* [71] found that the potassium and oxygen signals increased after exposure to CO_2 at 650° C or O_2 at room temperature. The signals decreased upon evacuation at 650° C, with a concurrent shift in the potassium peak of about 1 eV. They attributed this effect to a redox cycle where K_2CO_3 is reduced by the carbon to K_2O at high temperature in a vacuum, and is then reduced further by the carbon to elemental potassium, resulting in a binding energy shift. The potassium then sinks into the bulk carbon, resulting in a decrease in the XPS signal. The potassium is then reoxidized to K_2O in the presence of CO_2 or O_2 .

This explanation has been shown to be at least partially invalid in the sense that intercalation compounds of the sort implied by the authors have been shown to be unstable under reaction conditions [25,26]. Saber, *et al.* [28] have, however, postulated that elemental potassium is part of the catalytic cycle and can be strongly bound to carbon. In addition to the evidence that intercalation compound are unstable, a redox cycle would not be supported in the presence of hydrogen. Based on the XPS evidence, it is therefore postulated that the phenomena observed here are not the result of metallic potassium formation. The apparent presence of large amounts of carbonate on the surface supports this hypothesis, and the 0.6 eV shift in the potassium peak can be explained by the removal of water of hydration. Metallic potassium is undoubtedly formed under gasification conditions, and is probably the primary mode of catalyst loss, but it was not observed in the XPS experiments.

The buildup of a catalyst layer at the surface upon exposure to hydrogen suggests that several atomic layers of carbon are being gasified, leaving a layer of catalyst behind on the surface of the pellet. In addition, oxidized sulfur is also bound to the surface, possibly by interaction with the catalyst to form K_2SO_4 . This is in contrast to uncatalyzed gasification, where sulfur would be expected to desorb as H_2S [16]. For the catalyzed reaction at high hydrogen pressure, any sulfur compounds such as K_2S or K_2SO_4 would likely react further with hydrogen to form H_2S , and thus sulfur would not be expected to play a role [16].

Gasification of a powder sample would also tend to prevent the formation of a catalyst layer at the nonporous surface of the pellets compressed at extremely high pressures and used for XPS analysis. Gasification would proceed more or less uniformly throughout the bed, rather than only at the surface of the compressed pellet, allowing the catalyst to remain dispersed. These hypotheses were confirmed by analyzing a sample partially gasified in high

pressure hydrogen by XPS. The catalyst was highly dispersed, and virtually no sulfur was present on the surface, as shown in Table 5.1.

The nature of the interaction between surface carbonyl and basic groups and the catalyst is not yet understood. The use of XPS on catalyzed carbon has provided little useful information on this subject thus far, although the presence of carbon singly bound to oxygen strongly suggests that formation of K-O-C groups is occurring. It is possible that surface oxidation simply allows the catalyst to better wet and disperse on the carbon during hydrogen gasification. It has been observed that surface oxygen stabilizes catalyst on the surface during gasification. Catalyst loss experiments [16] indicate that loss is more rapid for degassed samples than fresh carbon and slower for samples oxidized by partial combustion than for fresh. Stabilizing of catalyst alone, however, does not necessarily enhance the reaction rate, as shown by Zoheidi [16]. Finally, it is possible that surface oxygen may participate in one of the M-O-C surface oxides postulated as an active catalyst form.

In summary, the treatments performed in this chapter do affect the performance of the catalyst, demonstrating the importance of oxygen in the catalyzed hydrogen gasification reaction. The nature of the interaction between the catalyst and the carbon and/or oxygen groups on the surface of the carbon has yet to be clarified. As discussed in Chapters 1 and 3, the difference between K_2CO_3 and Na_2CO_3 can be explained by a weaker interaction of the Na_2CO_3 with the carbon and/or oxygen groups on the surface of the carbon.

Chapter 6

Conclusions and Recommendations

6.1 Uncatalyzed Gasification

The gasification and XPS results presented in Chapter 4 demonstrate that a strong correlation does exist between the initial surface oxygen content and the initial hydrogen gasification rate of both carbon black and coconut charcoal. Surface analysis shows that oxygen is not present on the carbon under reaction conditions, providing direct evidence that the oxygen groups participate indirectly in gasification by desorbing and forming nascent active sites.

Based on these observations, a general mechanism for hydrogen gasification similar to those proposed for steam and carbon dioxide gasification is postulated. First, oxygen groups on the carbon surface desorb as CO or CO₂ to form active carbon sites.





The concentration of C(O) and C(O)₂ on the surface of the carbon, and hence the number of active sites, can be increased or decreased to various degrees depending on the pretreatment procedures used. Oxidation increases the number of active sites on the carbon surface, while degassing anneals the active sites formed from C(O) and C(O)₂ desorption.

Hydrogen gasification then proceeds at active sites under the proper conditions of high temperature and hydrogen pressure, most likely by the two-step hydrogenation of active sites proposed by several investigators.



The role of oxidation is therefore to increase the number of active sites for hydrogen gasification to occur, not to change the fundamental reaction process.

Propagation of active sites must also be occurring, since rate enhancement by oxidation persists to moderately high conversions before decaying to approximately the same rate as an untreated sample. This effect may be related to the tendency for oxygen to attack edge sites in a different manner than hydrogen, rendering the surface more active for subsequent gasification by hydrogen. Thus, there is some probability that Reaction 6-2 will result in either an active or deactivated site, depending to some extent on the degree of structural order in the carbon.

As discussed in Chapter 1, dissociative adsorption of hydrogen (Equation 1-7) occurs at low hydrogen pressures and blocks the active sites (C_f), thus inhibiting the steam gasification reaction. This could also explain why hydrogen gasification requires high hydrogen pressures to proceed at an appreciable rate. Hydrogen gasification may be self-inhibiting at low pressures, as dissociatively adsorbed hydrogen blocks active sites and prevents rapid methane formation via two-step hydrogenation.

This general mechanism does not attempt to address the complicated processes that are most likely occurring on the surface of the carbon. It is postulated that desorption of oxygen groups as CO or CO₂ either opens or destabilizes the ring structure of the carbon, thus rendering the surrounding carbon atoms more susceptible to subsequent gasification. In addition, not all active sites necessarily have equal reactivity, depending on the oxygen groups from which they were formed and the local carbon structure.

Differences in enhancement of uncatalyzed gasification via oxidation by O₂ and HNO₃ can be explained by two factors: oxygen is able to remove annealed sites and access fresh surface area, and the proportion of oxygen groups which form active sites is postulated to be higher for O₂ than for HNO₃. Comparison of the results of oxidation by HNO₃ and O₂ also lends support to the previously set forth postulate [16] that desorption of acidic groups on the surface of carbon creates nascent active sites responsible for enhancement of the uncatalyzed reaction rate. Basic groups from the bulk carbon are proposed to form much less active sites and to thus be responsible for the low residual activity of degassed carbons.

Carbon structure also plays an important role in determining the effectiveness of pretreatment procedures. For graphitic carbon black, surface annealing of active sites during degassing most strongly affects gasification

activity, with oxidation having a lesser effect. This results from the fact that most oxygen and thus most active sites are initially on the surface of the carbon black particles. Once these sites are eliminated, gasification is slowed. This effect is most noticeable in the data for uncatalyzed carbon black gasification, where the rate is initially very high and then decays rapidly.

For uncatalyzed coconut charcoal, degassing and HNO_3 oxidation have opposite effects of about the same magnitude. The high bulk oxygen content makes initial removal of surface oxygen during degassing relatively unimportant. The amorphous structure allows extensive oxidation which facilitates an increase in the gasification rate. In other words, the ASA/TSA ratio for oxidation is much higher for coconut char than for carbon black. This suggests that preoxidation of coal prior to gasification in order to enhance the reaction rate has commercial potential. The properties of coal char should be more similar to those of the coconut char than those of the carbon black derived from partial combustion of petroleum residues.

The use of XPS to gain qualitative information about the nature of oxygen groups on the surface of carbon has thus far been unsuccessful. Much longer counting times and many replicates are necessary in order to determine whether differences in the position of the O(1s) peak, which are characteristic of differences in surface groups, can be detected after treatment procedures. Variations in the shape of the C(1s) peak have been noted, but the changes were too small to make any conclusions about the nature of oxygen groups on the surface. The use of software to account for asymmetry in the carbon peak may provide results that correlate better with the results for total oxygen. By determining the asymmetric factor for a carbon with little or no surface oxygen, subsequent curve fitting to determine the area of the shifted carbon peaks may indeed give results that are proportional to the value for total oxygen.

6.2 Catalyzed Gasification

The results in Chapter 3 demonstrate that the characteristics of alkali-catalyzed hydrogen gasification are very similar to those of steam and carbon dioxide gasification. Catalyst activity increases with increasing cation size, reaching saturation at an M/C ratio of approximately 0.1. The catalytic effect is very strong, enhancing the reaction rate by a factor of approximately 200 at 725° C. The catalyst initially becomes highly dispersed on the carbon under reaction conditions, indicating the method of catalyst addition is relatively unimportant.

Because of the aforementioned similarities, it is proposed that the same active species which are responsible for catalysis of steam and carbon dioxide gasification are also responsible for catalysis of hydrogen gasification. The presence of a C(1s) peak shifted 1.5-2 eV from the bulk carbon peak after exposure to hydrogen is tentatively assigned to the presence of K-O-C groups postulated to catalyze steam and carbon dioxide gasification. Thus the primary difference in hydrogen is the inability of the hydrogen environment to support a catalyst redox cycle. In steam or carbon dioxide, there is some probability that Reaction 1-12 will occur, regenerating the active form of the catalyst. In hydrogen, the probability of Reaction 1-13 occurring is much greater, because no oxygen is present in the reactant gas to regenerate reduced catalyst species. This results in catalyst loss which is much higher in hydrogen gasification than in oxidizing environments.

Oxidation with HNO₃ moderately enhances the reactivity of catalyzed carbon black and coconut charcoal. The results support the postulate of Zoheidi [16] that the catalyst interacts with basic groups on the surface of the carbon to enhance the reactivity. He showed that oxidation by partial combustion at

400° C fixes predominantly acidic groups on the surface and does not enhance the catalyzed reaction rate. Partial combustion at 800° C fixes predominantly basic groups on the surface and was shown to enhance the catalyzed reaction rate. Oxidation with HNO₃ fixes both acidic and basic groups on the surface, thus moderately enhancing the catalyzed reaction rate.

XPS experiments have shown evidence of several phenomena which would not be expected to occur under normal, high pressure gasification conditions. These include gasification of the carbon black pellet from the top surface only, with formation of a residual catalyst layer on the surface. In addition, sulfur is retained on the surface by formation of species tentatively identified as K₂SO₄. The observation of these phenomena demonstrates the need for care in making comparisons between effects observed in the vacuum pretreatment reactor and those observed in the high pressure gasification reactor. It also leads to the recommendation that an extremely pure carbon with both ash and low oxygen contents be used for the study of catalyst-carbon interactions.

The results for catalyst O/K ratio were quite high even after exposure to hydrogen at 800° C. The value for O/K of about 1.8 does not compare well with that of any postulated active species on the surface, and is even too high if all of the catalyst remained in the carbonate form. The close proximity of the C(1s) peak to the K(2p) peak could be affecting the accuracy of the results, but not enough to explain the extremely high O/K ratio. The use of AES instead of XPS should eliminate the interference between the two peaks and show whether the quantitative XPS results for catalyzed samples are accurate.

LIST OF REFERENCES

List of References

- [1] Tomita, A. and Y. Tamai, *J. Catal.*, **27**, 293 (1972).
- [2] Taylor, H.S. and H.A. Neville, *J. Am. Chem. Soc.*, **43**, 2065 (1921).
- [3] Epperly, W.R. and H.M. Siegel, *11th Intersoc. Energy Conv. Eng. Conf., Proc. Am. Soc. Mech. Eng.*, 249 (1976).
- [4] Moulijn, J.A. and F. Kapteijn, "Carbon and Coal Gasification", *NATO ASI Series, E*, **105**, 181 (1986).
- [5] Rivin, D., *Rubber Chem. Technol.*, **35**, 729 (1962).
- [6] McKee, D.W. and V.J. Mimeault, *Chemistry and Physics of Carbon*, Dekker, New York, **8**, 151 (1973).
- [7] Hart, P.J., F.J. Vastola and P.L. Walker, Jr., *Carbon*, **5**, 363 (1967).
- [8] Nemerovets, N.N., V.F. Surovikin, S.V. Orekhov, G.V. Sazhin and N.G. Sadovnichuk, *Solid Fuel Chem.*, p. 104 (1980).
- [9] Proctor, A. and P.M.A. Sherwood, *Carbon*, **21**, 53 (1983).
- [10] Koszowski, C. and P.M.A. Sherwood, *J. Chem. Soc. Faraday Trans. I*, **80**, 2099 (1984).
- [11] Voll, M. and H.P. Boehm, *Carbon*, **9**, 481 (1970).
- [12] Barton, S.S. and B.H. Harrison, *Carbon*, **13**, 283 (1975).
- [13] Papirer, E., S. Li and J.-B. Donnet, *Carbon*, **25**, 243 (1987).
- [14] Otake, Y. and R.G. Jenkins, *ACS Div. Fuel Chem. Prepr.*, **32(1)**, 310 (1987).

- [15] Marchon, B., J. Carrazza, H. Heinemann and G.A. Somorjai, *Carbon*, **26**, 507 (1988).
- [16] Zoheidi, H., *Ph.D. Dissertation*, Michigan State University, East Lansing, MI (1987).
- [17] Phillips, R., F.J. Vastola and P.L. Walker, Jr., *Carbon*, **8**, 197 (1970).
- [18] Giberson, R.C. and P.L. Walker, Jr., *Carbon*, **3**, 521 (1966).
- [19] Keleman, S.R. and H. Freund, *ACS Div. Fuel Chem. Prepr.*, **32(1)**, 318 (1987).
- [20] Keleman, S.R. and H. Freund, *Carbon*, **23**, 723 (1985).
- [21] Jalan, B.P. and Y.K. Rao, *Carbon*, **16**, 175 (1978).
- [22] McKee, D.W. and D. Chatterji, *Carbon*, **16**, 53 (1978).
- [23] Wen, W.Y., *Catal. Rev. Sci. Eng.*, **22**, 1 (1980).
- [24] Rao, Y.K., A. Adjorlolo and J.H. Haberman, *Carbon*, **20**, 207 (1982).
- [25] Tromp, P.J.J. and E.H.P. Cordfunke, *Thermochim. Acta*, **77**, 49 (1984).
- [26] Mims, C.A. and J.K. Pabst, *Proc. Int. Conf. Coal Sci.*, Verlag Gluckauf GmbH, Essen, 730, (1981).
- [27] Saber, J.M., J.L. Falconer and L.F. Brown, *J. Catal.*, **90**, 65 (1984).
- [28] Saber, J.M., J.L. Falconer and L.F. Brown, *Fuel*, **65**, 1356 (1986).
- [29] Saber, J.M., K.B. Kester, J.L. Falconer and L.F. Brown, *J. Catal.*, **109**, 329 (1988).
- [30] Cerfontain, M.B., F. Kapteijn and J.A. Moulijn, *Carbon*, **26**, 41 (1988).
- [31] Cerfontain, M.B., R. Meijer, F. Kapteijn and J.A. Moulijn, *J. Catal.*, **107**, 173 (1987).

- [32] Mims, C.A. and J.K. Pabst, *J. Catal.*, **107**, 209 (1987).
- [33] Keleman, S.R., H. Freund and C.A. Mims, *J. Catal.*, **97**, 228 (1986).
- [34] Keleman, S.R. and H. Freund, *J. Catal.*, **102**, 80 (1986).
- [35] Randall, M. and A. Mohammad, *Ind. Eng. Chem.*, **21**, 1048 (1929).
- [36] Redmond, J.P. and P.L. Walker, Jr., *J. Phys. Chem.*, **64**, 1093 (1960).
- [37] Bansal, R.C., F.J. Vastola and P.L. Walker, Jr., *Carbon*, **12**, 355 (1974).
- [38] Blackwood, J.D., *Aust. J. Chem.*, **12**, 14 (1959).
- [39] Blackwood, J.D., *Aust. J. Chem.*, **15**, 397 (1962).
- [40] Blackwood, J.D. and D.J. McCarthy, *Aust. J. Chem.*, **19**, 797 (1966).
- [41] Cao, J.-R. and M.H. Back, *Carbon*, **20**, 505 (1982).
- [42] Zielke, C.W. and E. Gorin, *Ind. Eng. Chem.*, **47**, 820 (1955).
- [43] Anthony, D.B. and J.B. Howard, *AICHE J.*, **22**, 625 (1976).
- [44] Tomita, A., O.P. Mahajan and P.L. Walker, Jr., *Fuel*, **56**, 137 (1977).
- [45] Makino, M. and Y. Toda, *Fuel*, **60**, 321 (1980).
- [46] Mühlen, H.-J., K.H. van Heek and H. Jüntgen, *Fuel*, **65**, 591 (1986).
- [47] Gulbransen, E.A., K.F. Andrew and F.A. Boassart, *J. Electrochem. Soc.*, **112**, 49 (1965).
- [48] Gill, P.S., R.E. Toomey and H.C. Moser, *Carbon*, **5**, 43 (1967).
- [49] Wood, B.J. and H. Wise, *J. Phys. Chem.*, **73**, 1348 (1969).
- [50] Yang, R.T. and R.Z. Duan, *Carbon*, **23**, 325 (1985).
- [51] Casanova, R., A.L. Cabrera, H. Heinemann and G. Somorjai, *Fuel*, **62**, 1138 (1983).

- [52] Cao, J.-R. and M.H. Back, *Carbon*, **23**, 141 (1985).
- [53] Gardner, N., E. Samuels and K. Wilks, *ACS Adv. in Chem. Ser.*, **131**, 209 (1974).
- [54] Walker, P.L. Jr., S. Matsumoto, T. Hanzawa, T. Miura and I.M.K. Ismail, *Int. Symp. on Fund. Cat. Coal and Carbon Gas.*, Amsterdam, p.11 (1982).
- [55] Kokorotsikos, P.S., G.G. Stavropoulos and G.P. Sakellaropoulos, *Fuel*, **65**, 1462 (1986).
- [56] Cypres, R., M. Ghodsi and D. Feron, *Thermochim. Acta*, **81**, 105 (1984).
- [57] Mims, C.A. and J.J. Krajewski, *J. Catal.*, **102**, 140 (1986).
- [58] Keleman, S.R., H. Freund, *ACS Div. Fuel. Chem. Prepr.*, **33(4)**, 706 (1988).
- [59] McKee, D.W. and D. Chatterji, *Carbon*, **13**, 31 (1975).
- [60] Huhn, F., J. Klein and H. Jüntgen, *Fuel*, **62**, 196 (1983).
- [61] Kapteijn, F., G. Abbel and J.A. Moulijn, *Fuel*, **63**, 1036 (1984).
- [62] Mims, C.A. and J.K. Pabst, *Fuel*, **62**, 176 (1983).
- [63] Sams, D.A., T. Talverdian and F. Shadman, *Fuel*, **64**, 1208 (1985).
- [64] Hftinger, K.J. and R. Minges, *Fuel*, **64**, 1112 (1985).
- [65] Proctor, A. and P.M.A. Sherwood, *J. Electron Spectr. Rel. Phenom.*, **27**, 39 (1982).
- [66] Ishitani, A., *Carbon*, **19**, 269 (1981).
- [67] Proctor, A. and P.M.A. Sherwood, *Carbon*, **21**, 53 (1983).
- [68] Perry, D.L. and A. Grint, *Fuel*, **62**, 1024 (1983).

- [69] Clark, D.T. and R. Wilson, *Fuel*, **62**, 1034 (1983).
- [70] Thomas, J.M., E.M. Evans, M. Barber and P. Swift, *Trans. Faraday Soc.*, **67**, 1815 (1971).
- [71] Yokoyama, S., K. Tanaka, I. Toyoshima, K. Miyahara, K. Yoshida and J. Tashiro, *Chem. Lett.*, p. 599 (1980).

APPENDIX A

Appendix A

Data for Figures 3.1 and 3.2

The following curves of specific rate versus conversion (Figures A.1-A.11) were used to generate Figures 3.1 and 3.2. Duplicate experiments are shown with different symbols. Table A.1 contains information regarding any extrapolations that were made to obtain a rate at 30% conversion.

Table A.1. Extrapolations made to obtain rates at 30% conversion.

Catalyst	M/C	Comment
None	--	Extrapolated from 3%
Li ₂ CO ₃	0.025	Extrapolated from 5%
Li ₂ CO ₃	0.043	Extrapolated from 7%
Na ₂ CO ₃	0.012	Extrapolated from 5%
Na ₂ CO ₃	0.024	Extrapolated from 6%
Na ₂ CO ₃	0.046	Extrapolated from 20%
K ₂ CO ₃	0.0095	Extrapolated from 3%
K ₂ CO ₃	0.019	Extrapolated from 11%
Cs ₂ CO ₃	0.009	Extrapolated from 6%
Cs ₂ CO ₃	0.020	Extrapolated from 11%

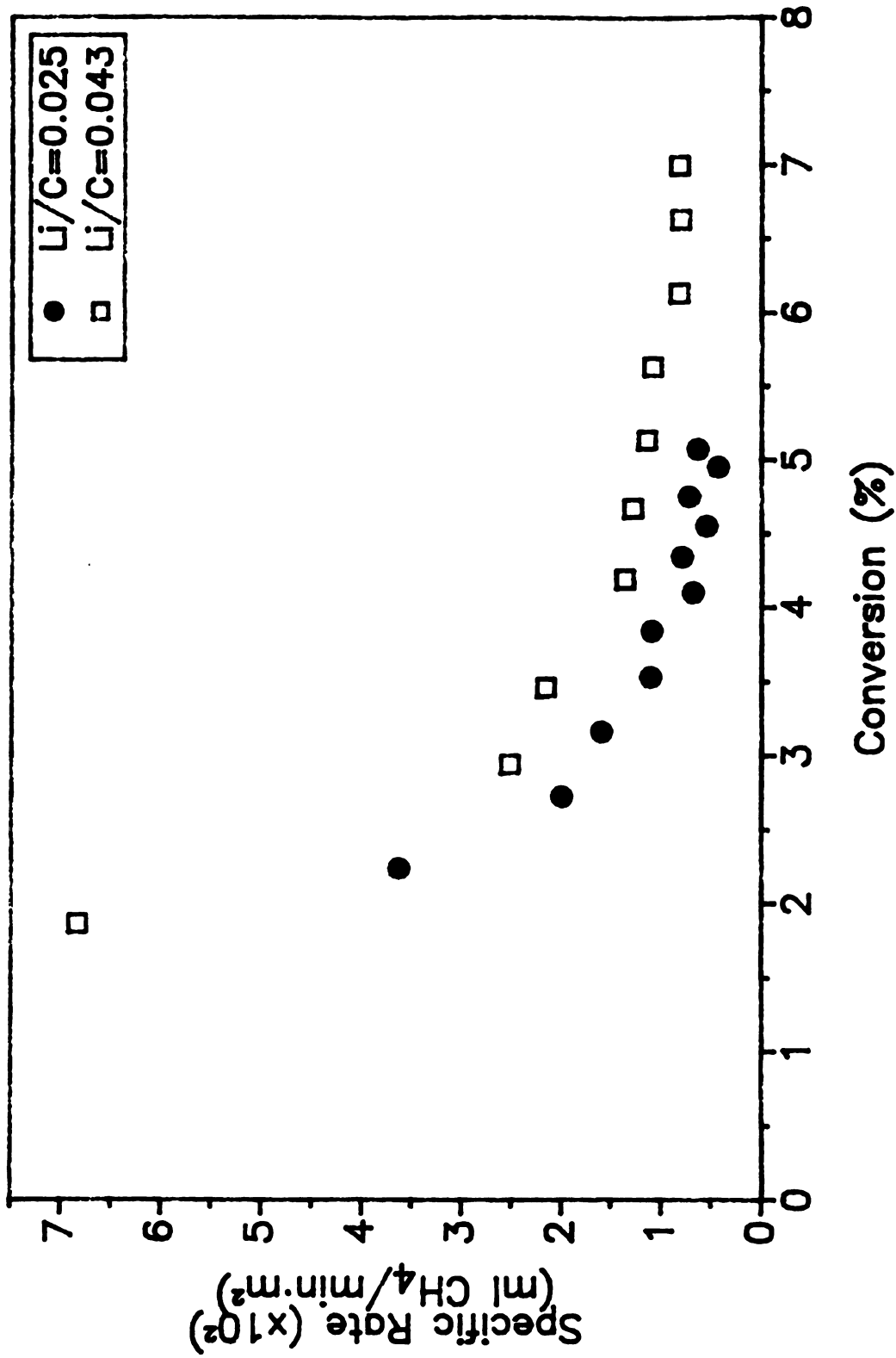


Figure A.1. Specific rate versus conversion for Li₂CO₃-catalyzed carbon black at 725° C, 500 psig H₂.

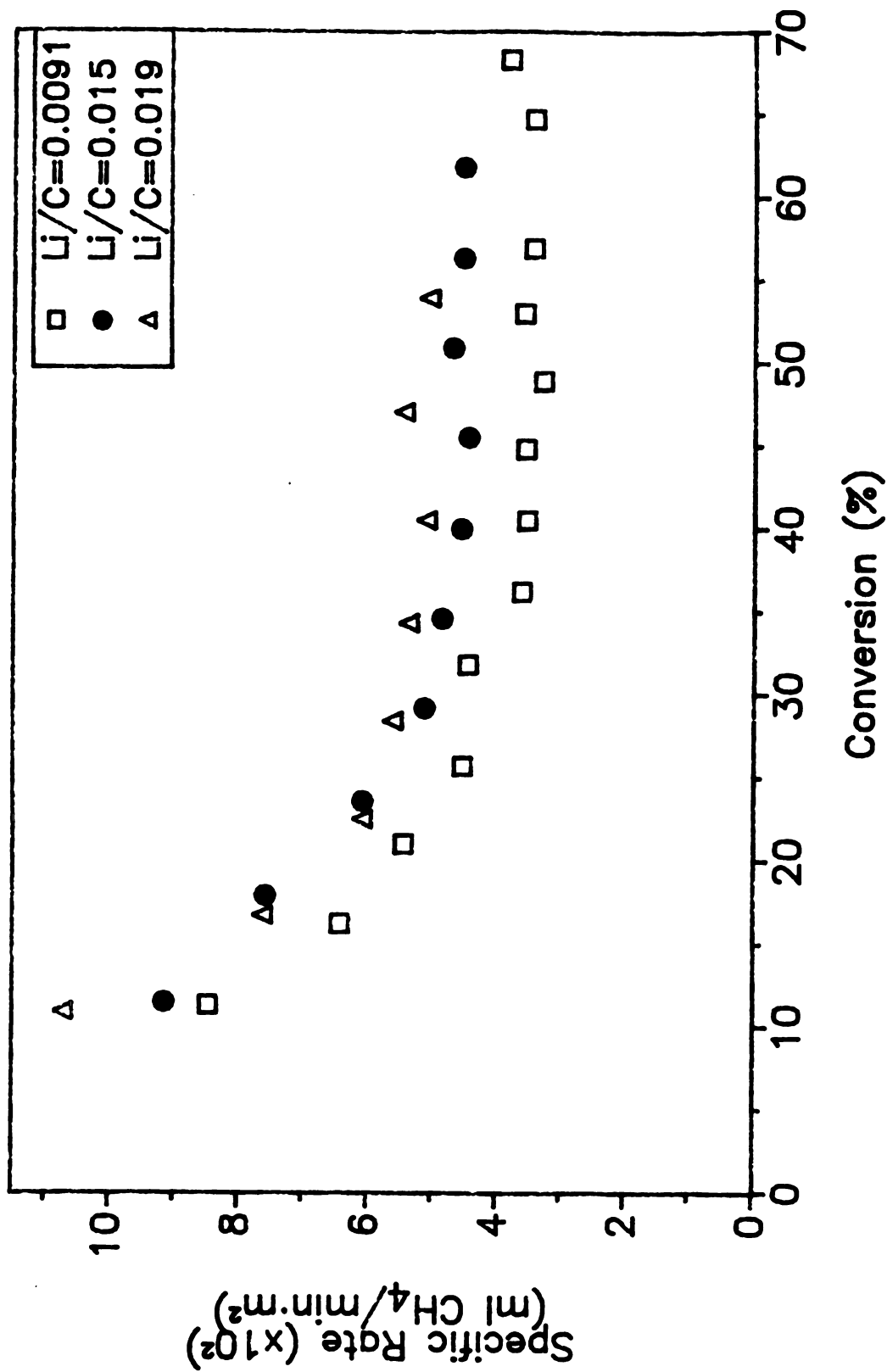


Figure A.2. Specific rate versus conversion for low Li_2CO_3 loadings on carbon black at 865°C , 500 psig H_2 .

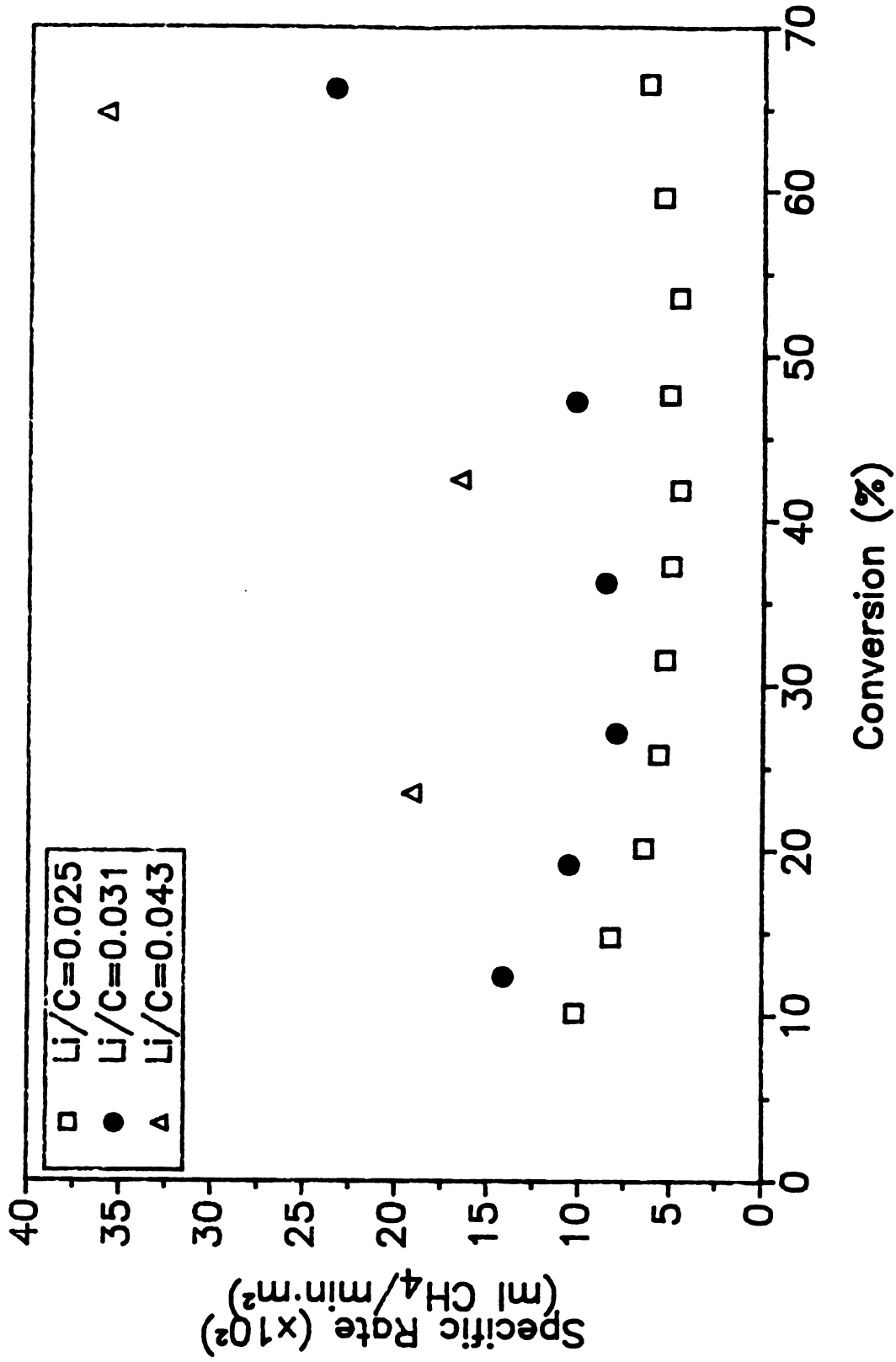


Figure A.3. Specific rate versus conversion for high Li₂CO₃ loadings on carbon black at 865° C, 500 psig H₂.

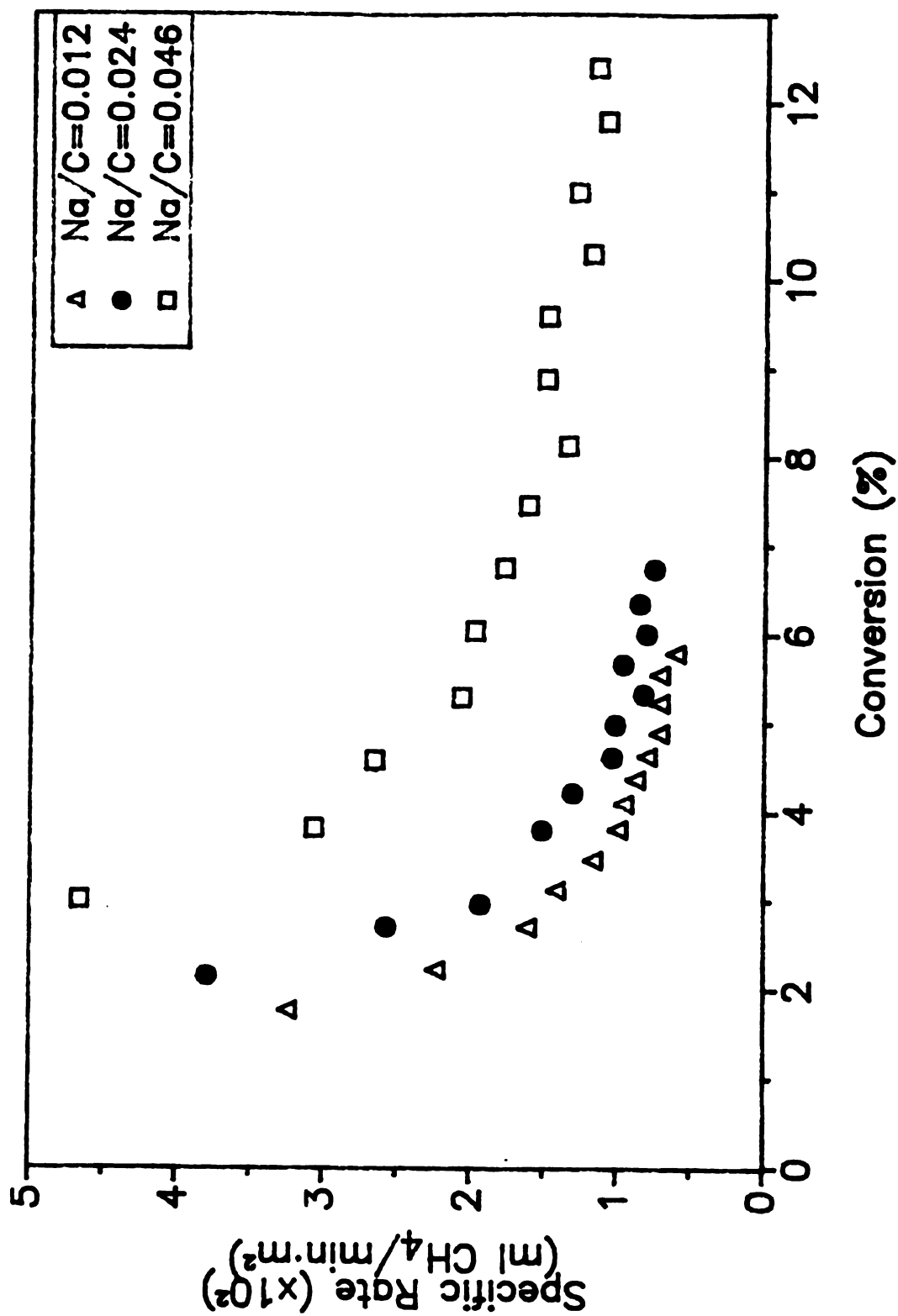


Figure A.4. Specific rate versus conversion for low Na₂CO₃ loadings on carbon black at 725° C, 500 psig H₂.

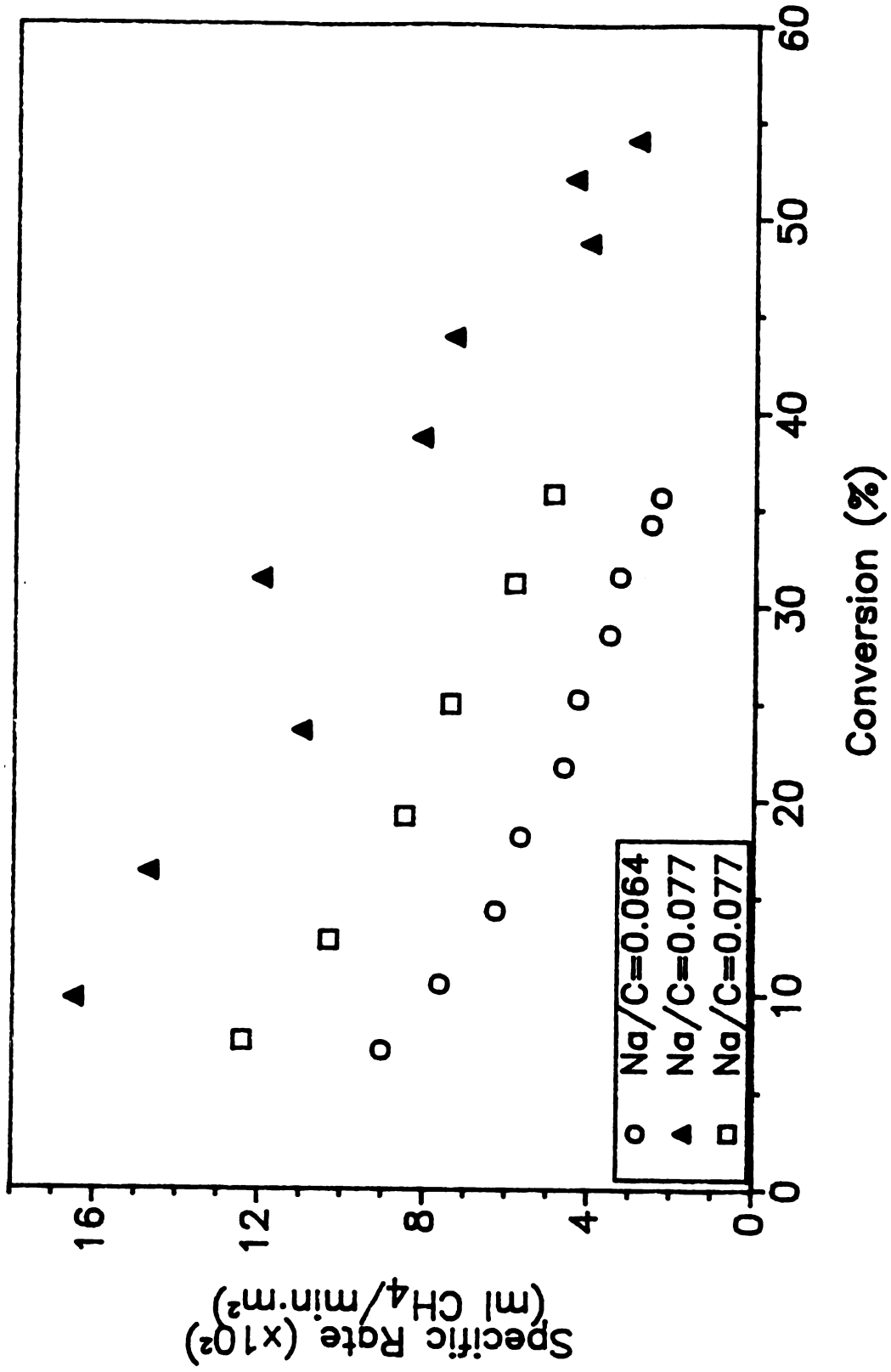


Figure A.5. Specific rate versus conversion for high Na₂CO₃ loadings on carbon black at 725° C, 500 psig H₂.

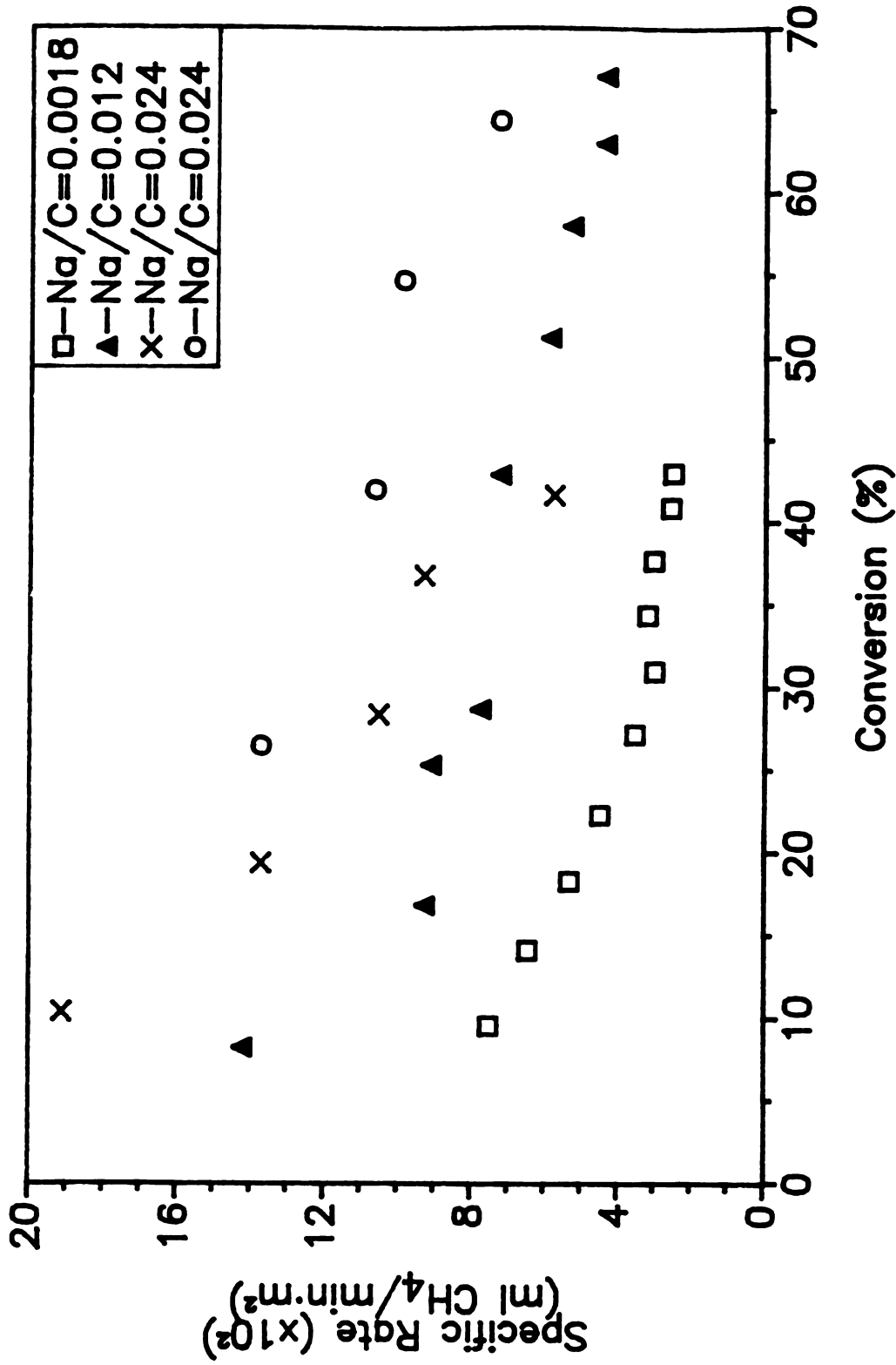


Figure A.6. Specific rate versus conversion for Na₂CO₃-catalyzed carbon black at 865° C, 500 psig H₂.

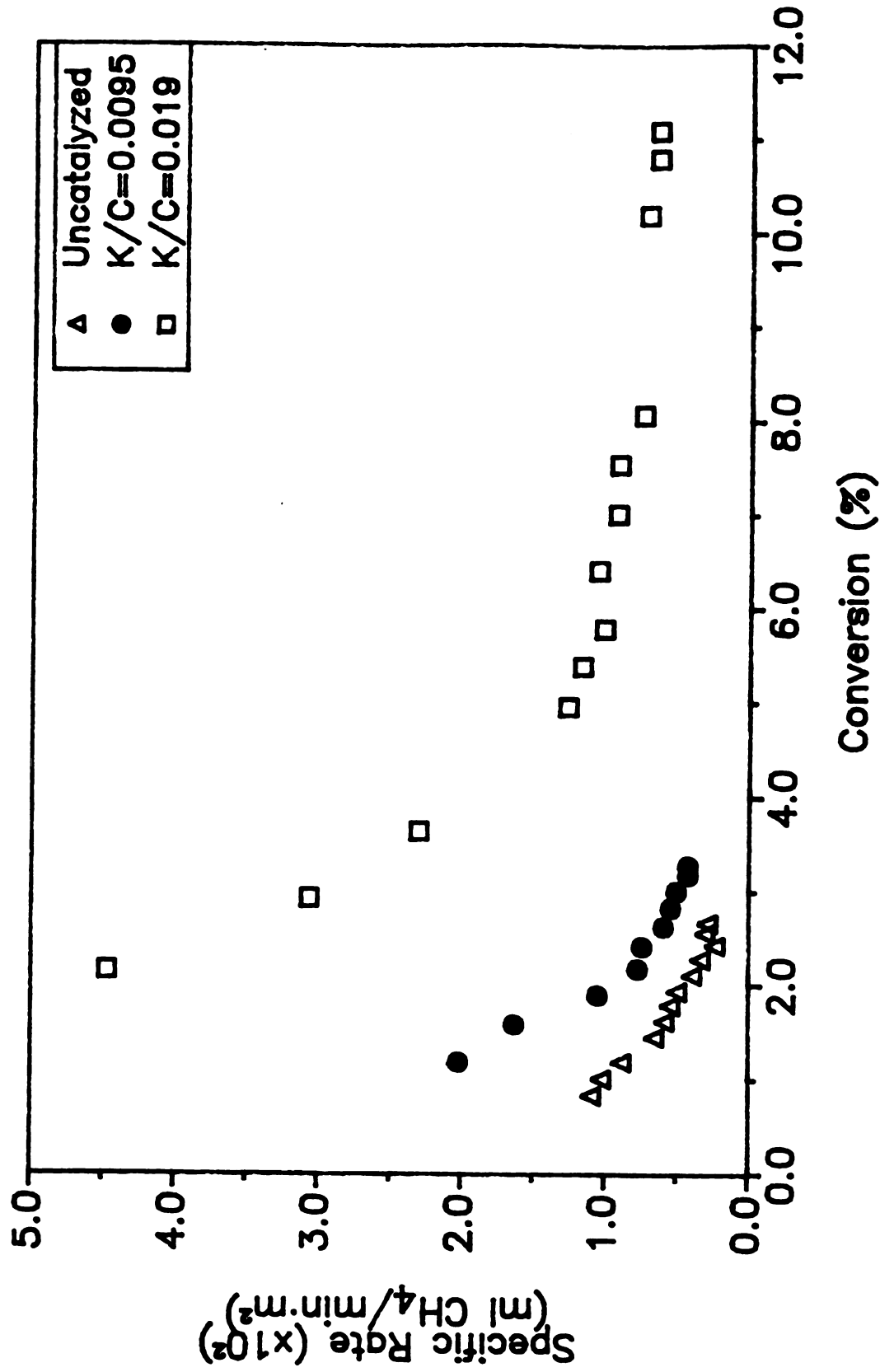


Figure A.7. Specific rate versus conversion for low K₂CO₃ loadings on carbon black at 725° C, 500 psig H₂.

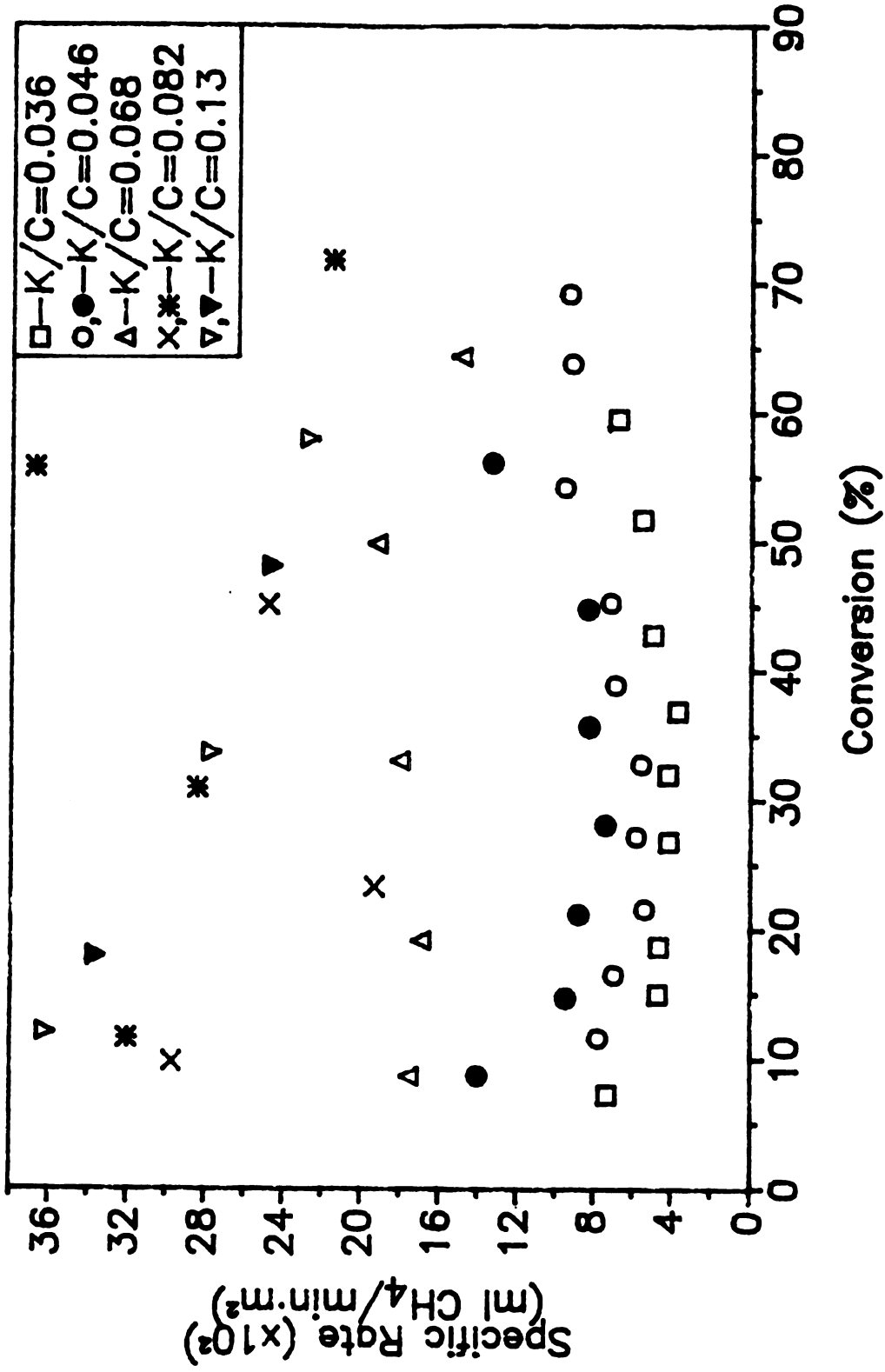


Figure A.8. Specific rate versus conversion for high K_2CO_3 loadings on carbon black at $725^\circ C$, 500 psig H_2 .

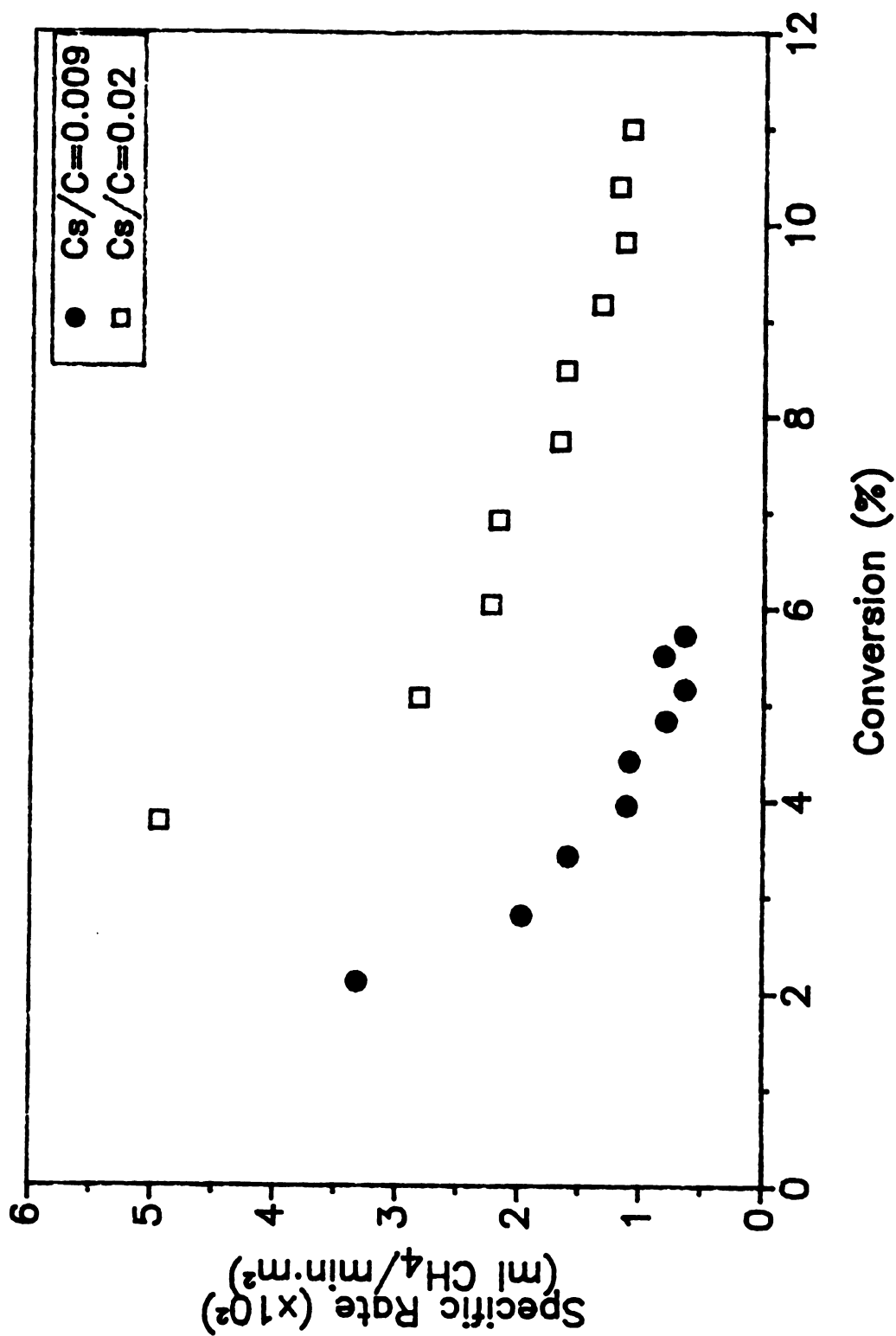


Figure A.9. Specific rate versus conversion for low Cs₂CO₃ loadings on carbon black at 725° C, 500 psig H₂.

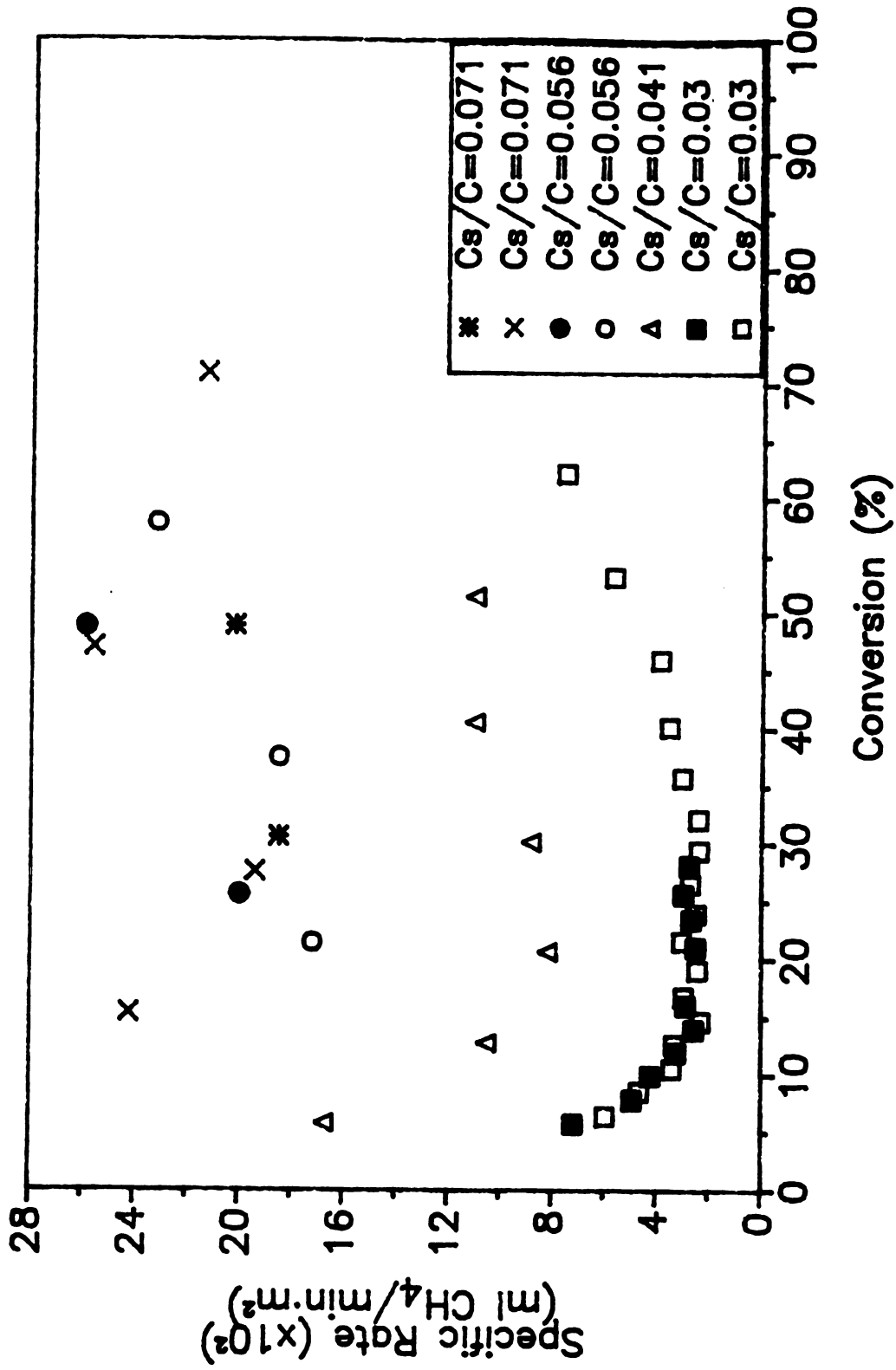


Figure A.10. Specific rate versus conversion for high Cs_2CO_3 loadings on carbon black at 725°C , 500 psig H_2 .

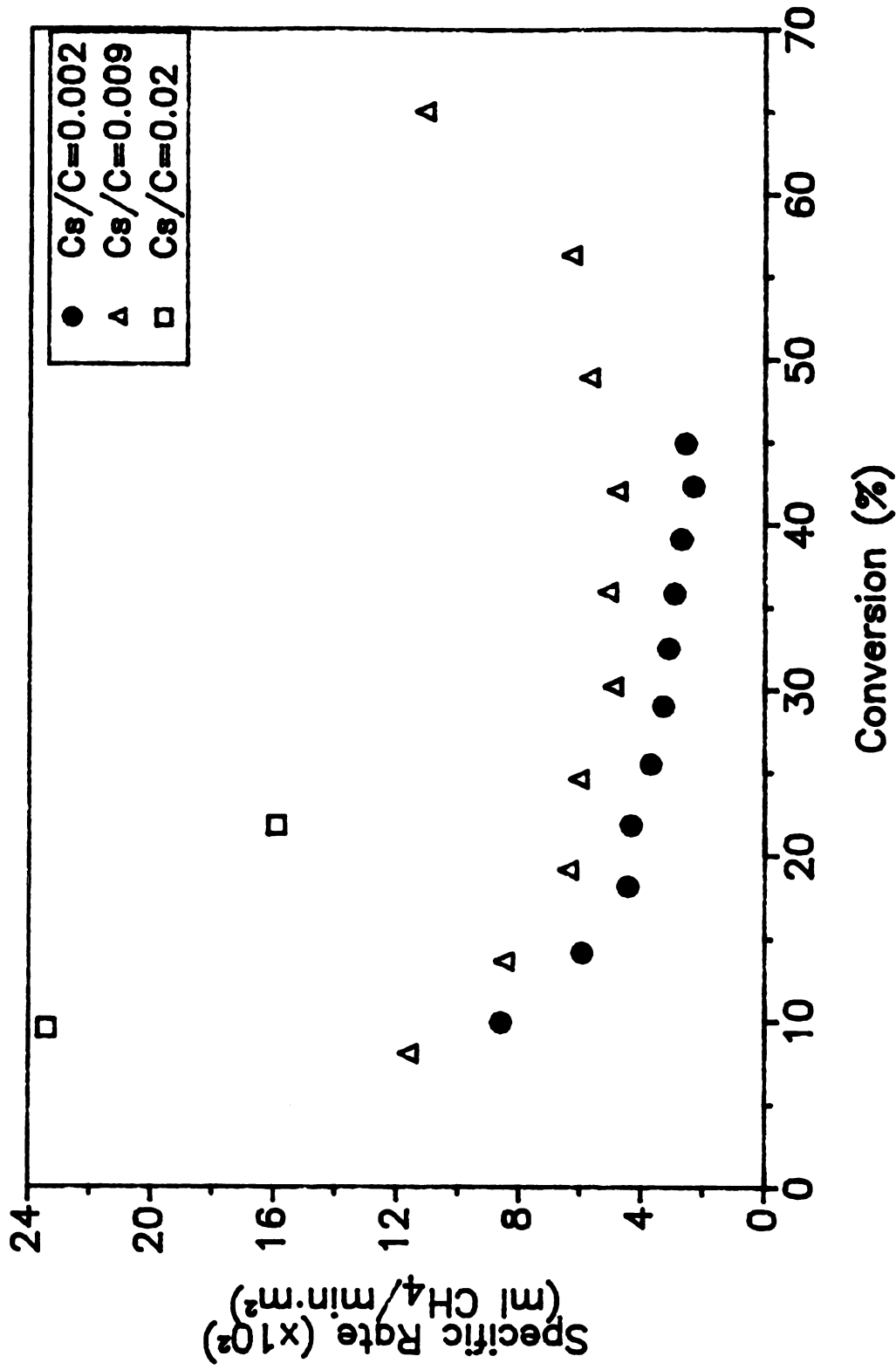


Figure A.11. Specific rate versus conversion for Cs₂CO₃-catalyzed carbon black at 865° C, 500 psig H₂.

APPENDIX B

Appendix B

O(1s) Peaks

The following figures (Figures B.1-B.21) present the O(1s) peaks and curve fit components (if a fit was performed) for uncatalyzed and K_2CO_3 -impregnated carbon black.

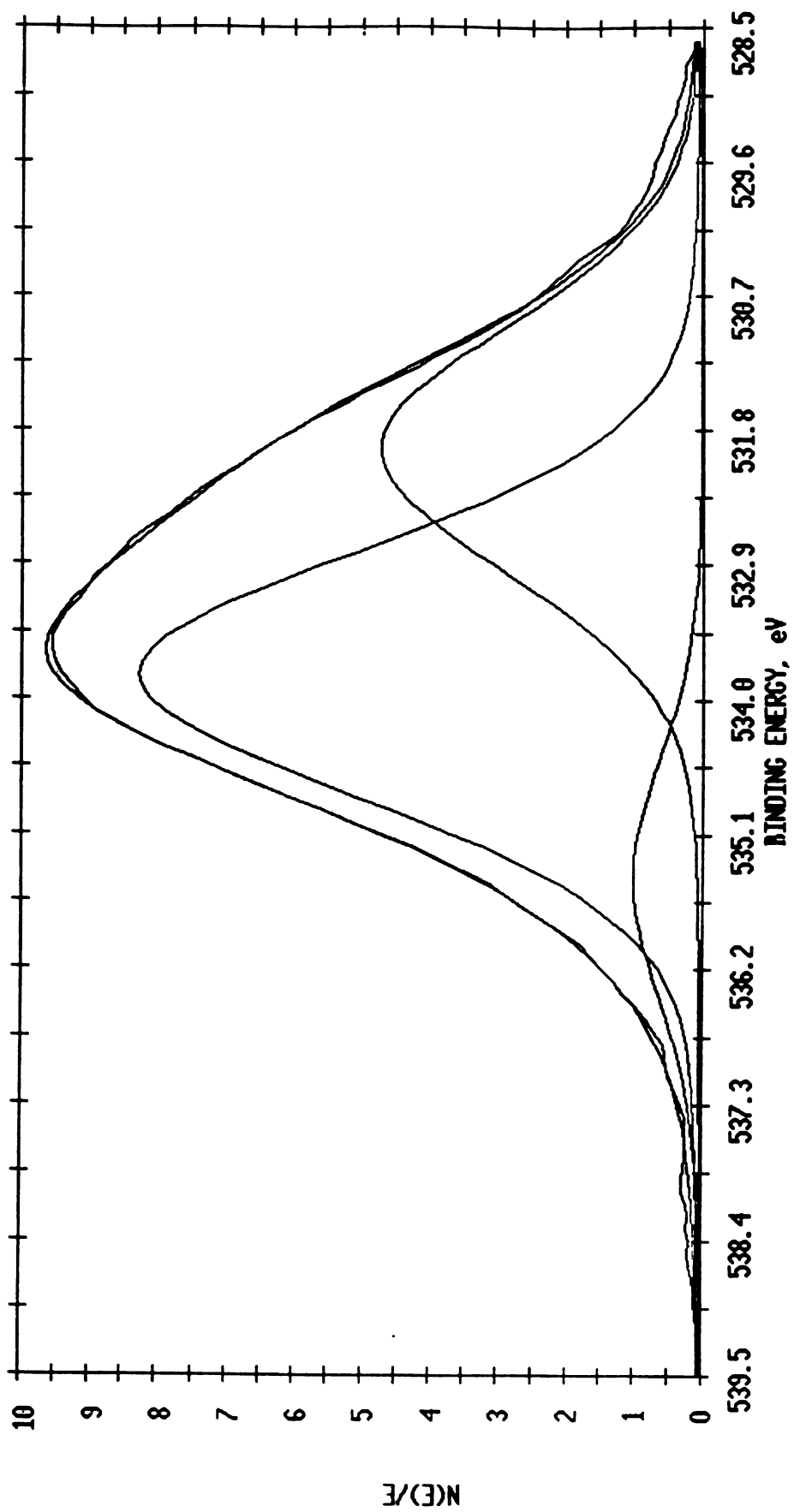


Figure B.1. O(1s) peak of untreated carbon black.

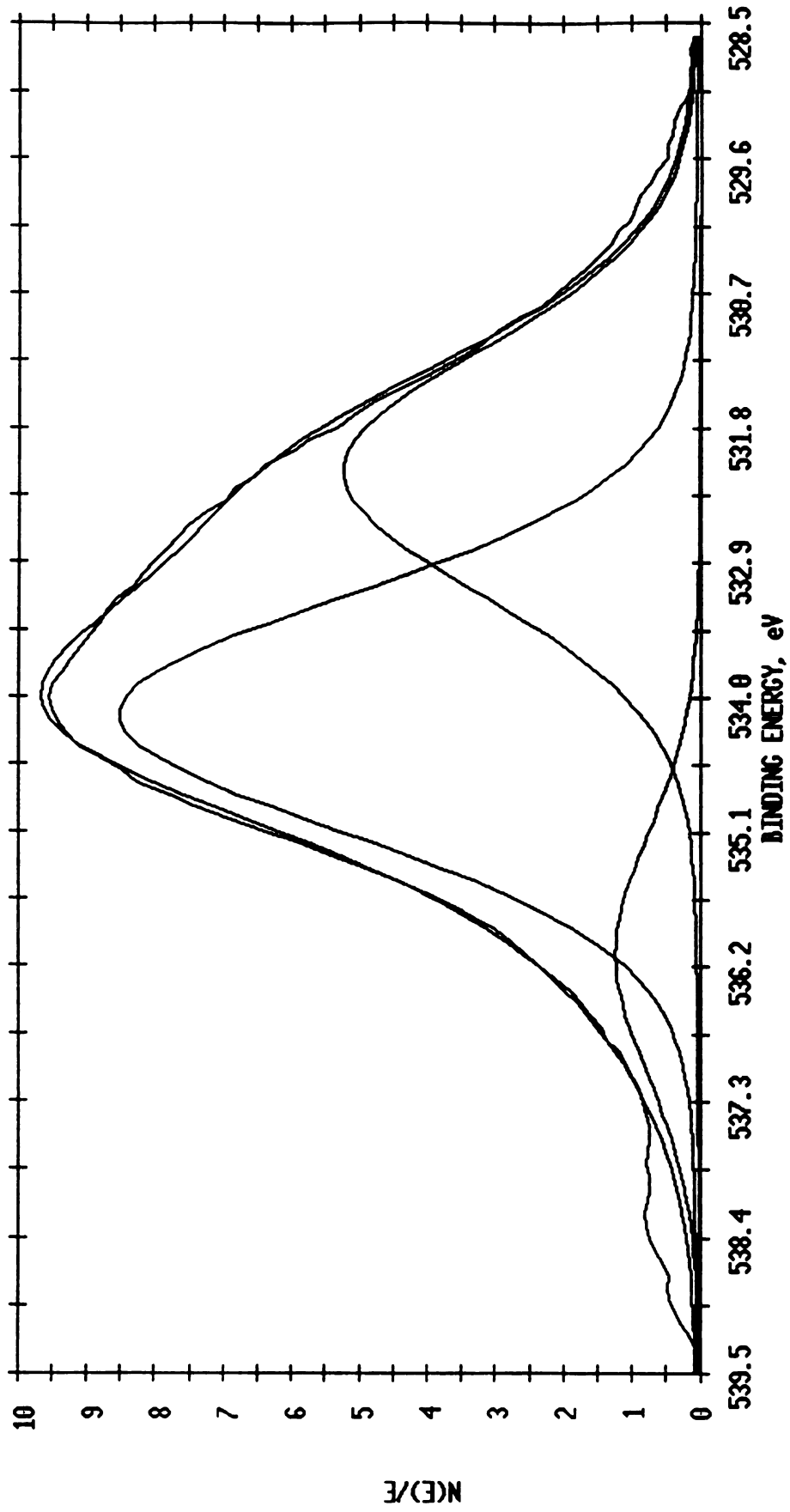


Figure B.2. O(1s) peak of carbon black heated to 200° C.

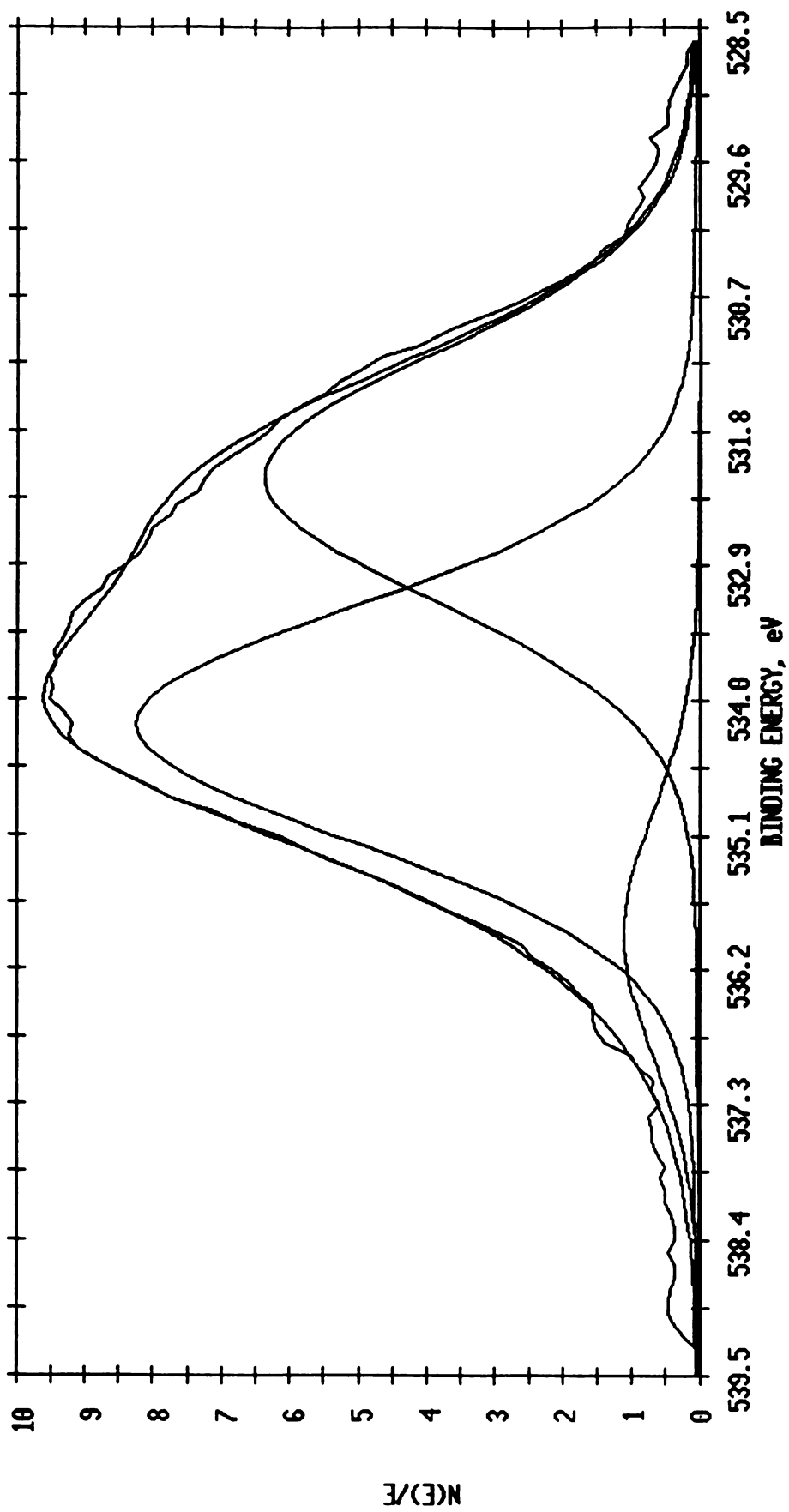


Figure B.3. O(1s) peak of carbon black heated to 400° C.

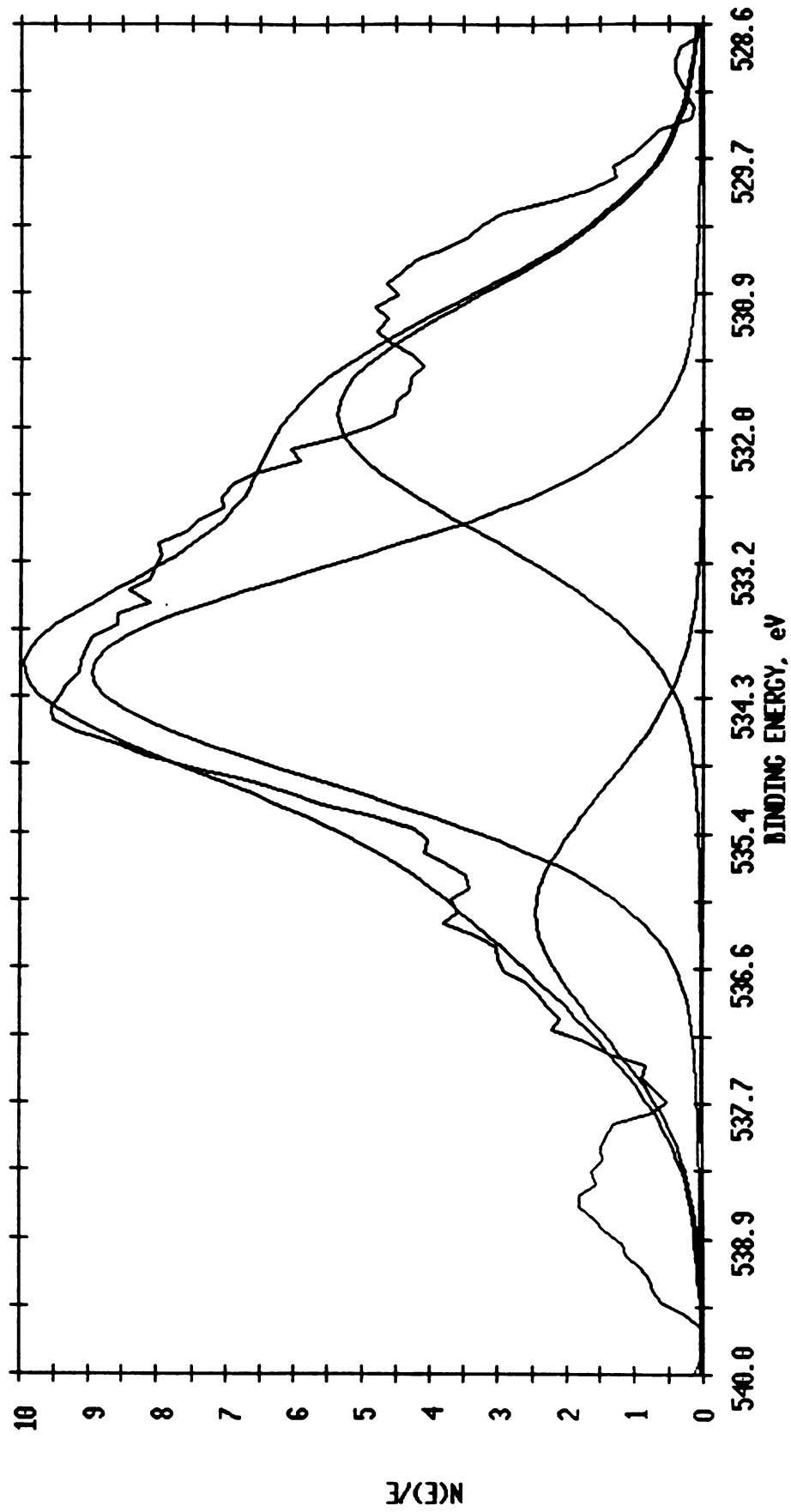


Figure B.4. O(1s) peak of carbon black heated to 600° C.

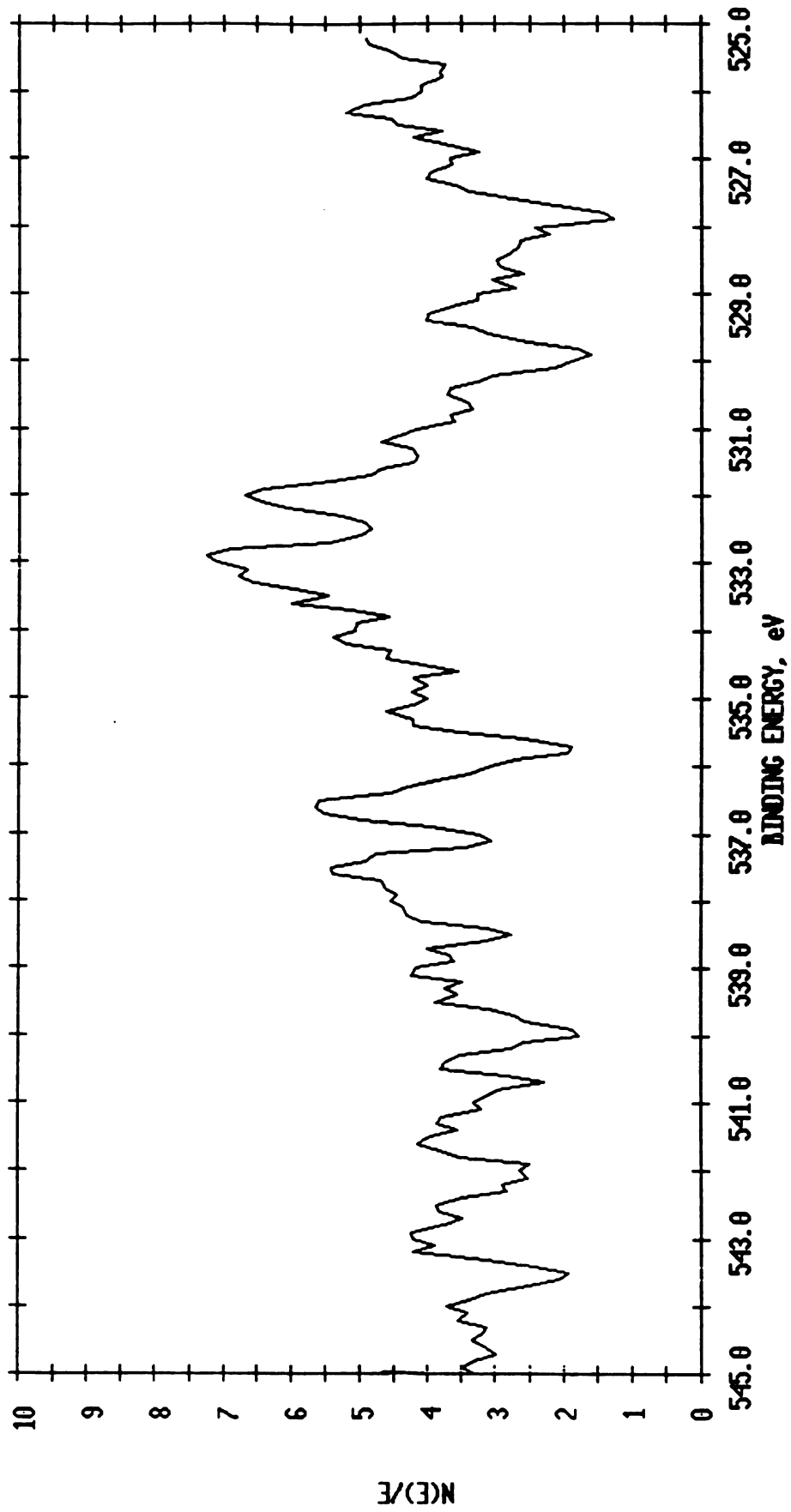


Figure B.5. O(1s) peak of carbon black heated to 1000° C.

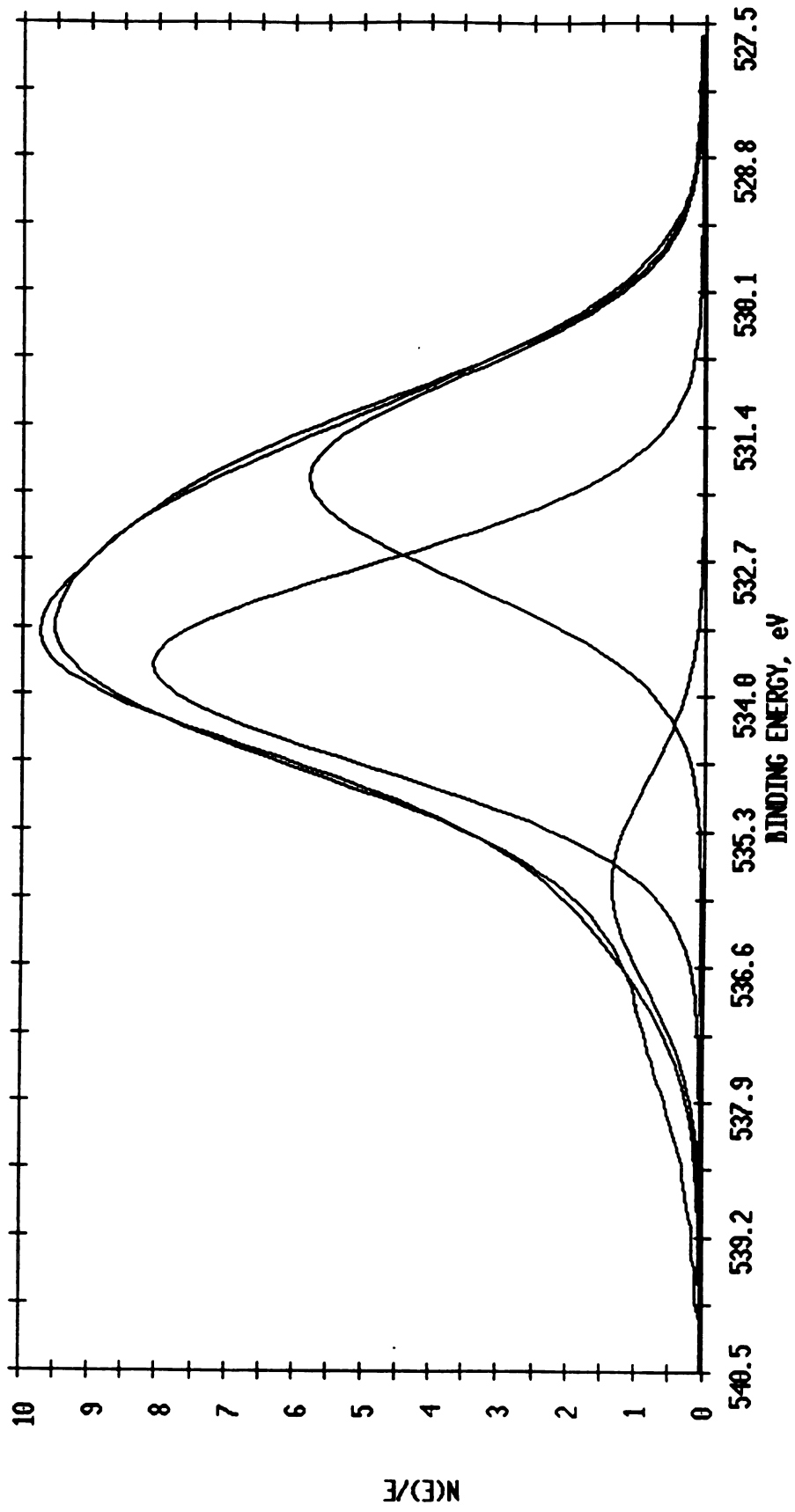


Figure B.6. O(1s) peak of HNO₃ oxidized carbon black.

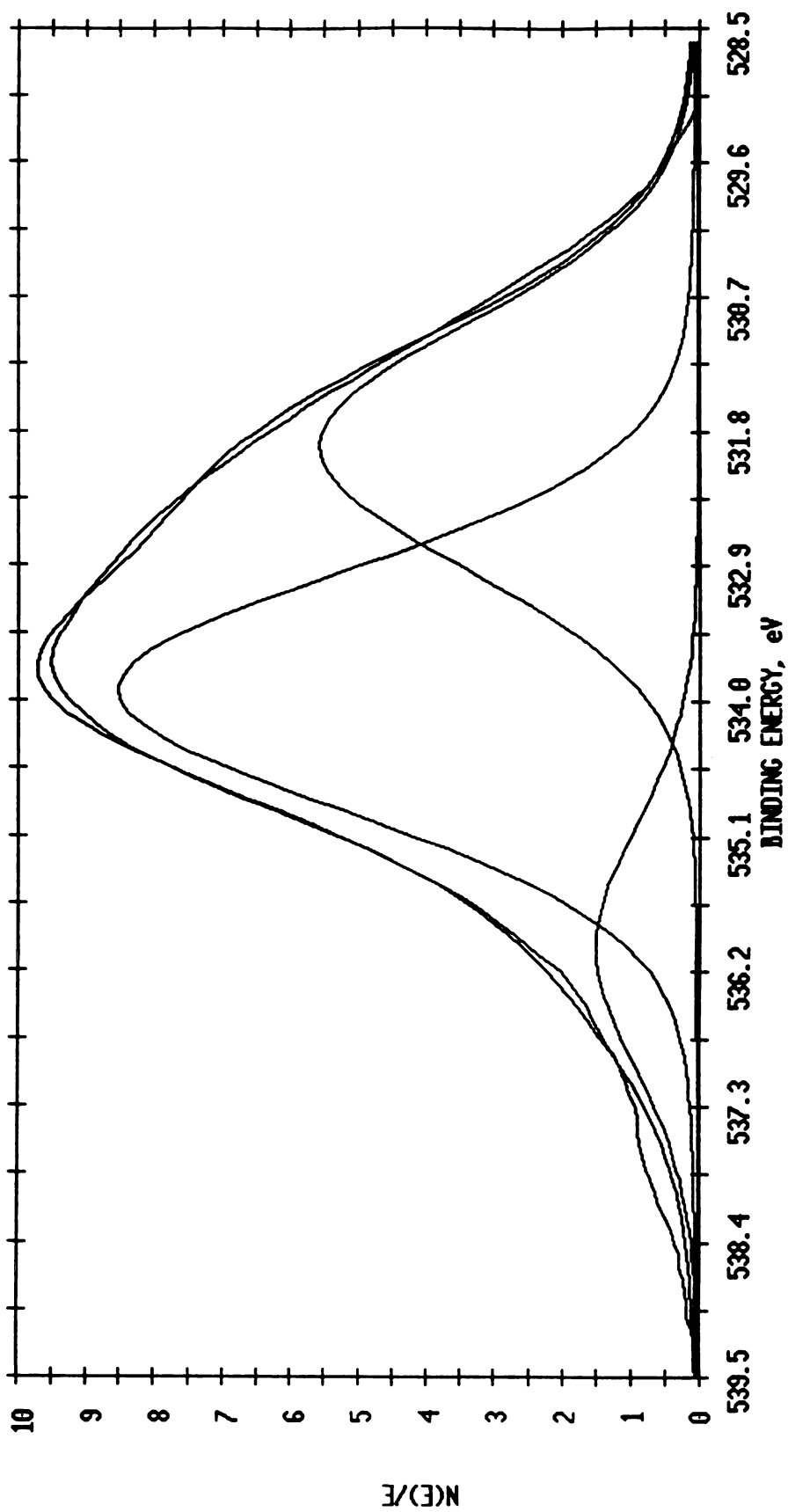


Figure B.7. O(1s) peak of carbon black; HNO₃ oxidized, heated to 200° C.

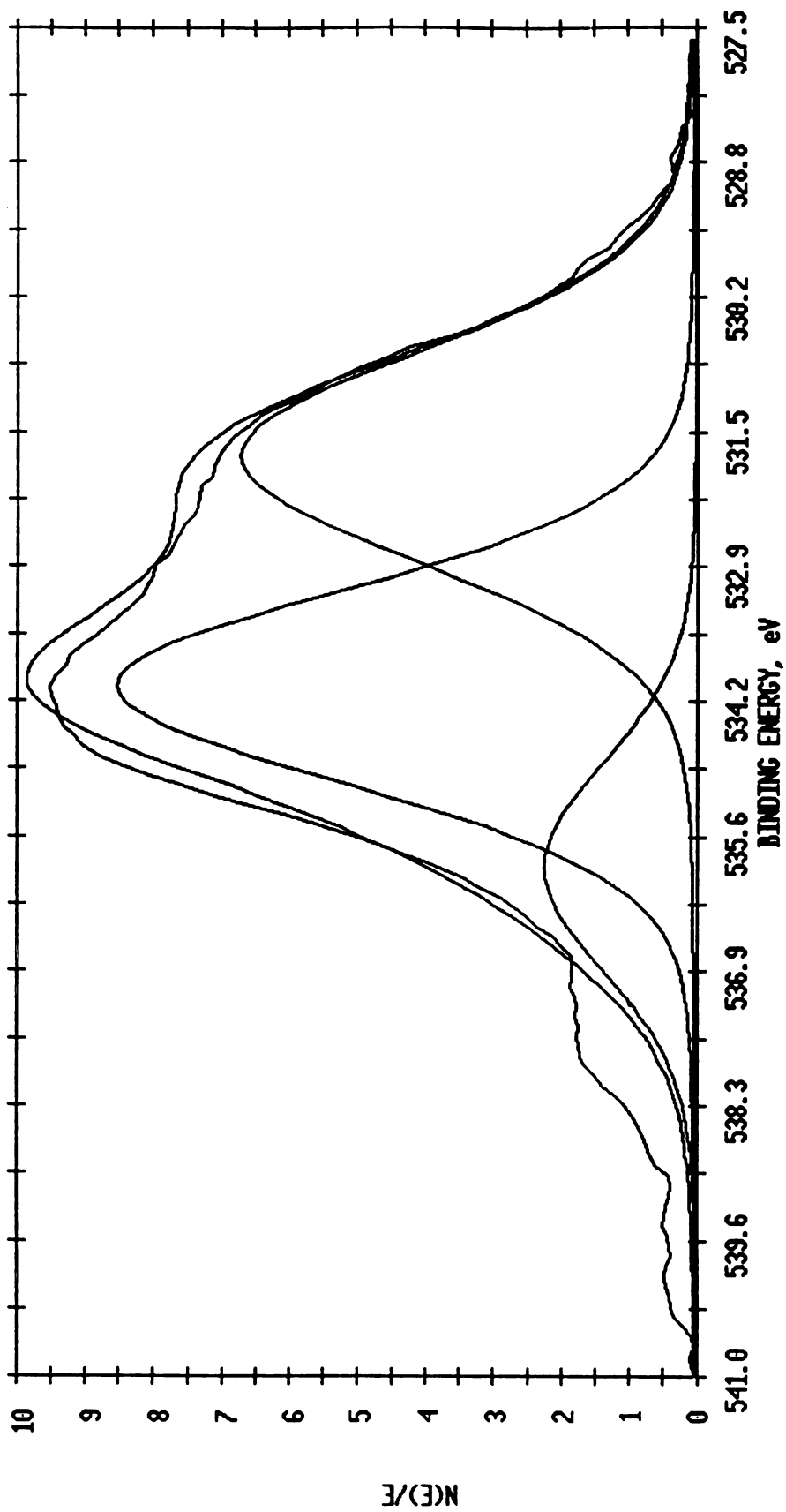


Figure B.8. O(1s) peak of carbon black; HNO₃ oxidized, heated to 400° C.

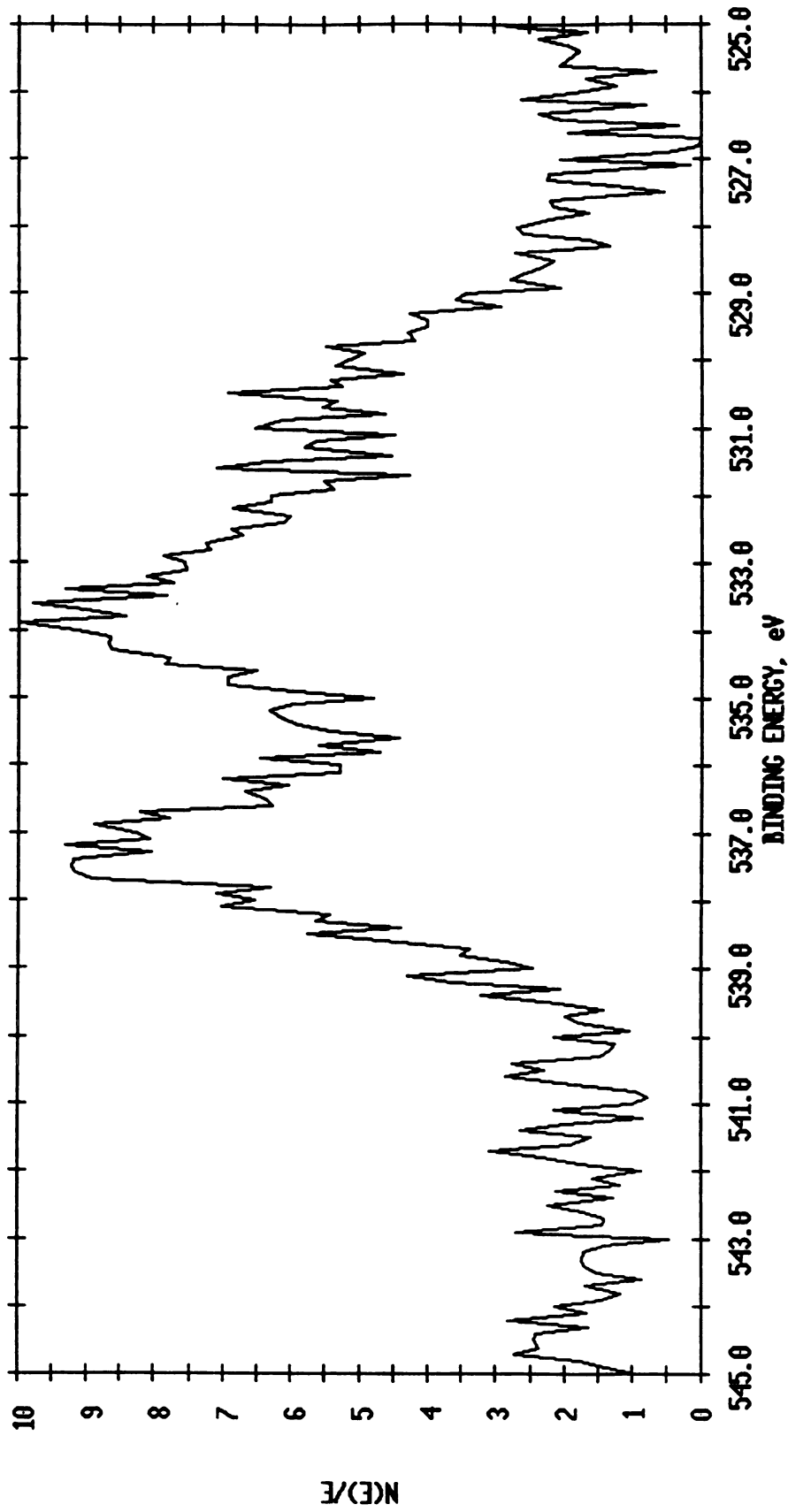


Figure B.9. O(1s) peak of carbon black; HNO₃ oxidized, heated to 600° C.

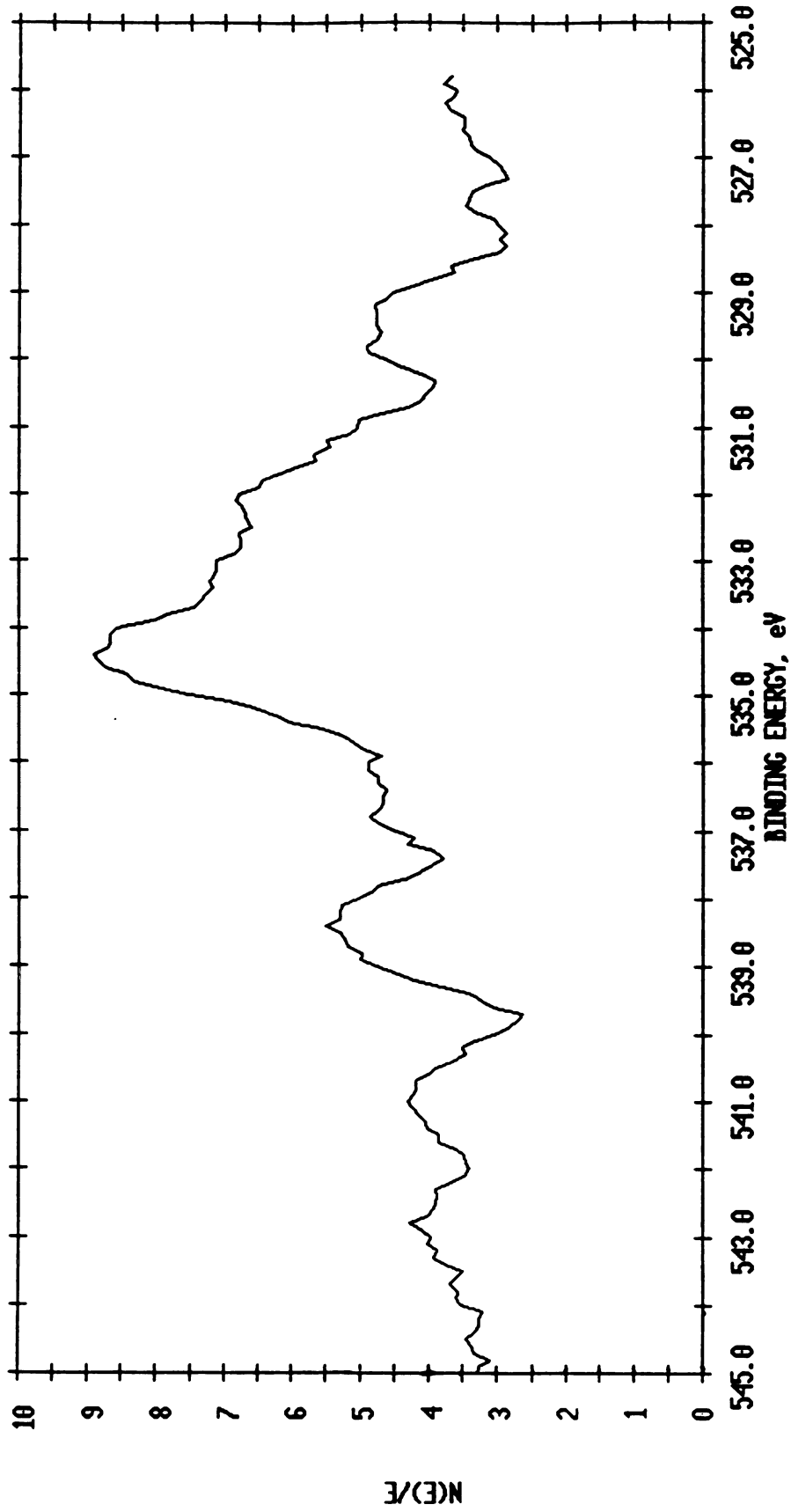


Figure B.10. O(1s) peak of carbon black; HNO₃ oxidized, exposed to H₂ at 750° C, 1 atm.

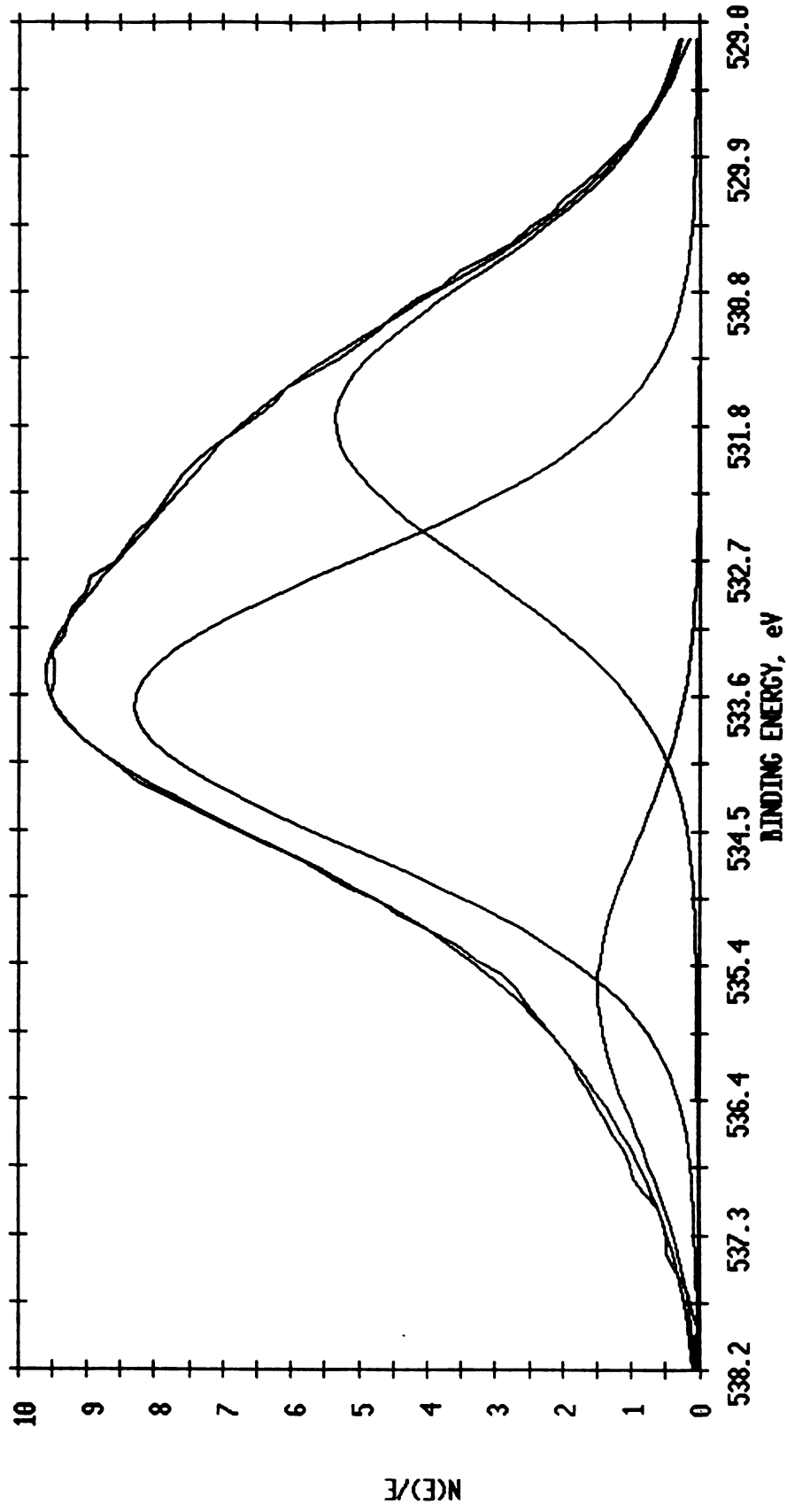


Figure B.11. O(1s) peak of carbon black; degassed, HNO₃ oxidized, heated to 200° C.

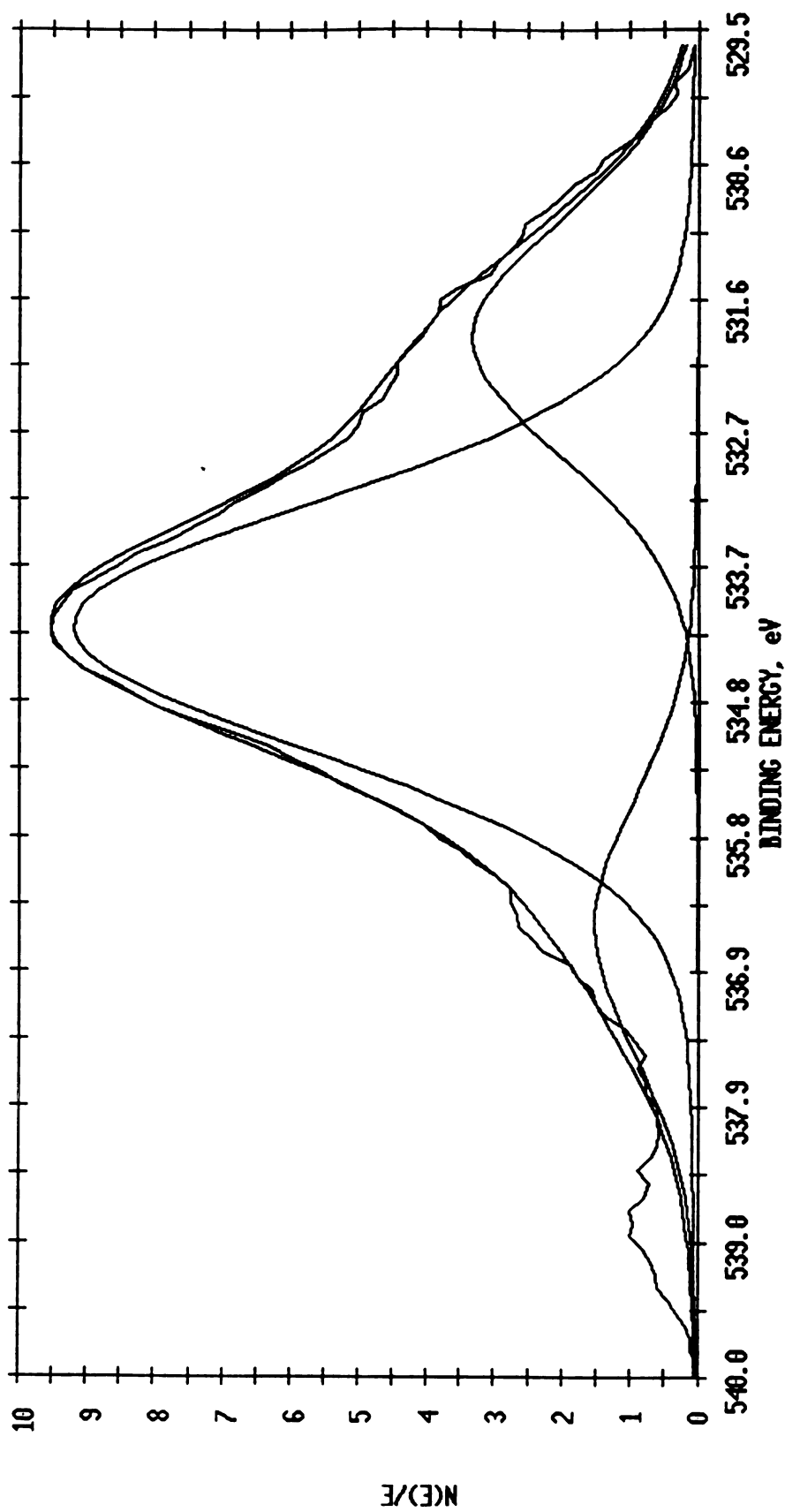


Figure B.12. O(1s) peak of carbon black; degassed, HNO₃ oxidized, heated to 400° C.

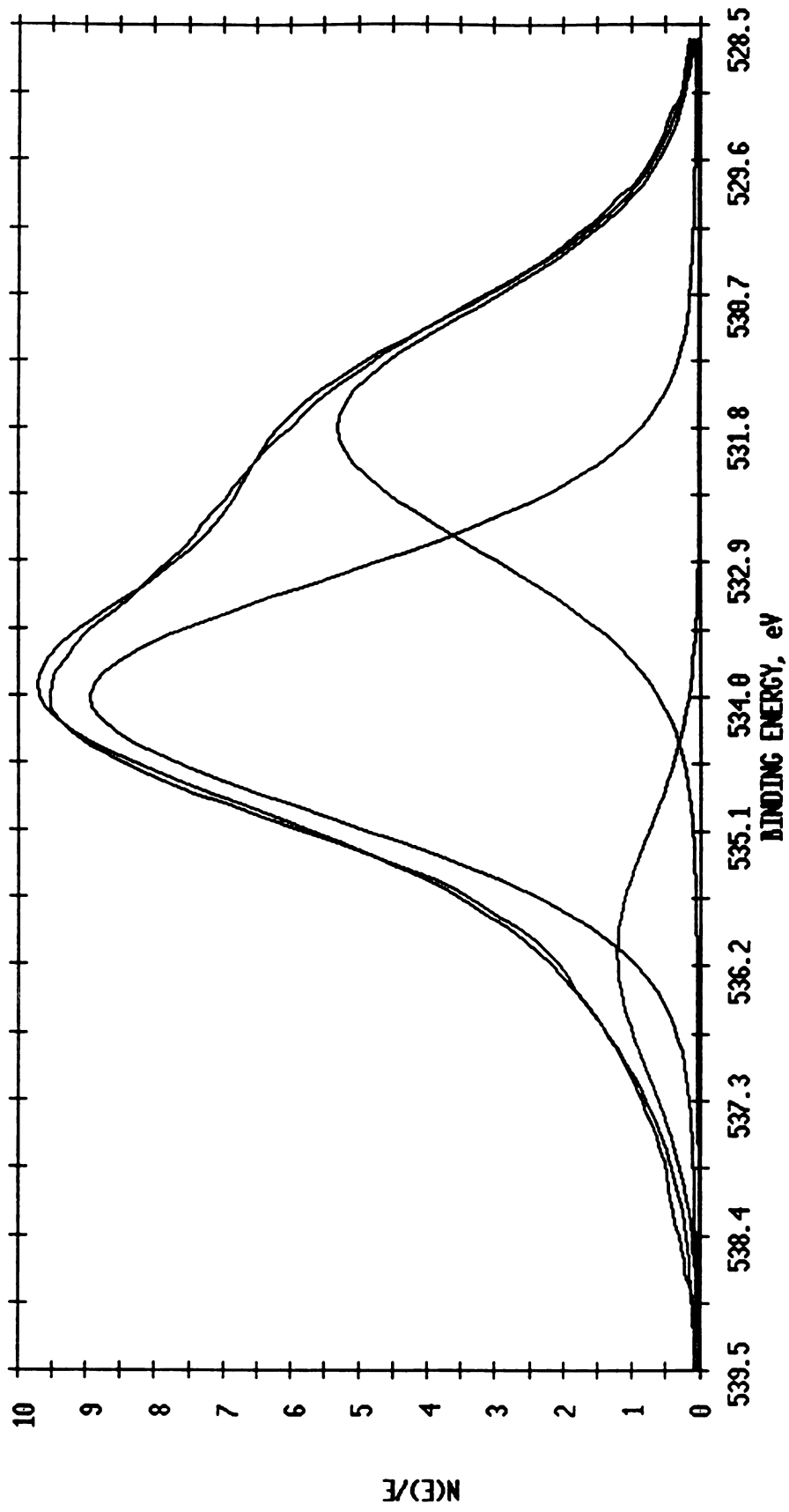


Figure B.13. O(1s) peak of carbon black O_2 oxidized at 400°C.

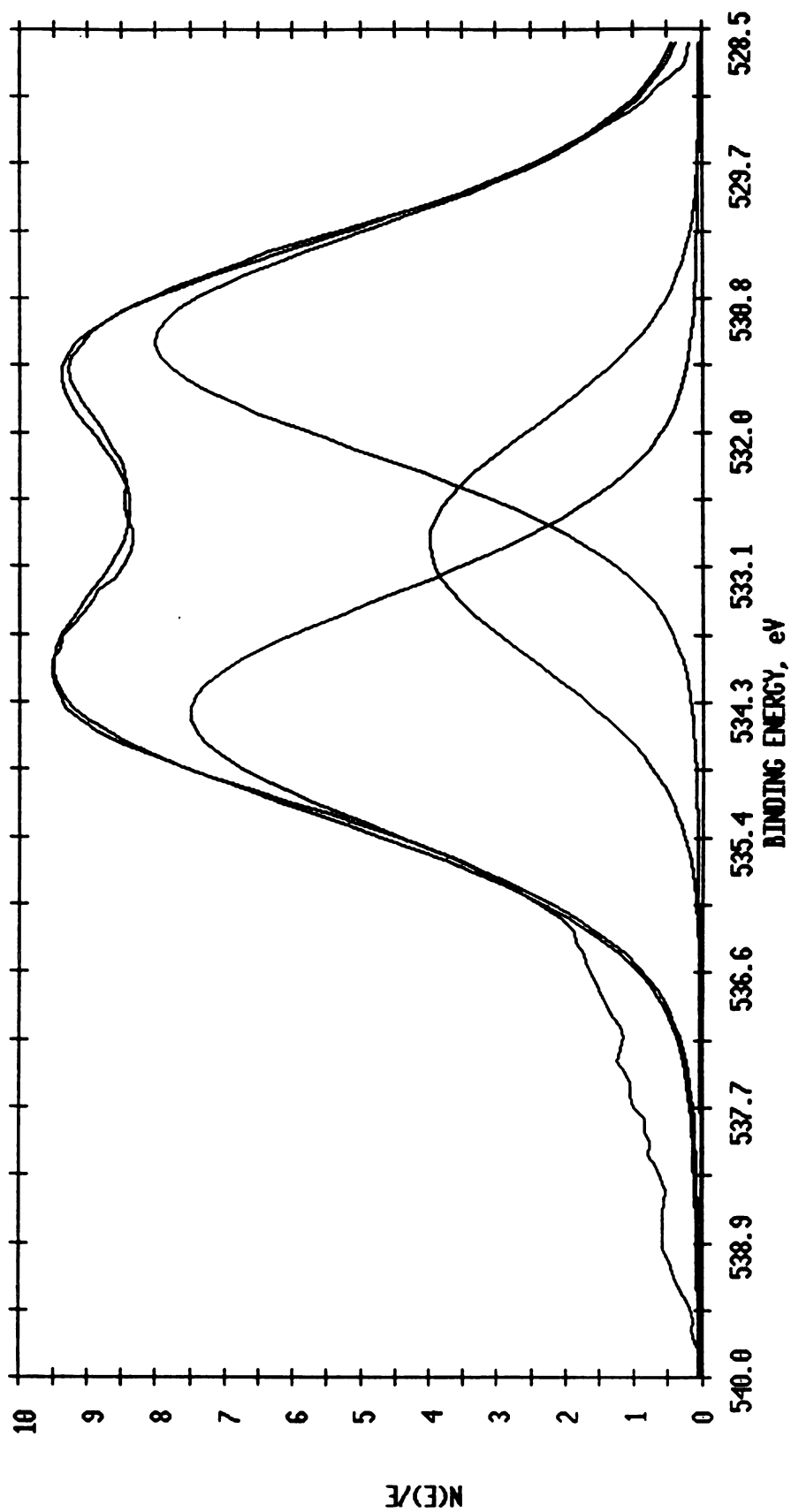


Figure B.14. O(1s) peak of carbon black; O₂ oxidized at 400° C, heated to 600° C.

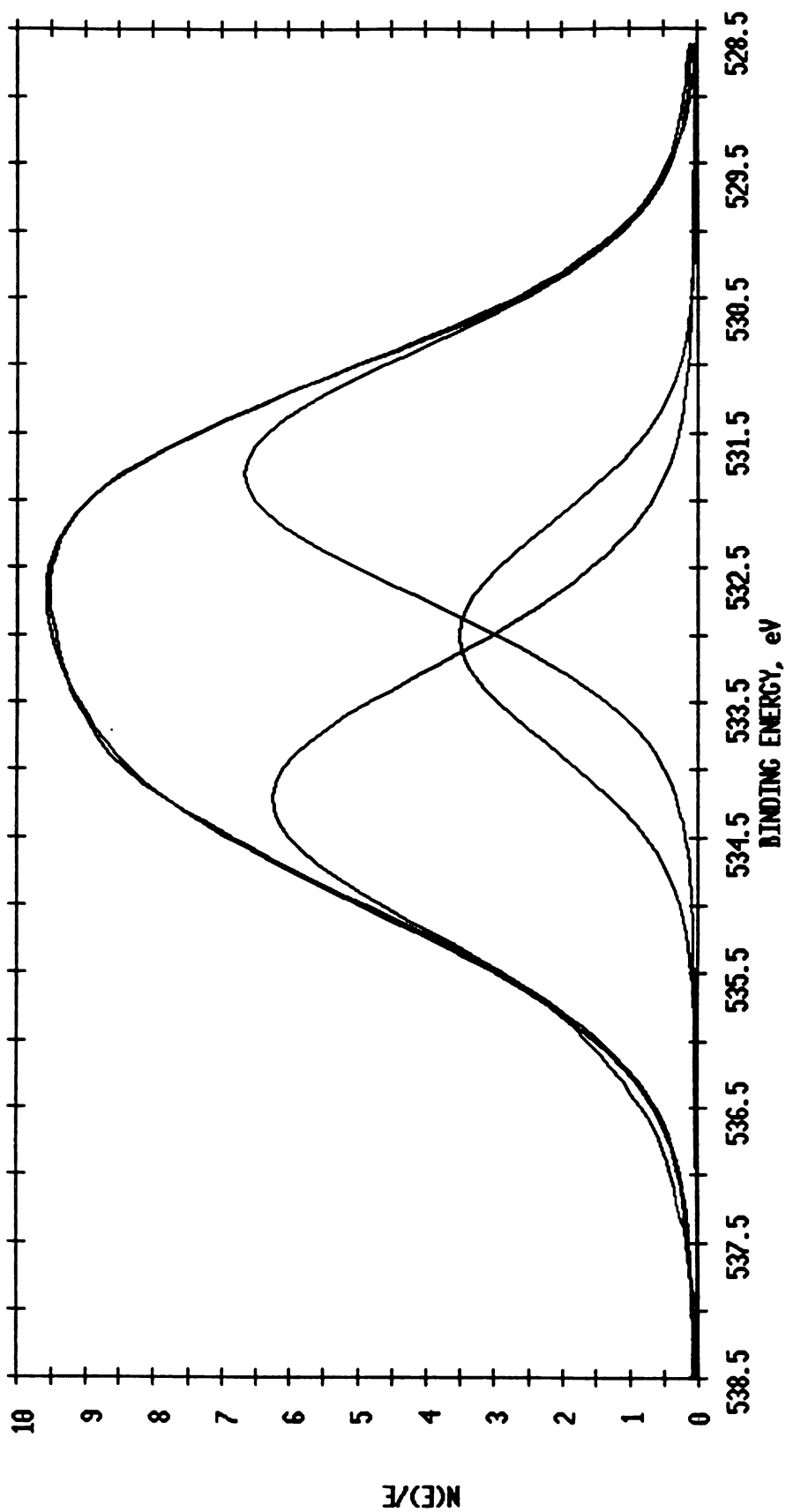


Figure B.15. O(1s) peak of untreated K_2CO_3 -impregnated carbon black.

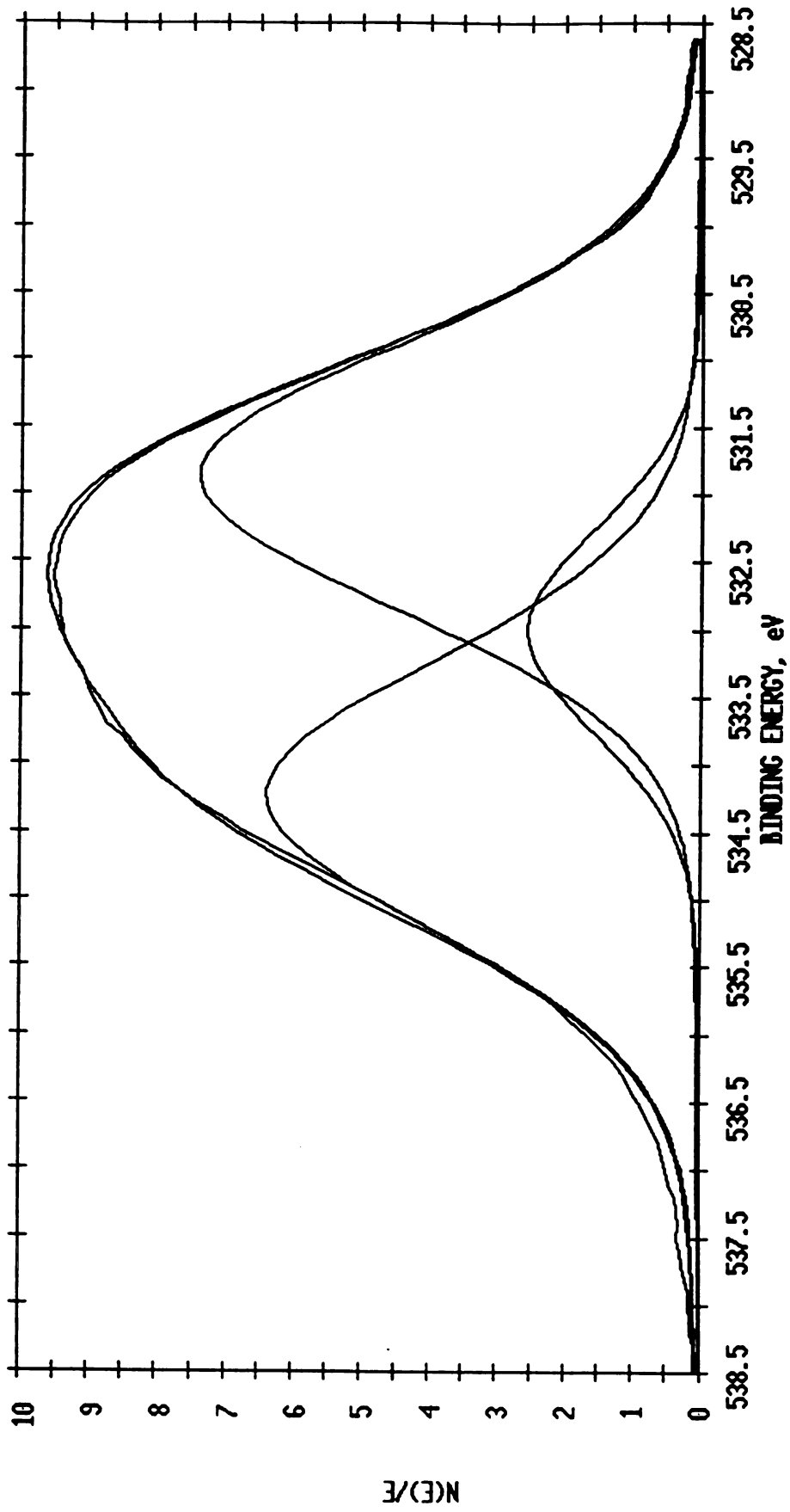


Figure B.16. O(1s) peak of K₂CO₃-impregnated carbon black heated to 200° C.

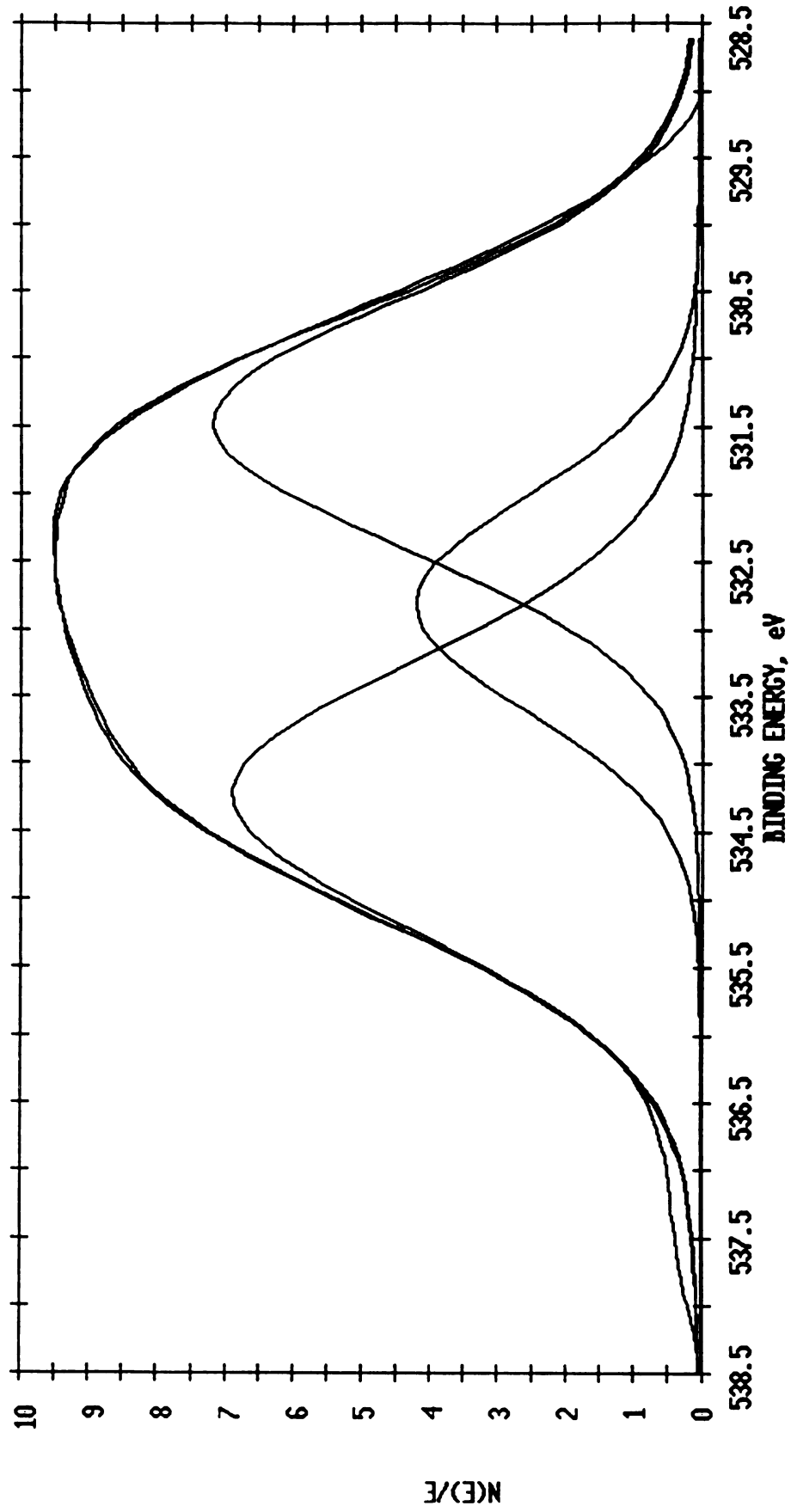


Figure B.17. O(1s) peak of K₂CO₃-impregnated carbon black heated to 500° C.

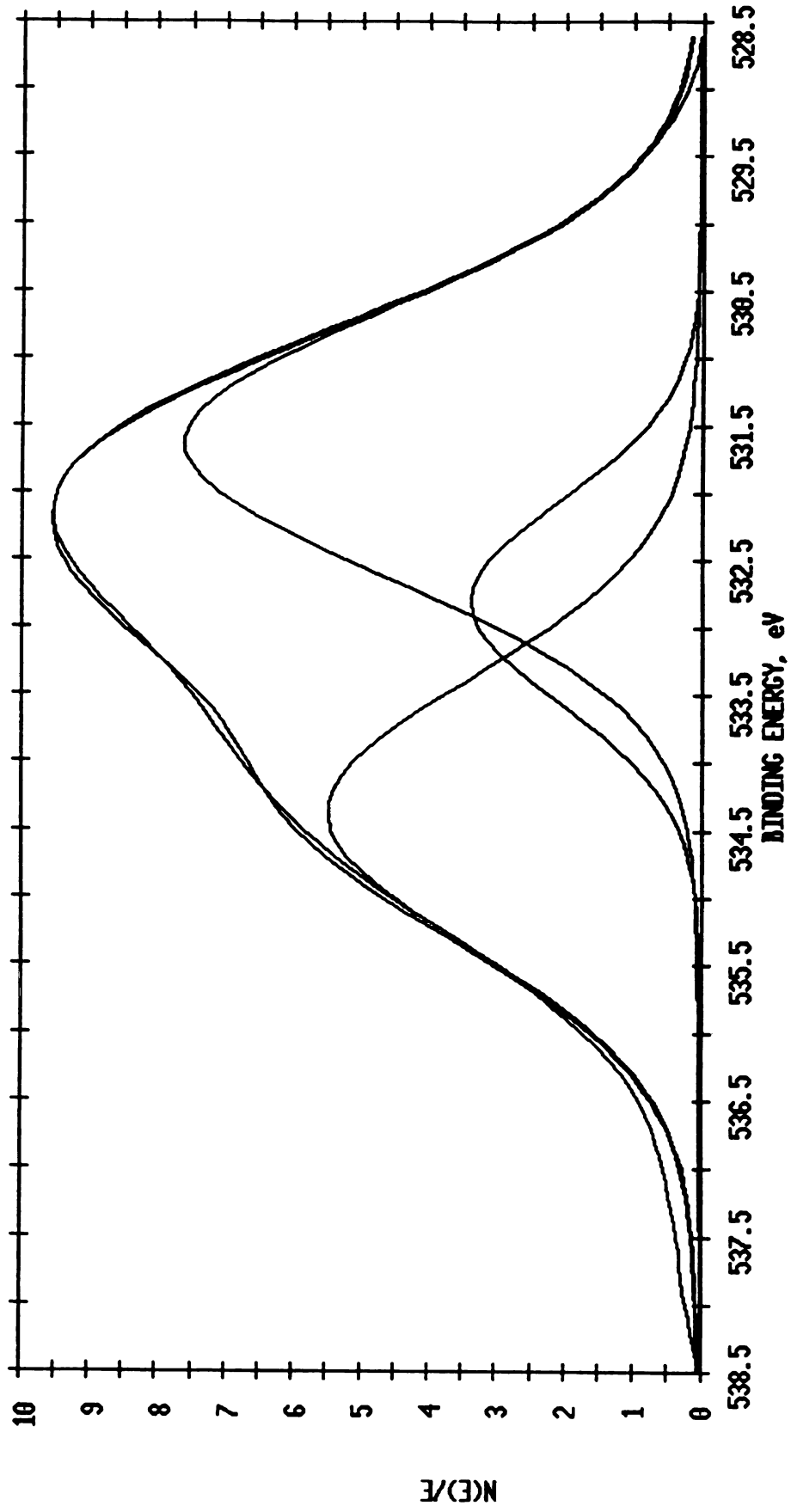


Figure B.18. O(1s) peak of K₂CO₃-impregnated carbon black heated to 750° C.

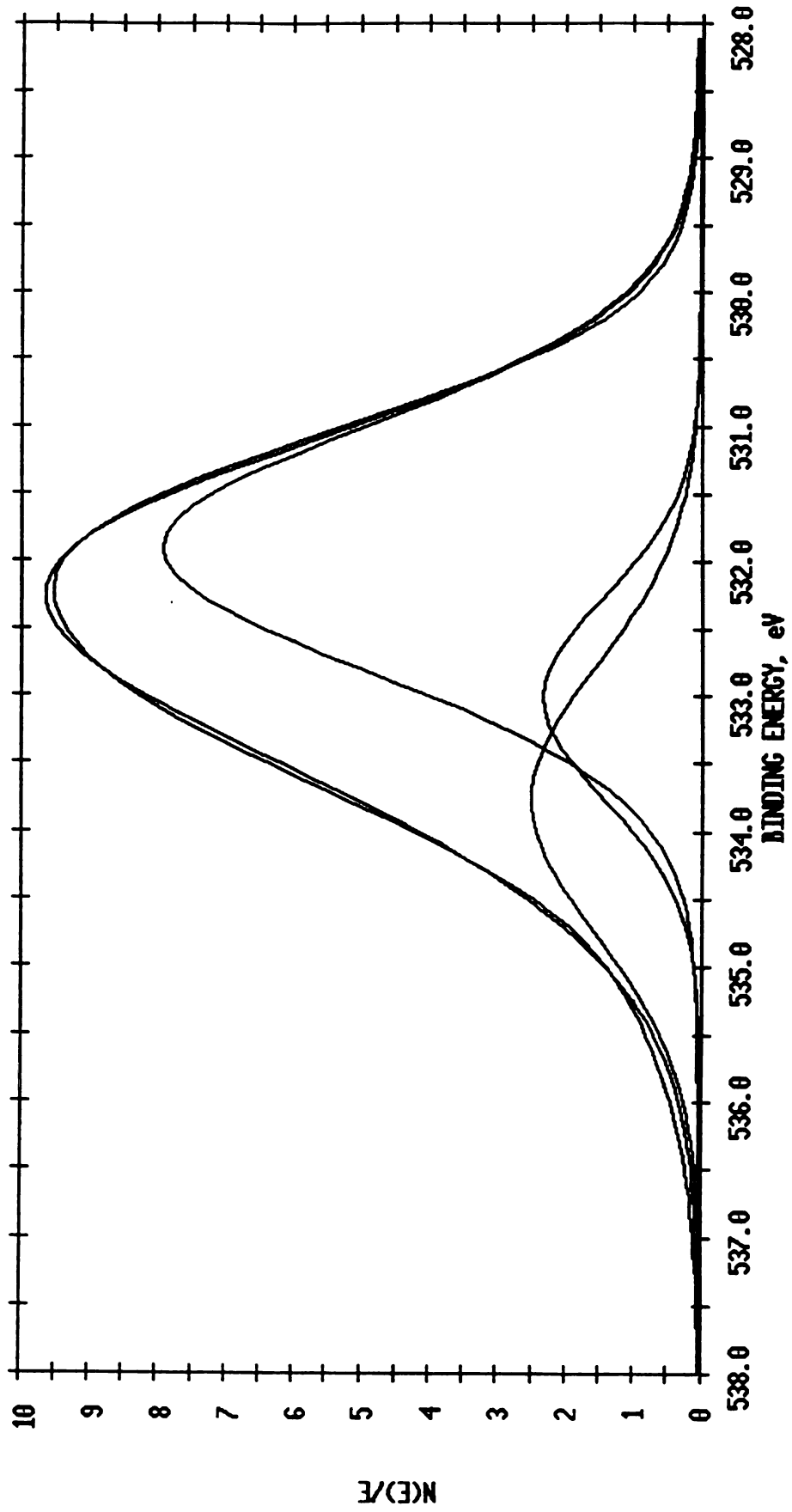


Figure B.19. O(1s) peak of K_2CO_3 -impregnated carbon black exposed to H_2 at $750^\circ C$, 1 atm.

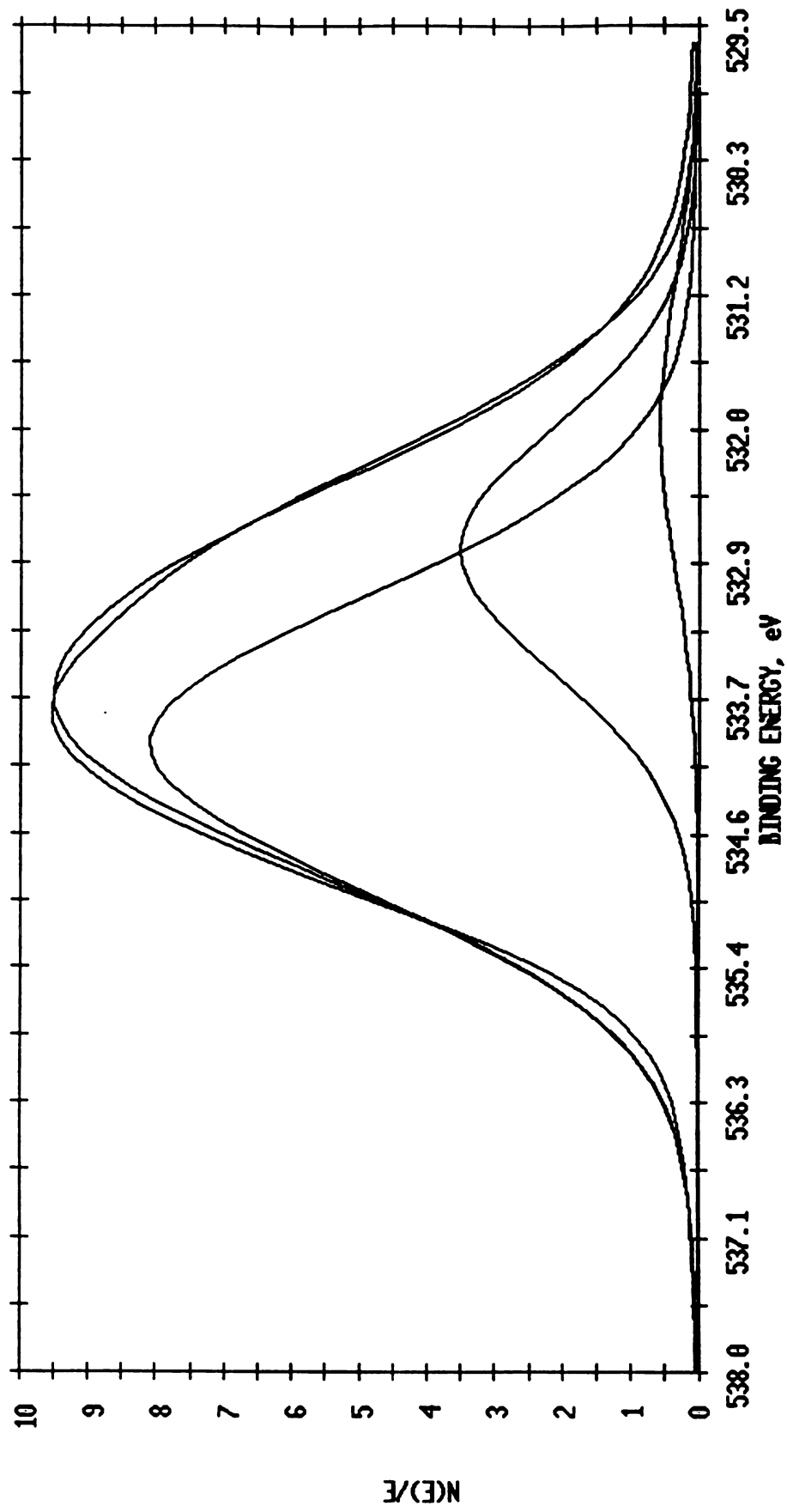


Figure B.20. O(1s) peak of K_2CO_3 -impregnated carbon black exposed to H_2 at 800°C, 1 atm.

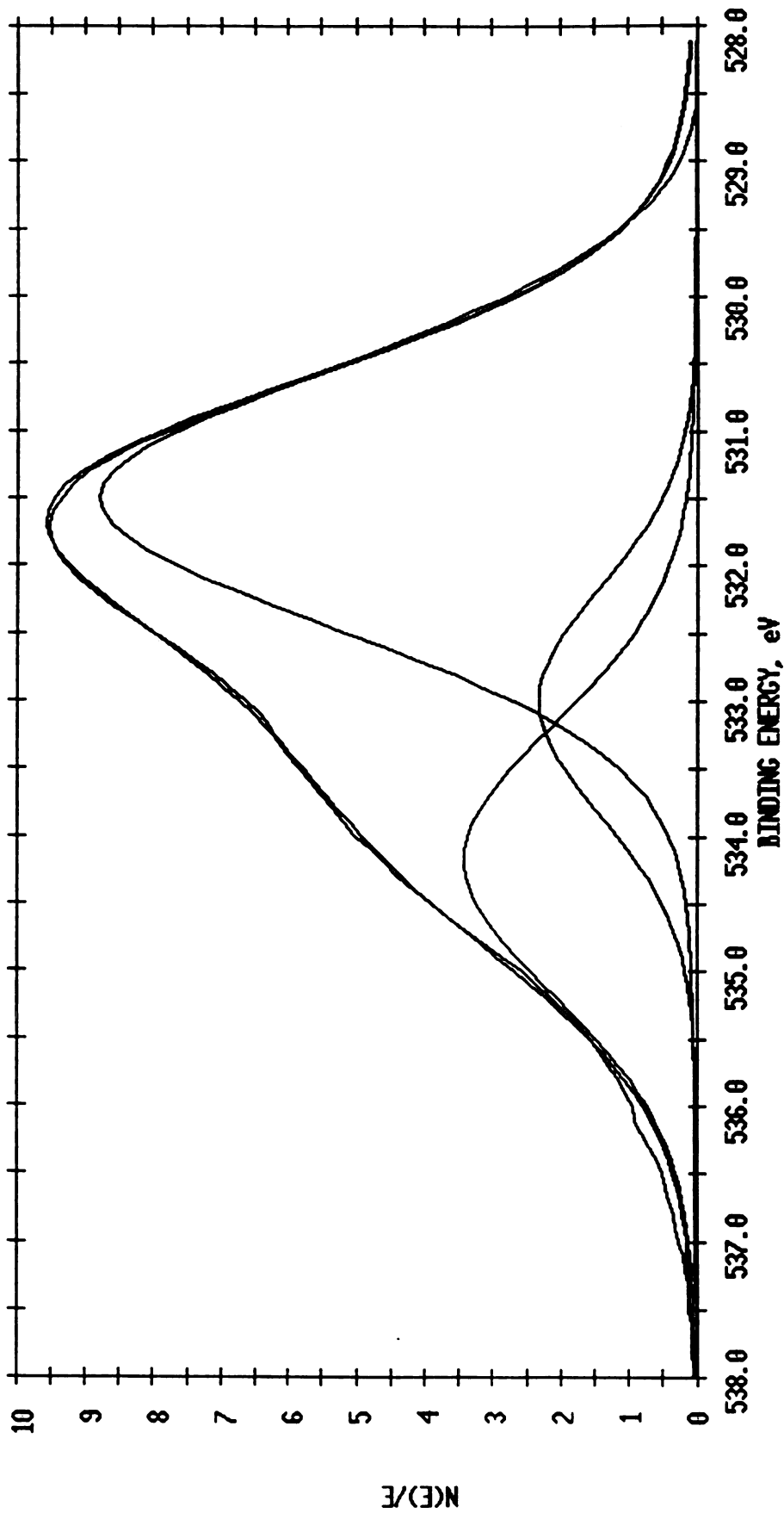


Figure B.21. O(1s) peak of K₂CO₃-impregnated carbon black 10% gasified, reheated to 200° C.

MICHIGAN STATE UNIV. LIBRARIES



31293007885928